Redox-dependent regulation of molecular crowding barrier in the nuclear pore

Wanzhen ZHANG

To my parents

Abstract

As a primary gateway of nucleocytoplasmic transport, the nuclear pore complex (NPC) plays important roles in cellular homeostasis and regulation. The NPC is a large macromolecular assembly that contains more than 30 proteins called nucleoporins (Nups), forming a molecular crowding barrier inside the pore. Although oxidative stress is known to affect the transport/permeability through the NPC, the molecular mechanism of this adaptive control remains unknown. In this study, redox-dependent responses of nuclear transport were investigated from a structural aspect of the NPC. Molecular crowding states of individual Nups were examined with a help of a crowding-sensitive fluorescent probe. Based on the detail analyses of the obtained images, Nups were classified into three categories: DTT-sensitive, H_2O_2-sensitive and insensitive Nups. Amino acid substitutions of cysteine residues to serine in H_2O_2-sensitive Nups partly abolished the H_2O_2-dependent crowding control, demonstrating that disulfide bonds play critical roles in this regulation. Fluorescence recovery after photobleaching analyses of importin α/β-dependent nuclear transport under oxidative stress also revealed that disulfide bonds are involved in the redox-dependent regulation of the nuclear transport. Combine with previous achievements from single molecular transport assays, a cysteine-based proximal control model was proposed to explain the adjustment of the molecular crowding barrier of the NPC under redox conditions. Taken together, this study demonstrated that redox environments can control the NPC-mediated nuclear transport via directly inducing disulfide bonds among channel-forming Nups.

Table of Contents

Acknowledgment I

This thesis is based on material contained in the following scholarly paper:

Wanzhen Zhang, Ryuji Watanabe, Hide. A Konishi, Takahiro Fujiwara, Shige H. Yoshimura, and Masahiro Kumeta.
Redox-sensitive Cysteines Confer Proximal Control of the Molecular Crowding Barrier in the Nuclear Pore. *Cell reports,* volume 33, issue 11, page108484, 2020

Acknowledgment II

Approaching the end of an incredible journey, I want to express my gratitude to those who helped me generously, without them I won't be able to finish my study in Japan.

My supervisors:

I would like to thank Dr. Shigehiro Yoshimura, who provided so much support for my life and study in Japan. He is a diligent supervisor who is always being around in the laboratory for students. With his constructive suggestions and comments, I've been motivated to improving constantly my experimental techniques and analytical methods. Thanks to him, I became a better person in research. I am very lucky to have such a caring supervisor in my doctoral study. Thank you so much!

I also would like to express my gratitude to Dr. Masahiro Kumeta. As the supervisor of my project, he offed me so much support that is beyond the words. He cares about us, either scientific problem or life situation, you can always talk to him. He taught me every experimental procedure with patience, and he made sure that I've learned everything correctly too. He's always available to help us in the lab; his hard-working attitude inspired me deeply. He is a role model to me in every aspect and I am truly grateful to have him as my supervisor.

I would like to express my gratitude to Pr. James Hejna, who provided so much help to me, for both my research and my life in Japan. His enthusiasm for science and literature enlightened me to pursue my interests in life. I was so lucky to be around such a good professor for these years. I'll be always grateful to him.

I am also very thankful for my sub-supervisors, Dr. Peter Carlton and Pr. Takane Katayama, for their constructive suggestions and kind instructions on my project. I also want to express my gratitude to Prof. Masaya Nagao and Prof. Yuichi Taniguchi for your efforts on my defense and suggestions about my thesis, thank you so much!.

I also want to thank Pr. Osamu Chisaka, who was always so nice to me. I received so many snacks and so much kind help from him. Thank you so much!

Members of Yoshimura Lab:

Fukuda-san, thank you so much for taking good care of me. I am also very lucky to know Yanshu as my good friend; she gave me a lot of support and counsel genuinely. I also owe Dr. Konishi so many thanks for his selfless help regarding my presentations, experiments, and so on. I am so grateful to Watanabe, who paved the foundation for our project with solid results. I also appreciated the kind help provided by Itagaki for my mechanobiology project, he designed and built the device for me. I can't thank my friends in the lab enough for their support and help, I will miss you all: Diyana, Ayumi, Yamazaki, Dodo-san, Sayuri, Deguchi, Jiang, and Takemoto.

I want to thank Nishimoto-san for her constant help and support for administrative issues. You made my life so much easier in Japan!

Mentors:

I also want to thank my supervisors of the master program back in France: Dr. Jean-Michel Jault and Dr. Pierre Falson. They provided me so much attention and care during my Master's internship. Dr. Jault was the person who encouraged me to take the first step in research, for that I will always be thankful to him.

Many thanks for Pr. James Sturgis, who kindly provided me the opportunity to learn in his lab. I had wonderful summer memories of Côte d'Azur in 2013.

I want to thank my excellent high school teacher: Shengli Qu. His good teaching led me interested in Biology in the first place, thank you so much.

Family and Friends:

I want to express my sincere gratitude to my parents. What they did for me is beyond any kind of expression. They supported me with nothing but love and care. I also want to thank my brother, my sister-in-law, my nephew, and my niece. They give me so much joy in my life.

I thank my best friends (my sisters from other mothers): Jie Meng and Dr. Lu Tian. For better and for worse, I know you will always be there for me.

I am very thankful to have so many good friends: Qinging Lidu, Xiaolin Yan, Dr. Rashad Nasr, Fei Hong, Rao Fu, Yu Zhang, Liwei Yu, Thev JayMahan, and so on. Thank you all for your support to me!

Abbreviations

NPC: nuclear pore complex

Nups: nucleoporins

FG: phenylalanine-glycine

NE: nuclear envelope

IDR: intrinsically disordered region

TR: transport receptor

NLS: Nuclear Localization Signal

NES: Nuclear Export Signal

Kap: karyopherin

Crm1: chromosome region maintenance 1

HEAT: **H**untingtin-**E**longation factor 3-Protein phosphatase 2**A** -yeast kinase **T**OR1

IBB: importin β-binding

LINC: linker of nucleoskeleton and cytoskeleton complex

YAP (Yes-associated protein)

ROS: reactive oxygen species

Nrf2: nuclear factor erythroid 2-related factor 2

Keap1: Kelch-like ECH-associated protein 1

FRET: Förster resonance energy transfer

FRAP: fluorescence recovery after photobleaching

WT: wild-type

CS: cysteine-to-serine

CFP: cyan fluorescent protein

YFP1G: glycine-inserted yellow fluorescent protein

DMEM: Dulbecco's Modified Eagle's Medium

FBS: fetal bovine serum

NEM: N-ethylmaleimide

DTT: Dithiothreitol

ROI: regions of interest

NT: non-treated condition

ZnF: zinc finger

ASK1: apoptosis signal-regulating kinase 1

ATM: Ataxia telangiectasia mutated kinase

JNK: c-Jun N-terminal kinase

MAPK: Mitogen-activated protein kinase

PI3K: Phosphatidylinositol 3-kinase

AKT: protein kinase B

NF-κB: nuclear factor kappa B

p53: tumor protein p53

HIF-1: Hypoxia-inducible factors 1

PKG: cGMP-dependent protein kinase

PKA: protein kinase A

Chapter 1 General Introduction

1.1 Nuclear Pore Complex

1.1.1 Structure of nuclear pore complex

As the solo guardian to control the nucleocytoplasmic molecular exchanges in eukaryotic cells, the nuclear pore complex (NPC) plays a crucial role in cellular homeostasis and regulations. From its first identification in the 1950s (Tomlin, 1950; Watson, 1959), the structure and function of the NPC have been intensively studied (Lin et al., 2016) (Kim et al., 2018) (Hampoelz et al., 2019).

The NPC is a large complex of proteins with a molecular mass from 60 MDa (yeast) to 112 MDa (human) depending on species, which is comprised of more than 30 protein subunits called nucleoporins (Nups). It forms a cylindrical structure that spans across the nuclear membrane with a predominant octagonal symmetry. Structurally, the NPC is made of three major substructures that are sparsely connected one to another: the cytoplasmic filaments, the central transport channel, and the nuclear basket. The molecular architecture and spatial organization of each substructure depend also on species (Lin and Hoelz, 2019) (Figure 1-1). In metazoan, the central channel of the NPC has a dimension of ~90 nm long and ~50 nm in diameter, with the extension of cytoplasmic filaments up to ~200 nm and an opposite extension towards nucleoplasm, ~75 nm connected to a ~55 nm-diameter distal ring (Stoffler et al., 2003).

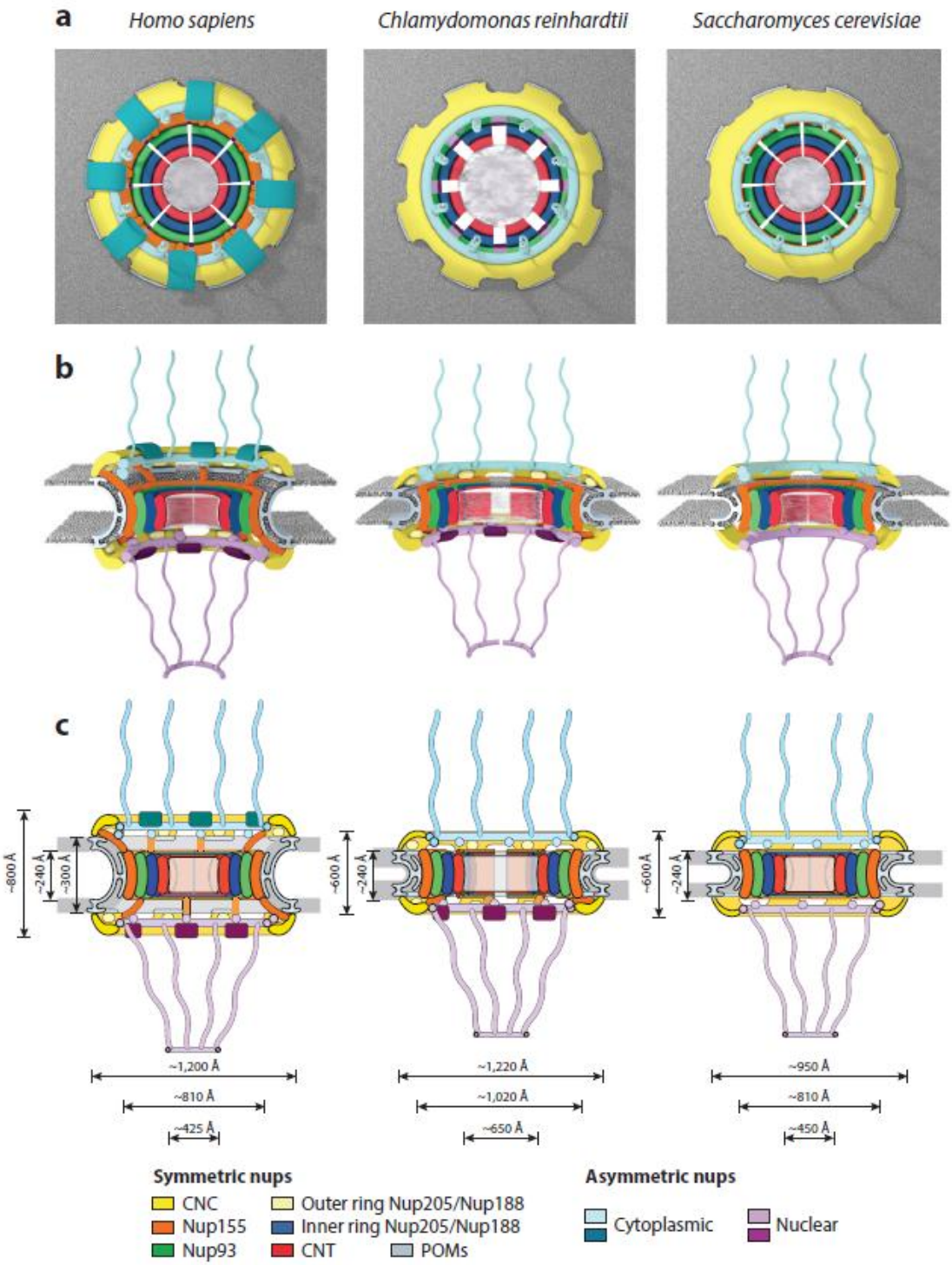

Figure 1-1 Structure of NPC from different species (Lin and Hoelz, 2019)

The structure of NPC from *homo sapiens*, *Chlamydomona reinhardtii*, and *Saccharomyces cerevisiae*. Different illustrations from (a) top view, (b) side view, and (c) schematic architecture are shown. The molecular details for two-dimensional schema are marked with different color codes for coat nucleoporin complex (CNC), channel nucleoporin heterotrimer (CNT), pore membrane protein (POMs), and other Nups. Sizes of each part of NPC from different species are marked.

Functionally, the cytoplasmic filaments serve as the docking harbor for nuclear transport of macromolecules, which facilitate the recognization step for import and release step for export of molecules, respectively. The nuclear basket plays a similar role with the reverse order compared to cytoplasmic filaments. On the other hand, the central transport channel is considered as the pivotal structure controlling nucleocytoplasmic exchange under given circumstances. The central channel cavity is filled with a high concentration of phenylalanine-glycine (FG) repeat motifs (up to 240 mM) extended from pore-forming Nups, which also provides an area with intensive binding sites (Aramburu and Lemke, 2017) that contribute to the nuclear transport process (See 1.2). Detailed molecular structures of individual Nups from each substructure are shown in Figure 1-2.

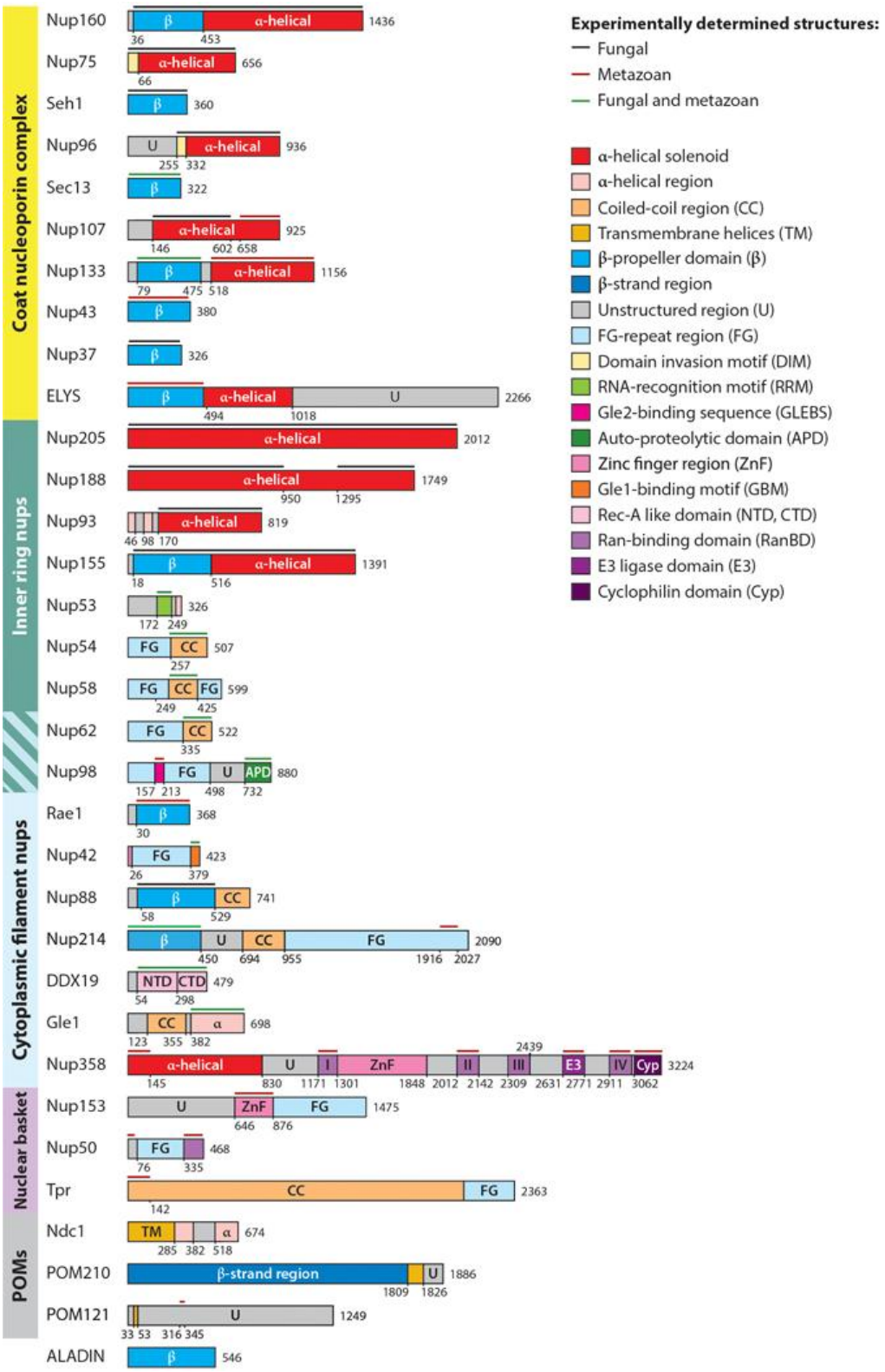

Figure 1-2 The molecular structures of Nups (Lin and Hoelz, 2019).

Detailed domain architectures of human Nups. Bars above domain indicate the regions explicated by high-resolution methods of each Nup, with color code of species from which the structures were determined. Abbreviations: CTD, C-terminal domain; NTD, N-terminal domain; POMs, pore membrane proteins.

1.1.2 Nucleoporins and FG repeats

Based on their function, the Nups could be classified into three categories: the transmembrane Nups, the scaffold Nups, and the barrier Nups (Figure 1-3). The transmembrane Nups (Gp210, Pom121 and Ndc1) are responsible for the anchorage of the rest of Nups within NPCs to the nuclear envelope (NE). The Nups that share a common feature of FG-repeats enriched intrinsically disordered regions (IDRs) are categorized as barrier Nups; since they are indispensable for the formation of a selective barrier in the NPC. The scaffold Nups (Nup160, Nup93, Nup205, etc.) function as bridges between the anchor component of transmembrane Nups and the functional component of barrier Nups.

The FG-domain in Nups possesses a high mean hydrophobicity and a very low net charge, with a hydrophilic inter-motif sequence that contains 10-20 amino acids. Most characterized FG-motifs in vertebrate Nups are FXFG, Glycine-Leucine FG (GLFG), Proline-XFG (PXFG), Serine-XFG (SXFG), and FG, in which X represents any amino acid (Cushman et al., 2006; Denning and Rexach, 2007; Schmidt and Gorlich, 2015). Due to their structural features, FG-Nups have shown the ability to adapt to different states, from the collapsed extended state as individual protein to brush state when they assembled on surfaces (Aramburu and Lemke, 2017). They could also form the transitions to supramolecular assemblies (Labokha et al., 2013; Milles et al., 2013) with different physical properties (Lim et al., 2007; Yamada et al., 2010) (Eisele et al., 2010; Milles and Lemke, 2011; Schoch et al., 2012).

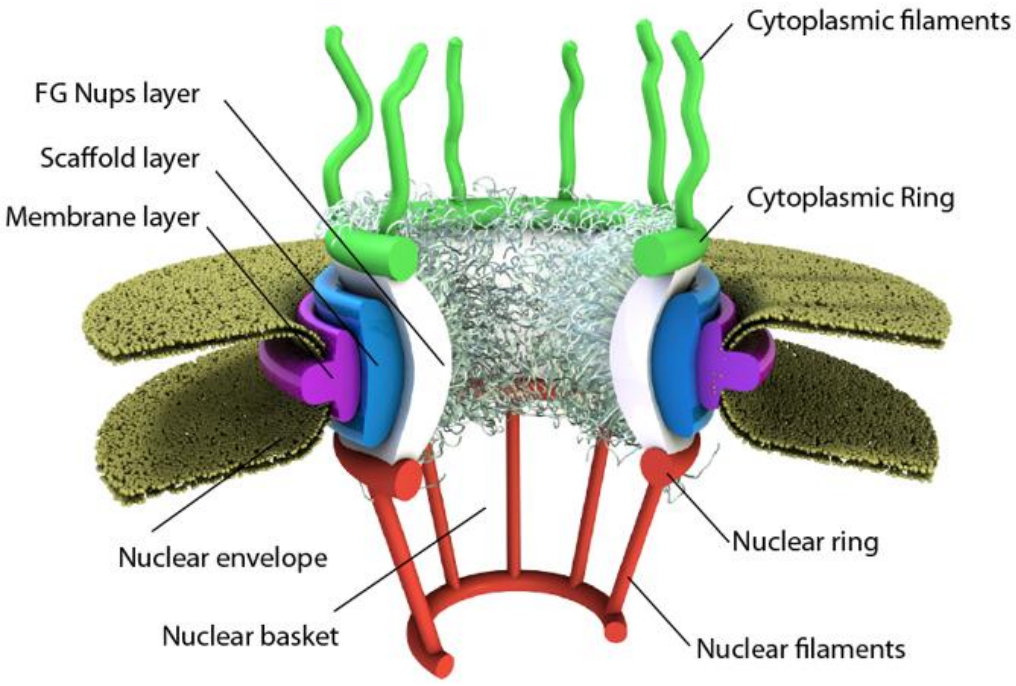

Figure 1-3 Architecture of NPC (Azimi and Mofrad, 2013).

The nuclear pore is anchored to the nuclear membrane with the membrane layer of Nups, the scaffold layer of Nups connected the membrane layer to the FG-Nups layer. IDRs of Nups in the FG-Nups layer constitute a selective barrier in NPC, which is important for nucleocytoplasmic transports through NPC. Vertically, the central channel of NPC protrudes both into cytoplasm and nucleoplasm, with cytoplasmic filaments and nuclear filaments, respectively.

1.1.3 Selective barrier

Translocation through the NPC is highly selective. Besides the passive diffusion of small molecules (< 40 kDa), only the passage for transport receptor (TR)-dependent cargos that contain nuclear signals are facilitated (Palmeri and Malim, 1999) (la Cour et al., 2004; Stewart, 2007). Although the underlying mechanism for NPC's selective barrier remains unclear, the molecular features of IDRs within FG-Nups surely contribute to NPCs' function as guardian gateway (Zeitler and Weis, 2004) (Kerr and Schirmer, 2011) (Fiserova et al., 2014).

For passive diffusion, the NPC functions as a size-filtration barrier, of which diffusion efficiency decreases dramatically with the molecular mass around 30-60 kDa. Based on dynamics simulation, this diffusion mode could be explained by a dual effect of molecules for constraining and competing within the limited volume of the NPC, which leads to an entropic repulsion force (Timney et al., 2016).

Opposite to the passive diffusion, multiple models are proposed to explain the TR-related active translocation through the NPC. A biomechanical study suggested that a delicate balanced FG-morphology between FG-Nup cohesiveness and entropic repulsion is essential for selective barrier (Stanley et al., 2017). Other studies are trying to explain the selective character of the NPC through binding affinities between FG-Nups and cargo complexes (Raveh et al., 2016). Based on a recent study, the recycling of nuclear import factors back to the cytoplasm is important for enhanced import and there is an optimal cytoplasmic concentration of cargo for import rate boost (Fogelson and Keener, 2018). Besides, it seems both hydrophobicity and surface properties of cargo molecules affect its passage rate through NPCs (Yoshimura et al., 2014) (Frey et al., 2018).

From the perspective of phase separation among FG-Nups, several studies have

agreed on the dissolution process of either the TRs or the FG-Nups into the selective barrier is an important step for the cargo translocation through the NPCs (Ribbeck and Gorlich, 2001) (Frey et al., 2006) (Ma et al., 2016) (Stanley et al., 2017).

1.2 Receptor-dependent nucleocytoplasmic transport

1.2.1 Import and export signals

For the import and export of macromolecules, transport signals are generally required during the process. These signals are polypeptide chains that contain recognizable information to TRs, for ultimately either transport in or out of the nucleus.

Nuclear Localization Signal (NLS)

The NLSs are briefly classified into two types: the classical NLS (cNLS) and the proline-tyrosine (PY)-NLS.

The cNLS comprises either one (monopartite) or two (bipartite) cluster(s) of basic amino acids. The consensus sequence for monopartite is K-K/R-X-K/R; whereas for bipartite is K/R-K/R-$X_{10\text{-}12}$-$(K/R)_{3/5}$, in which X represents any amino acid and 3/5 means three out of five consensus amino acids are lysine or arginine (Soniat and Chook, 2015). The cNLS is recognized indirectly by importin-β (Impβ), one of the karyopherin (Kap) proteins, through an adaptor protein importin-α (Impα). The high affinity between cNLSs and Impα is mainly achieved by electrostatic and polar interactions between them, with the help of hydrophobic interactions (Conti et al., 1998).

On the other hand, the PY-NLSs consist of three important binding epitopes: the N-terminal hydrophobic/basic epitope, the middle epitope, and the C-terminal epitope of P-Y or homologous P-Φ motif (Φ for a hydrophobic amino acid). The consensus

motif of the middle epitope, together with the C-terminal epitope is R/K/H-X_{2-5}-P-Y. The PY-NLS is recognized directly by karyopherin-β2 (Kapβ2, also known as importin-β2 or transportin-1) via the large concave surface of Kapβ2 (Lee et al., 2006) (Imasaki et al., 2007) (Suel et al., 2008).

Furthermore, non-classified NLSs such as the Karyopherin 121 (Kap121)-specific lysine-rich NLSs (Kobayashi and Matsuura, 2013) and the RS-repeat NLSs (Lai et al., 2000) (Maertens et al., 2014) have been identified.

Nuclear Export Signal (NES)

The NESs share a consensus motif of Φ-X_{2-3}-Φ-X_{2-3}-Φ-X-Φ, where the Φ represents hydrophobic residues, X means any amino acids (Bogerd et al., 1996) (la Cour et al., 2003) (Engelsma et al., 2004) (Kutay and Guttinger, 2005) (Xu et al., 2012). The best-studied NES binds to an export mediator chromosome region maintenance 1 (Crm1) protein. Its fragment usually exposes 3-5 hydrophobic residues to hydrophobic pockets in Crm1. There is one turn of helix in this NES that is conserved, which binds to the central part of the Crm1 groove. Furthermore, the backbone structure of this NES forms a hydrogen bond with Crm1 to further stabilize the interaction (Fung et al., 2017).

1.2.2 Nuclear Transport receptors

As mentioned previously, most of the proteins larger than 40 kDa travel through the NPC mediated by TRs. One of the important TR families is the Kapβ family, including importins and exportins (Chook and Blobel, 2001) (Conti and Izaurralde, 2001) (Gorlich and Kutay, 1999) (Weis, 2003). 25 Kaps have been identified in the human genome (Cagatay and Chook, 2018). Even though the sequence similarity among Kaps is very low (15%-20%) (Xu et al., 2010) (O'Reilly et al., 2011), they share similar

molecular weights ranging from 90 kDa to 150 kDa and an isoelectric point (pI) between 4.0 and 5.0 (Chook and Suel, 2011). More importantly, they all contain 19-21 helical repeats named HEAT (**H**untingtin-**E**longation factor 3-Protein phosphatase 2**A** -yeast kinase **T**OR1) repeats (Andrade Ma Fau - Bork and Bork, 1995) (Chook and Blobel, 2001) (Conti et al., 2006) (Chook and Suel, 2011); each repeat contains two anti-parallel amphiphilic α-helices (A-helix and B-helix) which connected by a short loop region (Chook and Blobel, 1999) (Cingolani et al., 1999). The hydrophobic sides of the α-helices are facing one and another, toward inside of the molecule; whereas the hydrophilic sides are facing outside of molecule, with contact to solvent. These HEAT repeats provide a structural flexibility to Kaps, which is crucial for its functional role as nuclear transporters, that is to interact with cargo proteins and RanGTP (Chook and Blobel, 2001) (Conti et al., 2006) (Forwood et al., 2010) (Lee et al., 2000) (Stewart, 2007) (Yoshimura et al., 2014). The outer surface of HEAT repeats provides multiple hydrophobic pockets, which interact with FG-Nups of NPC (Bayliss et al., 2000; Bayliss et al., 2002) (Liu and Stewart, 2005) (Otsuka et al., 2008) (Milles et al., 2015).

One of the best-studied Kaps is Impβ, which contains 19 tandem repeats of HEAT motifs. Impβ usually forms a trimeric transport complex with Impα and the NLS-cargo. To form this transport complex with an optimal transport activity, a specific range of concentration for Impβ is needed (Yang and Musser, 2006). Impα contains both cargo-binding and importin β-binding (IBB) domains, and mediate the formation of the trimeric complex. Structural studies suggested that Impβ could drastically change its structure, from a highly flexible structure to a compact one when interacting with the IBB domain (Cingolani et al., 1999) (Cingolani et al., 2000) (Zachariae and Grubmuller, 2008).

1.2.3 RanGTP gradient

Besides TRs, a small Ras-like GTPase Ran (~25 kDa) also plays an essential role in the nuclear transport process. In general, a GTP-bound form of Ran (RanGTP) is dominant in the nucleus, and a GDP-bound form of Ran (RanGDP) is dominant in the cytoplasm. This spatial distribution of Ran is called the RanGTP gradient (Nemergut and Macara, 2000). The RanGTP gradient is a fundamental feature for efficient nuclear transport because the different form of Ran directs nuclear transport via its selective binding to TRs to regulate association/dissociation of their cargos (Abu-Arish et al., 2009). Ran also affects Nup153-Impβ interaction for the importing process, especially for large cargoes (Lowe et al., 2015). This gradient is maintained by the isolated distribution of the nucleoplasmic regulator of chromosome condensation 1 (RCC1, also known as guanyl nucleotide exchange factor, RanGEF) and the cytoplasmic Ran GTPase-activating protein (RanGAP) (Gorlich et al., 1996) (Gorlich et al., 2003).

1.2.4 Nuclear import cycle

As shown in Figure 1-4, the classic nuclear import cycle mediated by Impα and Impβ includes four steps:

1) NLS-cargo in the cytoplasm is recognized by Impα with a high binding affinity (K_D ~ nanomolar range) (Hodel et al., 2001) (Hodel et al., 2006), then binds to Impβ through IBB domain of Impα (K_D~2 nM) (Cingolani et al., 1999) to form trimeric transport complexes (Impα•Impβ•NLS-cargo).

2) Transport complexes translocate the NPC with the help of interaction between Impβ and FG-Nups.

3) Once the transport complexes arrive in the nucleoplasm, binding of RanGTP to Impβ triggers the dissociation of this complex and releases the cargo.

4) Finally both Impα and Impβ are recycled to the cytoplasm with the help of other proteins, such as the cellular apoptosis susceptibility (CAS) protein.

Approximately 100~1000 cargos per minute per NPC are transported by the classic nuclear import cycle (Ribbeck and Gorlich, 2001) (Stewart, 2007). Although the nuclear import time and transport efficiency depend on Impβ concentration (Yang and Musser, 2006), recent studies agreed that the cargo molecule import process takes less than 10 ms (Kubitscheck and Siebrasse, 2017).

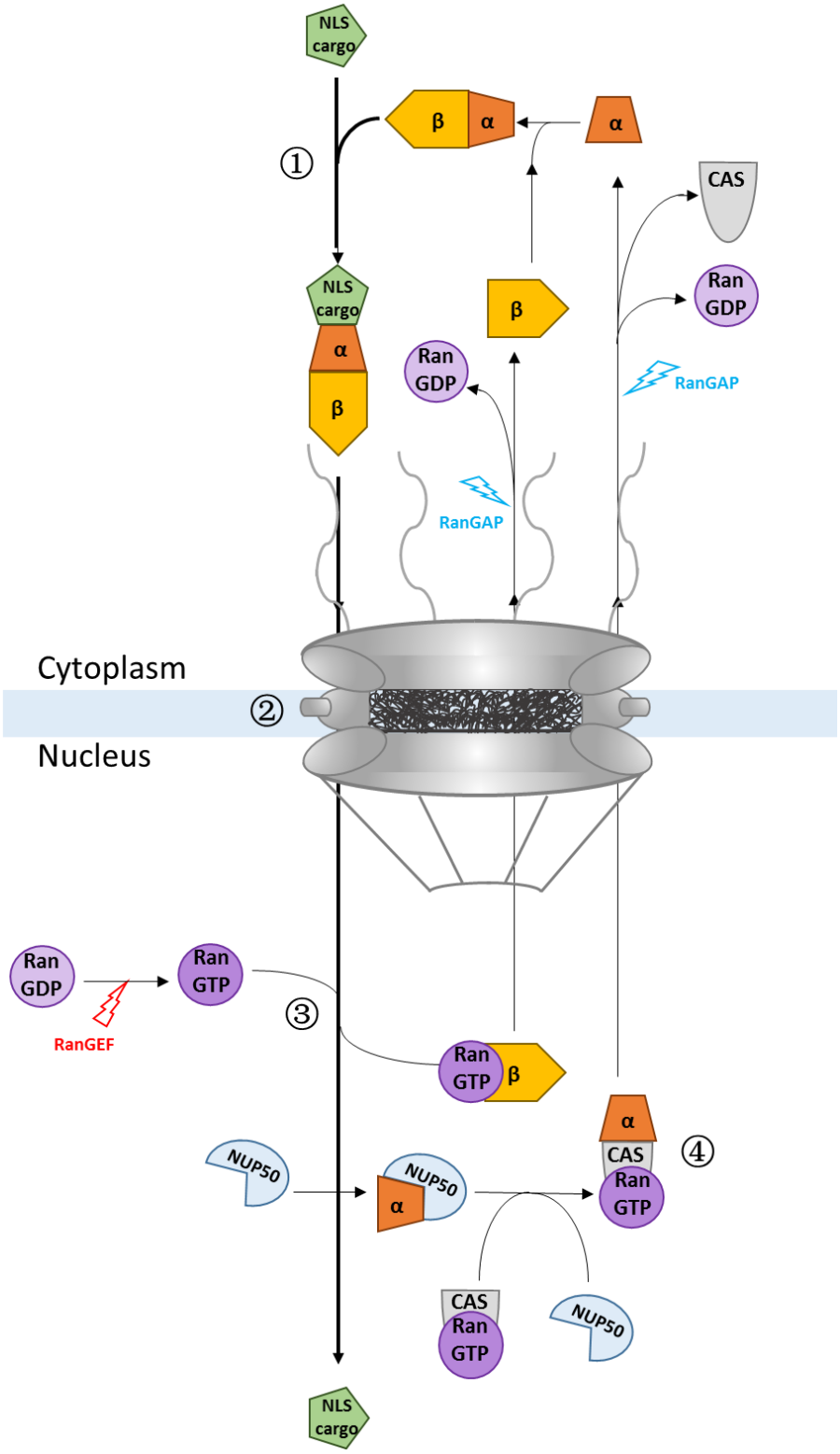

Figure 1-4 Nuclear import cycle (Adapted from (Stewart, 2007))

Four steps of the nuclear import cycle that are mediated by Impα and Impβ are shown. The transport process is assisted by various proteins, such as RanGAP (Ran GTPase-activating protein), RanGEF (guanyl nucleotide exchange factor), CAS (cellular apoptosis susceptibility), and Nup50.

1.2.5 Nuclear export cycle

Correspondently, the nuclear export cycle is a reverse process to the import cycle, as shown in Figure 1-5, with an example of a well-known exportin, Crm1 (Hutten and Kehlenbach, 2007). The nuclear export cycle also has four steps:

1) A cargo protein with NES in the nucleus is recognized and bound to Crm1, then RanGTP is recruited to form an export complex: NES-cargo•Crm1•RanGTP.

2) The export complex is translocated to the cytoplasm through NPC, which is also mediated via interaction with FG-Nups (Yang et al., 2004).

3) Upon binding to cytoplasmic filament Nups (Nup88, Nup98, Nup214 and Nup358) (Fornerod et al., 1997) (Hutten and Kehlenbach, 2006) (Askjaer et al., 1999) (Bernad et al., 2004) (Oka et al., 2010), this export complex interacts with RanGAP, which leads to the hydrolysis of GTP to GDP and promotes the dissociation of export complex (Kehlenbach et al., 1999) (Bischoff and Gorlich, 1997) (Bischoff et al., 1995) (Seewald et al., 2002).

4) Once the cargo molecule is released in the cytoplasm, Crm1 is recycled back to the nucleus where the exportin get prepared for the next round of export (Floer and Blobel, 1999) (Koyama and Matsuura, 2010).

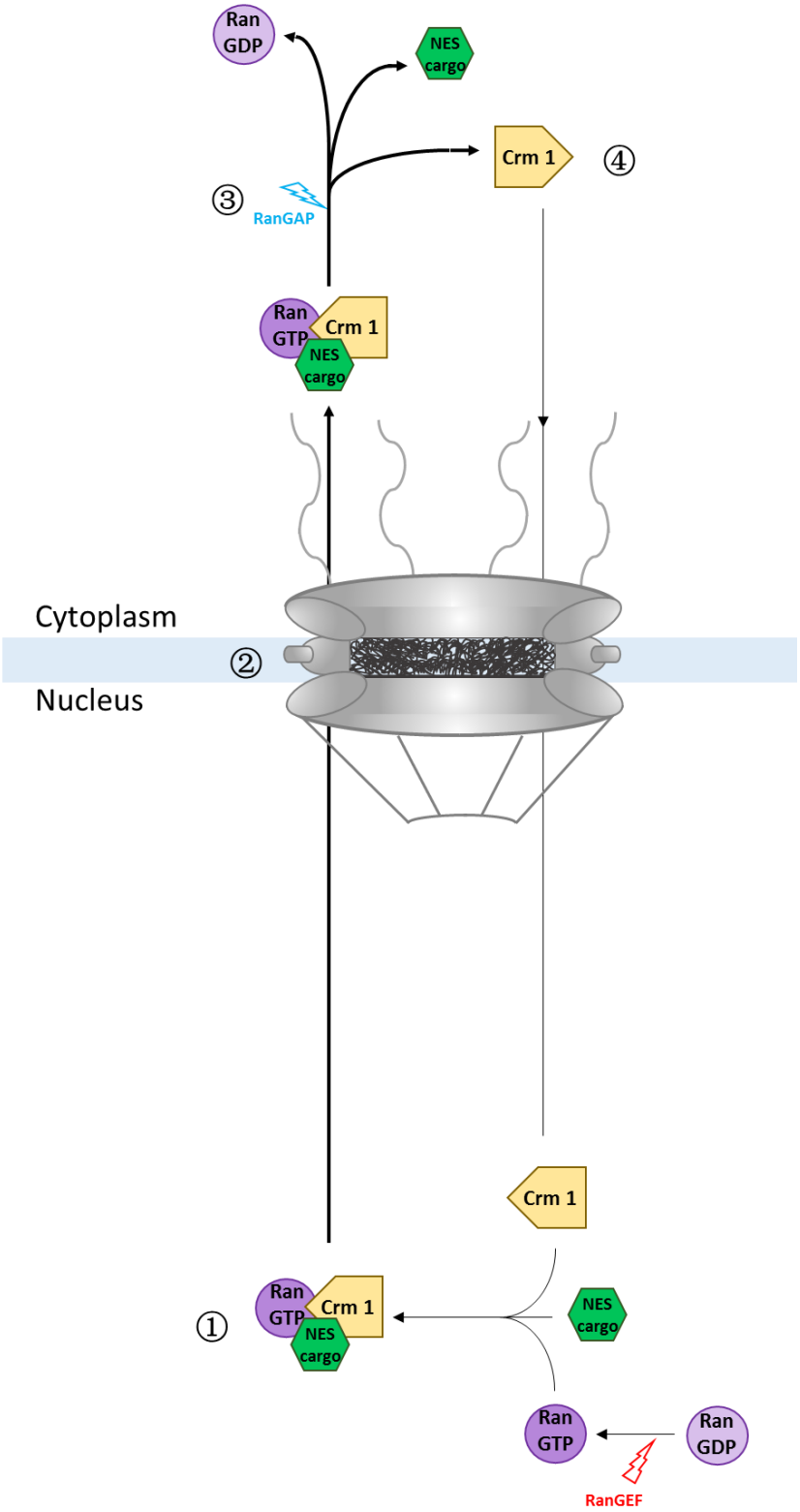

Figure 1-5 Nuclear export cycle (Adapted from (Weberruss and Antonin, 2016)

Four steps of the nuclear export cycle that are mediated by Crm1 are shown. The transport process is assisted by various proteins, such as RanGAP, RanGEF, and the cytoplasmic filament Nups (Nup88, Nup98, Nup214, and Nup358).

1.3 Models for nuclear transport through the NPC

Since selective nuclear transports through the NPC are mainly established by structural features of NPCs and coordinated ability of TRs, there are several nuclear transport models (Walde and Kehlenbach, 2010) (Donnaloja et al., 2019) proposed with different perspectives, as shown in Figure 1-6.

The virtual-gate model is proposed based on the preset that unstructured FG-Nups are non-cohesive with each other, thus they could form an entropic barrier due to the thermal movements of FG-repeats. Small molecules can pass through the NPC; the transport is mediated by transient binding events between TRs and FG-repeats (Miao and Schulten, 2010) (Moussavi-Baygi et al., 2011) (Gamini et al., 2014) (Figure 1-6A).

The forest model is proposed based on the heterogeneity of FG domains within NPCs (Yamada et al., 2010), Nups are classified into two categories of configurations, two distinct zones of traffic were proposed. Small molecules passively diffuse through NPCs mainly via zone 2 (close to the scaffold, indicate with yellow color), and active transport of macromolecules is conducted mainly through zone 1 (axial channel, indicate with green color) of the NPC (Figure 1-6B).

The reduction of dimensionality model suggested that active nuclear transport is carried out by sliding of TRs on the surface of FG-repeats through continuous binding sites, which makes the transport process mimic a 2D random walk (Figure 1-6C).

The hydrogel model proposed that the interaction among cohesive hydrophobic FG-repeats form a sieve-like hydrogel meshwork. Upon interacting with TRs, this meshwork is reversibly dissolved, in order to facilitate the passing through of cargos traverse NPCs (Ribbeck and Gorlich, 2002) (Miao and Schulten, 2009) (Gamini et al., 2014) (Figure 1-6D).

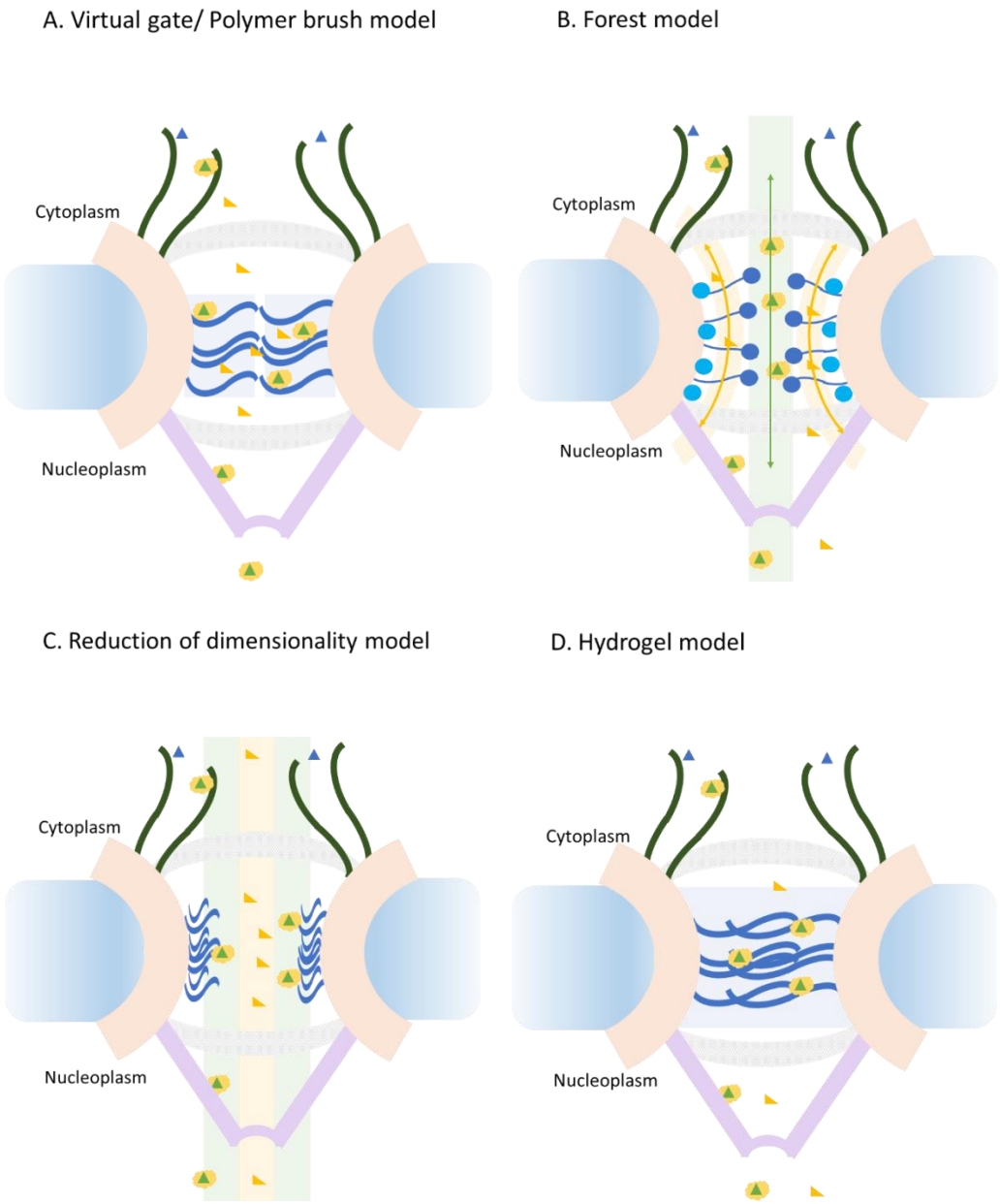

Figure 1-6 Nuclear transport models (Adapted from (Donnaloja et al., 2019))

The nuclear membrane is illustrated with blue color, a schematic NPC is simplified with different forms in color codes: the membrane and scaffold Nups in pink, the cytoplasmic filament Nups in dark green, the nucleoplasmic basket in violet. The boundary of NPC is shown with light grey. Small molecules within the 40 kDa threshold are shown in yellow triangles, large molecules are shown in blue isosceles triangles, transporters are shown in yellow rounds. FG-Nups are shown with dark blue wavy lines except for the Forest model. In the forest model, FG-Nups in 'shrub' conformation are shown in cyan disks, FG-Nups with 'tree' conformation are shown in dark blue disks with an extended coiled in the same color.

1.4 Stress-responses of nuclear transport

In recent years, more and more external stresses have been studied for a better understanding of physiology, from the individual level to the cellular level. I introduce here several stresses that have been reported to trigger cellular responses. Nuclear transports are generally involved in these regulatory processes.

1.4.1 Heat Stress

For homothermal animals, thermoregulation plays a vital function to keep the body core temperature at 37 ℃. Hypothermia (< 35.0 ℃) and hyperthermia (> 40.5 ℃) are life-threatening emergencies (Cheshire, 2016). Usually, this range of temperature between hypothermia and hyperthermia won't cause too much damage at the cellular level.

It has been reported that nuclear transports that were mediated only by Ran and Impβ family proteins (transportin- and Crm1- dependent transports, for example) were partially suppressed at temperatures < 44 ℃ (Ogawa and Imamoto, 2018), from an *in vitro* assay. The nuclear translocation of Impα seems to induce the import inhibition for transports that dependent on the Impα/β complex. This conclusion is supported by the fact that within a temperature range from 37.3 ℃ to 44.1 ℃, the RanGTP/RanGDP cycle and function of Impβ are quite stable compare to physiological conditions (37 ℃). Because the nuclear import efficiencies were not affected with either RanGDP or Impβ preincubated at high temperatures.

In addition, since Crm1-dependent export was still active while Impα/β-dependent import was inhibited, different types of localization signals are presumed to carry the information regarding the localization changes of cargo protein

under heat stress (Ogawa and Imamoto, 2018).

1.4.2 Mechanical Stress

Contrary to heat stress, cells are constantly facing various mechanical stimuli such as compression force, shear force, tensile force. As a principal regulation hub, the nucleus senses and reacts to the mechanical force that applied on cells through multiple molecules such as the linker of nucleoskeleton and cytoskeleton complex (LINC) (Crisp and Burke, 2008) (Alam et al., 2015), emerin (Guilluy et al., 2014), nuclear lamina (Folker et al., 2011) (Zwerger et al., 2013). It has been reported that cells react to force that applied on the cell surface by an instantaneous stretching of chromatin and a rapid transcription of transgene within the same chromatin regions (Tajik et al., 2016).

Apart from the transcriptional regulation, increased local tension upon the nuclear membrane would cause an alternation of NPCs' permeability. From a structural view, NPCs possess the conformational potential to restrict or dilate their central channel upon mechanical force stimulation (Solmaz et al., 2013) (Stuwe et al., 2015) (Chug et al., 2015). Several components of the nuclear envelope, such as Sun1 and lamin A/C, were shown to interact with Nup153 (Liu et al., 2007) (Jahed et al., 2016). Therefore, force-induced changes in NPC structure may be transmitted from the LINC complex and nuclear lamina. Indeed, the colocalization of NPCs with LINC proteins and actin was observed recently in cells under mechanical stimulation (Hoffman et al., 2020). In some cases, the translocalization of mechano-sensitive regulatory molecules such as YAP (Yes-associated protein) has been observed under mechanical stress, accompanied by an altered NPC conformation and nucleocytoplasmic transport (Elosegui-Artola et al., 2017).

1.4.3 Osmotic Stress

Cells adapt to osmotic stress by altering gene expression and metabolic activity. Usually, the osmotic stress affects directly the cell volume, thus directly changes the concentration of intracellular macromolecule. This concentration acts as an important physical factor for nucleus organization (Finan and Guilak, 2010).

The shrinkage of cell volume under hyper-osmotic stress results in an expanded nuclear pore and increases nucleocytoplasmic transport. On the other hand, hypo-osmotic stress has no such effect on nucleocytoplasmic transport (Finan et al., 2011).

1.4.4 Oxidative stress

For all the external stresses that may display on cells, oxidative stress has been considered as an important one that affects directly the nucleocytoplasmic transport. Aberrations in the nucleocytoplasmic transport would cause mislocalizations of proteins, which is often been found in neurodegenerative diseases (Patel and Chu, 2011).

Several regulatory factors of the nuclear transport system were known to be affected when cells are exposed to reactive oxygen species (ROS). For example, the nuclear factor erythroid 2-related factor 2 (Nrf2) has been found to mislocalize to the nucleus by ROS exposure due to its dissociation from cytoplasmic protein Kelch-like ECH-associated protein 1 (Keap1) (Kaspar et al., 2009) (Bellezza et al., 2018). As one of the important cellular regulators against oxidative stress, Nrf2 itself affects multiple cellular mechanisms by different signaling pathways (Zhang et al., 2015) (Sajadimajd and Khazaei, 2018).

At the structural level of the NE, A-type lamins act as a mediator of oxidative stress in cells (Sieprath et al., 2012) (Shimi and Goldman, 2014). Furthermore, oxidative stress has a direct effect on lipid peroxidation, thus the stability of lipid bilayer membranes of the NE could be compromised (Ramana et al., 2017).

Previous studies showed that oxidative stress has a direct effect on nuclear export; multiple FG-Nups are affected under this stress (Crampton et al., 2009) (Patel and Chu, 2011). It has also been reported that a mislocalization of nucleoporins such as Nup153 and Nup88 in the nucleus was observed under oxidative stress, and they form a high molecular mass complex with Impα inside the nucleus (Kodiha et al., 2008). In addition, other transport-related regulators such as the RanGTP gradient could be disrupted under oxidative stress (Chatterjee and Paschal, 2015).

1.5 Objective of Study

Living organisms are constantly facing various stimuli and very often need to overcome stress conditions, which processes are now considered as part of physiological regulations within certain realms (Pomatto and Davies, 2017). As the gateway to the nucleus, apart from its conventional role in nuclear transport, the NPC is considered a dynamic hub for multiple essential cellular activities including cell cycle, cell differentiation, and gene regulation (Capelson et al., 2010). To get a better understanding of cellular homeostasis, intensive studies have been carried out for different stimuli and nuclear transport processes (Gilbert and Weaver, 2017) (Goulev et al., 2017). However, the systematic control of NPCs at the molecular level remains unknown. In this study, I have chosen oxidative stress as stimulation to investigate the adjustment of NPCs while facing stressed conditions.

A previous study in my lab reported that the permeability through nuclear pore complexes could be suppressed by oxidative stress, which process has an affiliated formation of disulfide bonds among Nups (Yoshimura et al., 2013). With an established crowding-sensitive FRET (Förster resonance energy transfer) probe tools that were attached to individual Nups, molecular crowding states within different regions of NPC were directly measured *in vivo* (Konishi et al., 2017). By using this technique, I investigated the stress-induced alteration of the nuclear pore property. Several cysteine-to-serine (CS) mutants of Nups were designed for the investigation of molecular crowding. Furthermore, fluorescence recovery after photobleaching (FRAP) assay and previous single molecular transport assay provided more detailed information of the adaptive regulation in nuclear permeability/transport process under redox conditions. Finally, based on the experimental results mentioned above, I propose a proximal control model of molecular crowding *in vivo*, which is dynamically regulated at the molecular level.

Chapter 2 Alterations of the molecular crowding barrier in the NPC under different redox conditions

2.1 Introduction: Redox conditions and GimRET probe

In recent years, oxidative stress has been considered to play a key role in neurodegeneration diseases including Huntingtin disease, amyotrophic lateral sclerosis (Grima et al., 2017) (Fahrenkrog and Harel, 2018; Guo et al., 2018), etc. A previous work of my laboratory also demonstrated that the permeability of the NPC is reduced by oxidative stress, which is accompanied by the formation of intermolecular disulfide bonds among Nups and eventually affects Impβ-dependent nuclear transport (Yoshimura et al., 2013).

To investigate this *in vivo* process, a crowding-sensitive tool named GimRET has been implanted for individual Nup (Konishi et al., 2017), which was first developed based on a FRET principle (Morikawa et al., 2016) (Figure 2-1).

The GimRET probe uses a cyan fluorescent protein (CFP) as a donor and a glycine-inserted yellow fluorescent protein (YFP1G) as an acceptor. Under a low crowding environment, YFP fluorescence is observed by CFP excitation due to the energy transfer among them. When facing a highly crowded environment, the collapse of YFP1G protein leads to a reduced fluorescence signal in YFPG1. Therefore, GimRET could measure the local molecular crowding states *in vivo* by expressing together with the target protein.

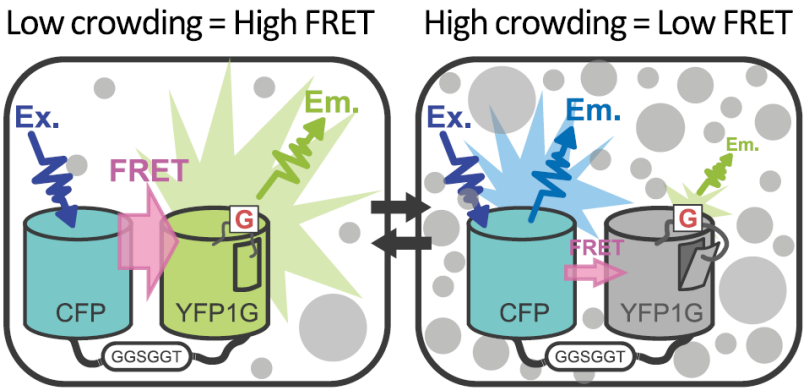

Figure 2-1 Schematic illustration of the GimRET probe

(Adapted from (Morikawa et al., 2016))

The illustration of crowding-sensitive probe GimRET. In a crowded environment, GimRET shows a low FRET signal due to the collapse of acceptor protein YFP1G.

2.2 Materials and methods

2.2.1 DNA constructs

Constructions of plasmids to express GimRET-Nups wild type (WT) were described in a previous report of my laboratory (Konishi et al., 2017). The CS mutants for Nup62, Nup98, Nup153, and Nup214 were constructed as described below.

GimRET-Nup62CS

Nup62 contains two cysteines (C478, C509) on its C-terminal region. A CS mutant for rat Nup62 was previously prepared using the GeneTailor Site-Directed Mutagenesis System (Invitrogen) (Yoshimura et al., 2013) in pcDNA3.1 vector, with an HA tag inserted at the N-terminus. To construct GimRET-Nup62CS mutant, CS containing region was amplified from the pcDNA3.1 construct and inserted into the GimRET vector (Figure 2-2). The CS mutated fragment of pcDAN3.1 construct (from 1035 bp to 1554 bp, a total 519 bp fragment) was amplified using forward and reverse primers of 5' ctcgacctcctggtcctcgccgtga 3' and 5' tcggccgcgttccttgtccttgcgt 3', respectively. GimRET vector with the rest part of Nup62 was amplified from GimRET-Nup62WT by PCR using forward and reverse primers of 5' tccttgtccttgcgtcggacgcgta 3' and 5' gacctcagacctcgacctcctggtc 3', respectively. The amplified fragments were combined using the InFusion® system (TAKARA).

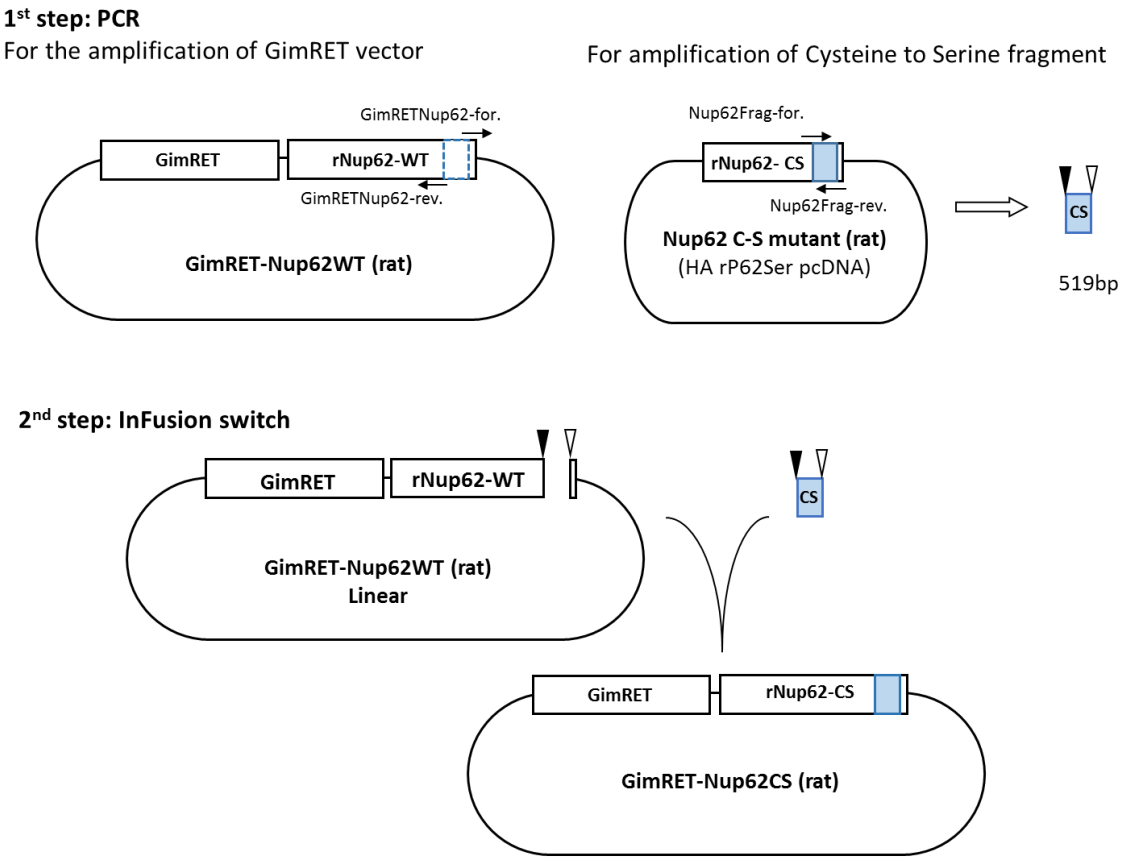

Figure 2-2 The strategy for GimRET-Nup62CS plasmid

CS fragment region was shown in the blue box. Complementary sequences (~15 bp) were shown in triangles: upstream sequence in black and downstream sequence in white. PCR primers were shown in black arrows. See text for more information.

GimRET-Nup98CS

For Nup98, a PCR-based mutagenesis strategy was used to mutate three cysteine residues (C188, C743, and C818). Two cycles of PCR-based mutagenesis were performed, as shown in Figure 2-3. A forward primer for the amplification of C188 to C743 fragment with both a ScaI site (indicated in italic letters) and a CS mutation (indicated in capital letters) at C188 was designed: 5' cactaacata*agtact*aagcaccagAGCat 3'. The reverse primer for the C743 side with a CS mutation at C743 was used: 5' gaaatcagagacaatGCTctctccttt 3'. However, after the InFusion reaction with the GimRET-Nup98WT construct, only the C743 site was mutated to S743. The same procedure was followed with the same C188 forward primer and C818 reverse primer with CS mutation at C818: 5' tgggctctttattaaGCTacgagatg 3'. After the second round of InFusion reaction, both C743 and C818 were mutated in the GimRET-Nup98 construct. The final mutation of C188 (capital letters) was proceeded by another round of two-step PCR based mutagenesis with amplification of fragment between BglII and HindIII restriction sites (italic letters) of GimRET-Nup98WT. Four primers are shown below:

BglII forward: 5' tccggactc*agatct*atgtttaacaaatca 3'

C188 forward: 5' accaagcaccagAGCattactgctatgaaa 3'

C188 reverse: 5' tttcatagcagtaatGCTctggtgcttggt 3'

HindIII revers: 5' tgtagt*aagctt*gttattgccaaacagggt 3'

Finally, the GimRET-Nup98CS construct with all three CS mutations was obtained.

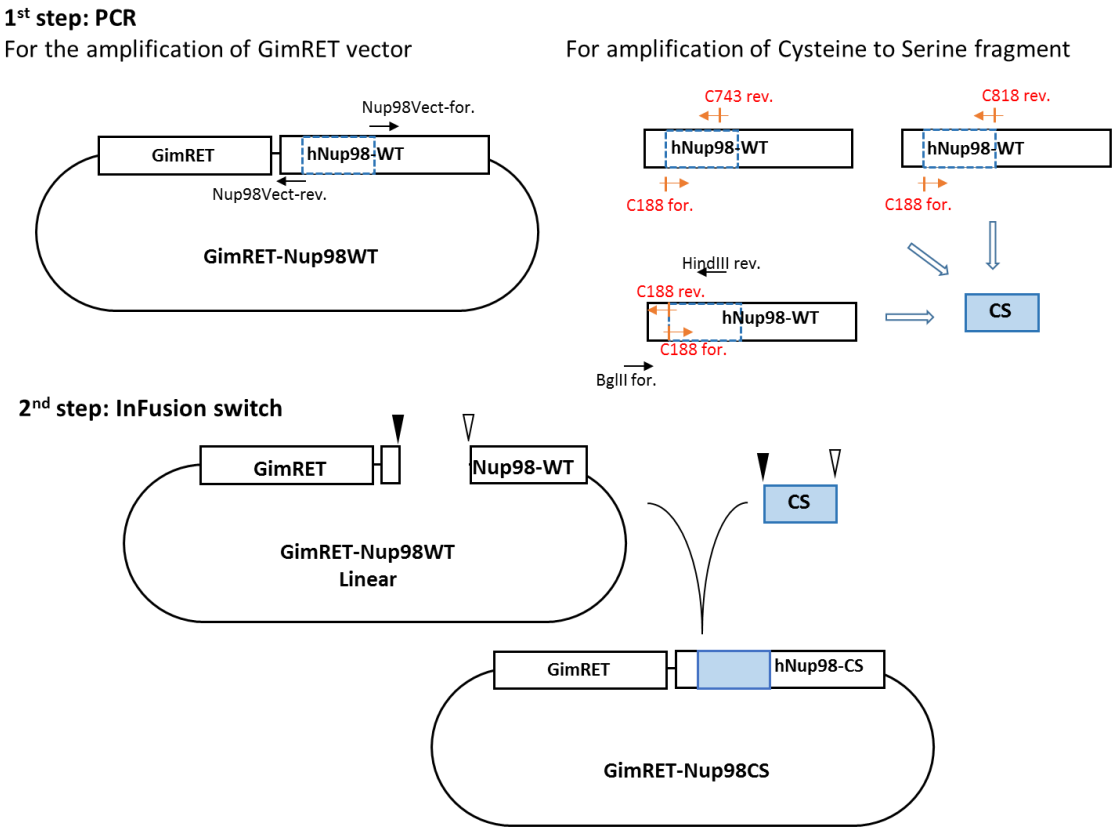

Figure 2-3 The strategy for GimRET-Nup98CS plasmid

CS fragment region was shown in the blue box. Complementary sequences (~15 bp) were shown in triangles: upstream sequence in black and downstream sequence in white. CS mutations were shown in red vertical lines, the correspondent PCR primers (including these CS mutations) were shown in orange arrows.

GimRET-Nup153CS and GimRET-Nup214CS

For Nup153, 21 cysteine residues among a total of 28 cysteine residues were substituted to serine residues. For Nup214, 8 cysteine residues among a total of 13 cysteine residues were mutated to serine residues. The correspondent CS fragments of Nup153 (C585 to C874) and Nup214 (C102 to C299) were synthesized (FASMAC), provided within the pMA-RQ vector. The strategies of these two plasmid constructs are shown in Figure 2-4; the fragments were amplified by PCR, with the insertion of silent XmaI (purple) and SacI (green) restriction sites for Nup153 and Nup214, respectively.

Primers for Nup153 are shown as below, restriction sites were indicated in italic letters:

153CS fragment PCR forward: 5' gtgaacagtacaaatagcaagsagacacca 3'

153CS fragment PCR reverse (+XmaI): 5' *ggg*ctttgcactttcgcttgccaagctttt 3'

GimRET-Nup153 forward (+XmaI): 5' gaaagtgcaaag*cccggg*acaaaatctgg 3'

GimRET-Nup153 reverse: 5' atttgtactgttcactgtagtgacatgatg 3'

Primers for Nup214 are shown as below:

214CS fragment PCR forward (+SacI): 5' atcacctggcctt*gagctc*cgataacctca 3'

214CS fragment PCR reverse: 5' tgatgctgtctctccgtgctgctgcc 3'

GimRET-Nup214 Vector PCR forward: 5' ggagagacagcatcattactacctca 3'

GimRET-Nup214 Vector PCR reverse: 5' tcaaggccaggtgatggattgggaat 3'

Amplified CS fragments are switched to the WT constructions of GimRET-Nup153 and GimRET-Nup214 respectively, using InFusion® enzyme.

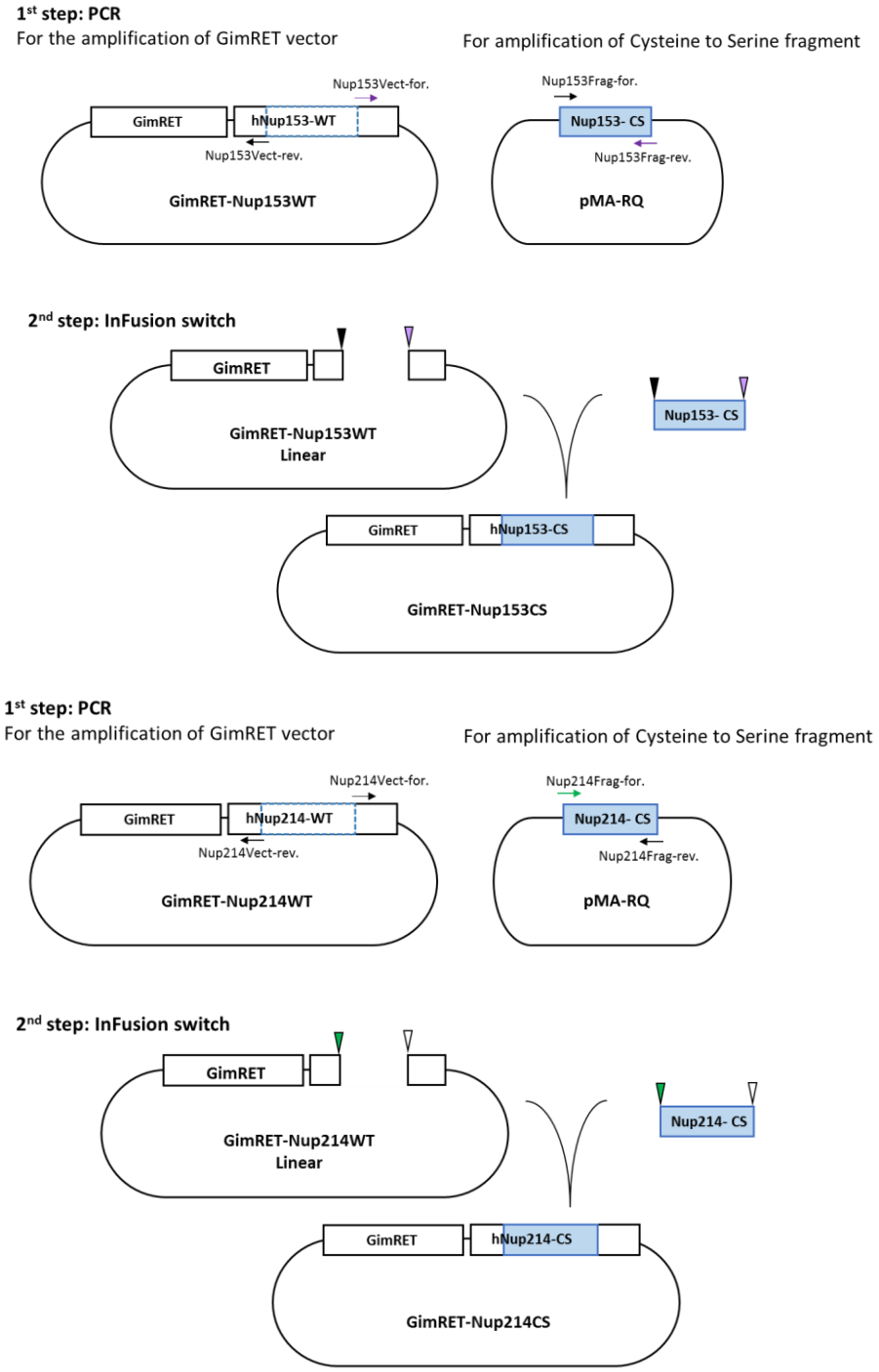

Figure 2-4 The strategies for plasmid constructs of GimRET-Nup153CS and GimRET-Nup214.

CS fragment regions were shown in the blue box. Complementary sequences (~15 bp) were shown in triangles, sequences with inserted restriction sites during PCR amplification were shown in colors: purple for Nup153 (XmaI), green for Nup214 (SacI); sequences without sites were marked in black (upstream) and white (downstream). Correspondent PCR primers were shown in vertical lines with the same color as sequences. PCR primers identical to templates were shown in black arrows.

2.2.2 Bulk GimRET assay

HeLa S3 cells (ATCC, CCL-2.2) were cultured in Dulbecco's Modified Eagle's Medium (DMEM) (Sigma) with 10% fetal bovine serum (FBS). Plasmid DNA was introduced to HeLa cells the next day of seeding (cellular confluency 60% ~ 70%), using an Effectene transfection reagent (QIAGEN). Depend on DNA constructs, either 23 h (Nups with small molecular weight, e.g. Nup62) or 29 h (Nups with large molecular weight, e.g. Nup153 and Nup214) after transfection, a new medium (DMEM+10% FBS) was supplied to the dishes. To prepare cells under oxidative condition, 2 mM H_2O_2 was added and incubated for 1 h before the sample processing. HeLa cells expressing GimRET-fused Nups (24 h or 30 h after transfection) with or without H_2O_2 treatment were semi-permeabilized by treating with 40 μg/mL digitonin in transport buffer (20 mM HEPES-KOH, pH 7.3, 110 mM CH_3COOK, 2 mM $(CH_3COO)_2Mg$, 5 mM CH_3COONa, 0.5 mM EGTA, and 1 mM Dithiothreitol (DTT)) for 5 min at 4℃, as described previously (Yoshimura et al., 2013). After digitonin treatment, the cells were washed twice using transport buffer with DTT (10 mM DTT for standard condition, 100 mM DTT for reduced condition) or without DTT (oxidative condition). A short incubation step of 10 min at 37℃ was performed afterward, with the same buffer as washing steps.

Microscopic observations were performed at room temperature for 30 min after the permeabilization. Microscopic images were captured using the FV1200 confocal laser-scanning microscope (Olympus) with a 60 × NA1.35 objective lens. The excitation wavelength was 433 nm, and the emission wavelength was set between 460 to 500 nm for the CFP channel, and 520 to 570 nm for the FRET (or YFP) channel. The NE area for each cell was selected using ImageJ (Version1.51W) software (Figure 2-5); The FRET ratios were calculated with YFP intensity over CFP intensity (YFP/CFP).

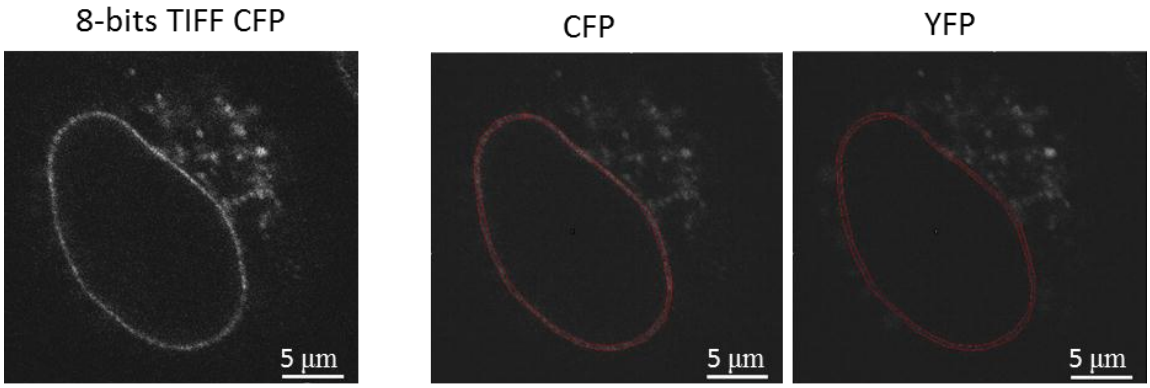

Figure 2-5 The CFP channel image (8-bits TIFF) of GimRET-Nup62 and the NE area selection by ImageJ for CFP and YFP images

The entire NE region was selected (indicate by the red line) for bulk FRET ratio analysis. Scale bar = 5μm.

2.2.3 Single-NPC-level GimRET assay: analysis methods

The same microscopy with the same objective lens and same setting as bulk assay were used for observation. The NE areas were largely zoomed; microscopic images with partial NE were captured for both CFP and YFP channels, in the format of 8-bits TIFF.

The detailed analysis method using ImageJ for GimRET crowding assays at a single-NPC-level is shown in Figure 2-6. Data processing was carried out with the following steps: 1) The CFP image was enhanced to get better contrast and then smoothed to reduce noise to be miss-detected as a signal in the latter step. The smooth step could decrease the automatic recognition of random noisy pixels in TIFF images by software. After this smooth step, only the spots (3x3 pixels averaged) with reasonable size and uniform signal intensity above the threshold (noise tolerant) would be recognized. 2) Areas outside/inside the nucleus are masked from the image and fluorescent spots corresponding to NPCs were detected using the 'Process—Find Maxima' tool. A threshold of 'noise tolerance' was settled for each image to get an optimum detection of individual NPC's maxima according to each image. 3) A list of XY coordination (X for horizontal and Y for vertical coordination) for the maxima of all the NPCs detected was provided by the same tool, and round regions of interest (ROI) with a diameter of 7 pixels (≈ 200 nm) were chosen as the standard area of individual NPCs. The XY coordination pairs for each NPC on images were confirmed during the repetitive selection process, remaining noisy spots after previous steps were finally eliminated. 4) By combining the XY coordination and the ROI manager, all the single-NPC areas were extracted for CFP images, and a list of fluorescent signal intensities for CFP of each NPC was obtained. 5) The same ROI was applied for FRET (or YFP) images and a list of fluorescent signal intensities for FRET images was obtained. 6) Calculation of ratios as FRET signal over CFP signal for all NPC detected.

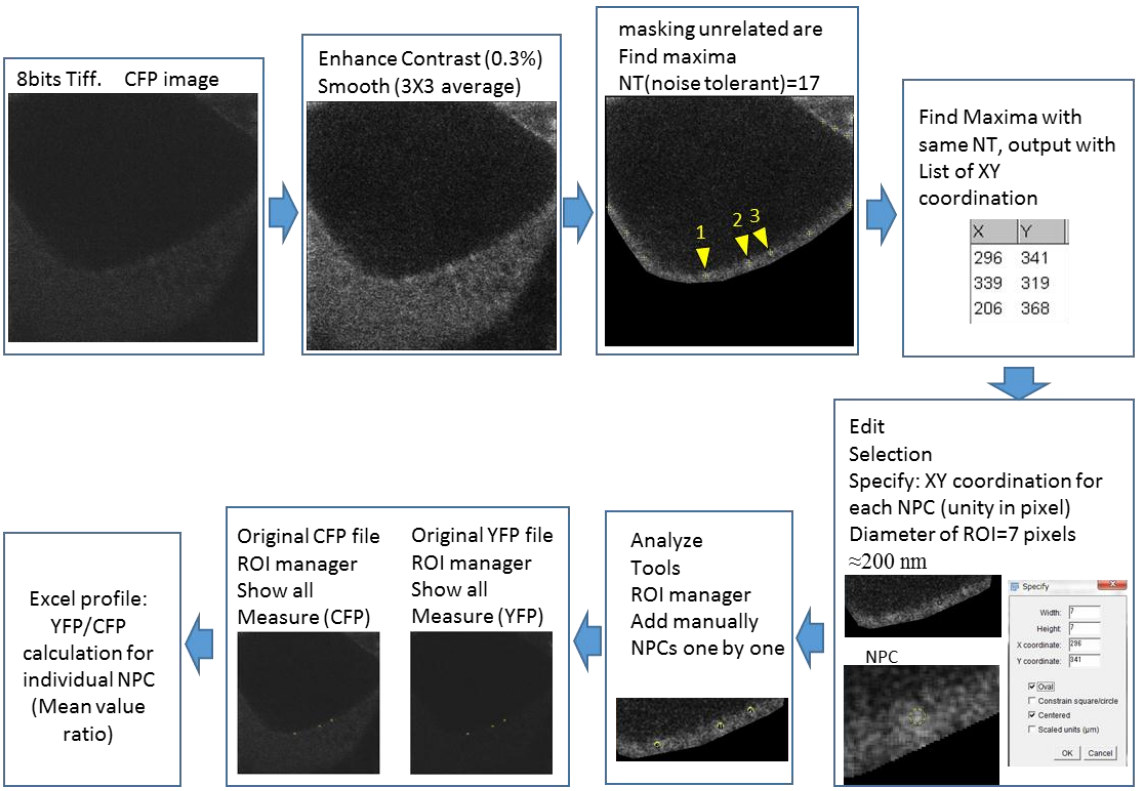

Figure 2-6 Analysis method for single-NPC-level crowding assays

Single-NPC-level analysis of molecular crowding for individual Nups, with ImageJ. Smooth and masking steps help to eliminate isolated noise signals and unrelated areas, respectively. The area corresponds to a single-NPC was limited by circle selection with a diameter of 7 pixels (≈ 200 nm). A list of detected circle areas was provided, fluorescent intensities in CFP and YFP (FRET) channels were recorded, and the final FRET ratios (YFP/CFP) were calculated for each NPC detected.

2.2.4 Evaluation of single-NPC identification method

The accuracy of the single-NPC detection was evaluated by comparative trials that overlaying the immunostaining signals on the GimRET fluorescent signals for individual NPCs. GimRET-Nup expressing HeLa cells on a coverslip were fixed and immunostained with the primary antibody of mAb414, an anti-FG Nups antibody that recognizes Nup62, Nup153, Nup214, and Nup358. A secondary antibody fused with Alexa 568 was used for observation. Same microscopic settings as single-NPC-level experiments were used for CFP and YFP channels. The excitation wavelength for the detection of immunostaining (Alexa 568) signal was 559 nm. In both CFP and mAb414 images, the fluorescent spots on the nuclear membrane, which correspond to individual NPCs, were distinguished as described in 2.2.3. An exemplary analysis from GimRET-Nup58 expressing cell is shown in Figure 2-7.

(A)

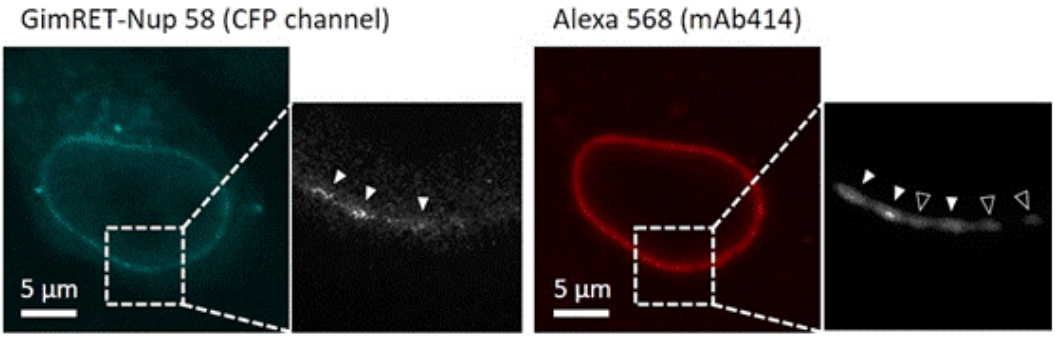

(B)

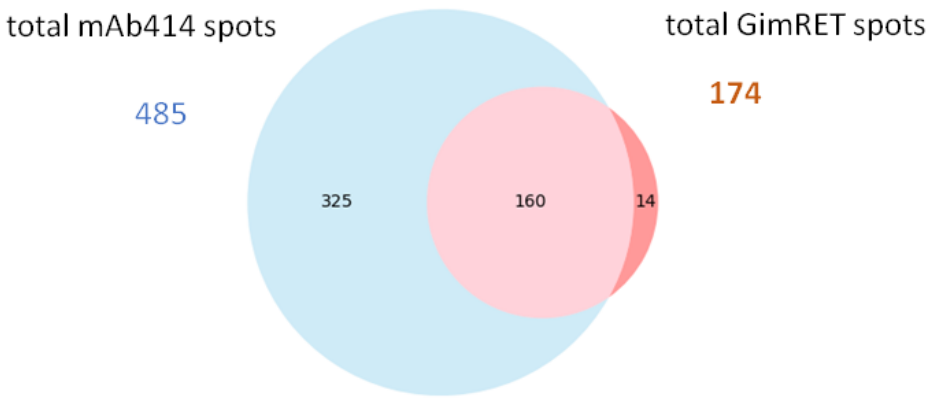

Figure 2-7 Colocalization analysis of GimRET and mAb414 spots

(A) GimRET-Nup58 and mAb414 images are shown. GimRET-positive and negative NPCs are indicated by white and black arrowheads, respectively, in zoomed images. Scale bars=5 μm. (B) Venn diagram for single-NPCs identification. Immunostaining of HeLa cells transfected by GimRET-Nup58. The number of individual NPCs identified by IgG-Alexa568 of anti-mAb414 antibody (sky blue, 485 spots) and number of NPCs identified by GimRET-Nup58 CFP (red, 174 spots) were shown. The number of NPCs identified by both methods was shown by overlap region (pink, 160 spots).

The total number of spots detected from the same set of samples was 174 for the GimRET signal and 485 for the mAb414 signal. Among the 174 GimRET spots, 160 of them were co-localized with mAb414 spots, which correspond to a 92.0% detection accuracy for the single-NPCs identification method.

2.2.5 Detection of disulfide bond formation in Nups

To confirm the deficiency in disulfide bonds formation of Nup62CS and Nup153CS mutants, nuclei lysate samples were collected as previously described (Yoshimura et al., 2013), with the presence of N-ethylmaleimide (NEM) to prevent oxidation during sample preparation, for HeLa cells expressing GimRET-Nup WT or CS mutants with or without 1 h H_2O_2 treatment. These samples were further treated with DTT (standard and reduced conditions) or without DTT (oxidative condition) during the sample preparation step for SDS-PAGE and western blot experiments. Anti-GFP (rabbit) antibody (MBL) was used for detection of GimRET tag, by recognition of consensus sequence between cyan variant (CFP) and GFP (Veening et al., 2004). Signal enhanced reagent Can Get Signal® (TOYOBO) was used for western blot signal detection.

2.3 Results

2.3.1 Subcellular localization of GimRET-Nups at the nuclear envelope was maintained in redox conditions

It was already reported that GimRET-fused Nups were localized correctly on the NE (Konishi et al., 2017). To assess the effect of redox treatments (DTT or H_2O_2) on subcellular localization of GimRET-Nups, cells treated with redox treatments were observed under the microscope, as shown in Figure 2-8.

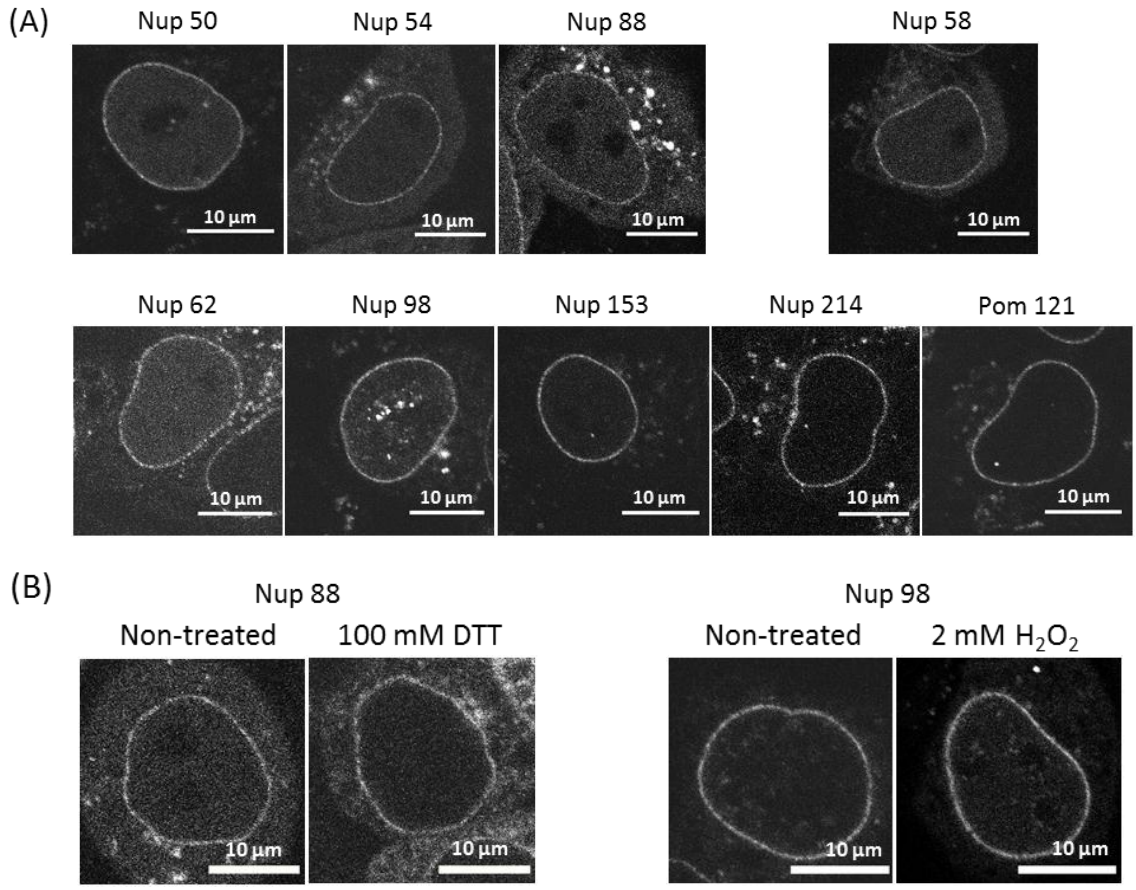

Figure 2-8 Fluorescent signal localization of GimRET-Nups tested in HeLa cells

(A) Digitonin-permeabilized HeLa cells expressing GimRET-Nups, fluorescent signals were detected at the NE. (B) Permeabilized HeLa cells after redox treatments, for reduced and oxidative treatment, the NE enriched fluorescent signals did not change.

The fluorescent signal enriched at NE was not affected during the permeabilization step. In addition, treatment of the permeabilized cells with redox reagents did not change the localization of GimRET-Nups, as shown in examples of GimRET-Nup88 and GimRET-Nup98 (Figure 2-8B). More than 15 cells were analyzed for each condition for all Nups tested; at least two independent experiments have been performed for the same GimRET-Nup expressing HeLa cells.

2.3.2 Nups responded differently for different redox conditions

Local molecular crowding states for each Nups were directly measured by analyzing FRET signals under different redox conditions. FRET ratios relative to the non-treated condition are shown in the graphs (Figure 2-9).

As shown in Figure 2-9A, Nup50, Nup54, and Nup88 showed a significant increase in the FRET ratio after DTT treatment, especially with 100 mM DTT; which means their local crowding states were decreased under reduced condition. In addition, the sensitivities for the reduced condition were clearly different for different Nups. Nup54 and 88 showed no obvious response under the 10 mM DTT condition, while Nup50 showed significant responses from 10 mM DTT. All of these three Nups showed no response to the oxidative environment (2 mM H_2O_2). Therefore, it is reasonable to see that a successive DTT treatment (100 mM) after 1 h incubation with H_2O_2 (recovery condition) leads to a similar level of crowding compare to the 100 mM DTT treatment alone.

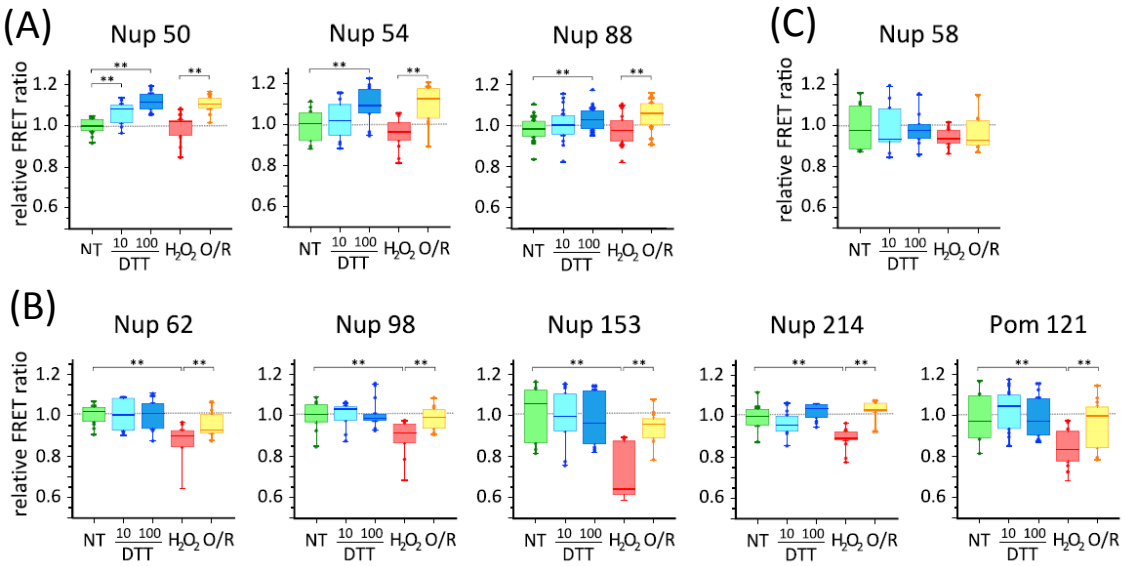

Figure 2-9 Effects of redox conditions on crowding states of HeLa cells expressing GimRET-Nups constructs (performed by Ryuji Watanabe)

Bulk analysis of relative FRET ratios of GimRET-Nups expressed in HeLa cells under standard condition (green), reduced conditions (10 and 100 mM DTT treatment, blue), oxidative condition (2 mM H_2O_2 treatment, red), and successive treatment of oxidative (2 mM H_2O_2) and reduced (100 mM DTT) conditions (O/R) for recovery assay (yellow) (*indicates $p<0.05$, **indicates $p<0.01$, by Welch's t-test). Nups tested were classified into three categories: DTT-sensitive Nups (Nup50, Nup54, Nup88), H_2O_2-sensitive Nups (Nup62, Nup98, Nup153, Nup214, Pom121), and insensitive Nup58, respectively.

On the other hand, Nup62, Nup98, Nup153, Nup214, and Pom121 showed significant responses against H_2O_2 treatment and no response to reduced conditions (Figure 2-9B). The degree of response among these Nups was more or less evident. A higher degree of fluctuation was observed for Nup153 and Pom121 compare to other Nups. This may be due to their spatial localizations (Nup153 on the nuclear basket and Pom121 is a transmembrane Nup), which are relatively remote from the direct contact area to the oxidative environment. The effect of oxidative stress for these H_2O_2-sensitive Nups was completely canceled by DTT treatment (100 mM DTT) in the recovery condition. Finally, there was one Nup, Nup58, which showed no response to any redox condition (Figure 2-9C).

Besides H_2O_2, another oxidative reagent diethyl maleate (DEM) was used to ensure the effect. Since the sulfhydryl group of glutathione (GSH) is alkylated by DEM, the function of GSH as an antioxidant is blocked by this reagent and ROS accumulate in cells (Kaur et al., 2006), which ultimately causes oxidative stress. Two representative GimRET-Nups, Nup62 and Nup153 were tested under this oxidative stress caused by DEM (Figure 2-10).

FRET ratios for both Nup62 and Nup153 showed a significant reduction by DEM treatments, which is consistent with H_2O_2 treatment. This indicates the H_2O_2-sensitive Nups are not exclusively reacted to H_2O_2; they also adapted their crowding states while facing an oxidative environment caused by another reagent.

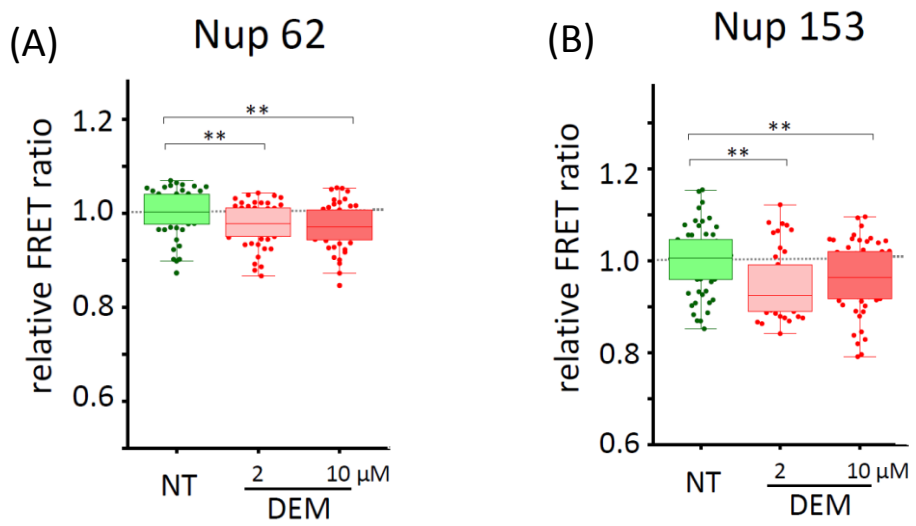

Figure 2-10 Effect of DEM induced oxidative stress on the crowding states of HeLa cells expressing H_2O_2-sensitive GimRET-Nups

(A) HeLa cells expressing GimRET-Nup62 were treated with 2 or 10 μM DEM, followed by the FRET measurement. The relative FRET ratio was statistically analyzed (**indicates $p<0.01$ tested by Welch's t-test). (B) The result for GimRET-Nup153.

When compare the molecular crowding response of Nups while facing oxidative stresses (Figure 2-9 and Figure 2-10), DEM did not induce a dramatic effect as H_2O_2, probably due to the property of reagents. As a pro-oxidant reagent, H_2O_2 has broader impacts on cells compare to DEM (Rahal et al., 2014), whereas the DEM is a glutathione-depleting reagent for mild oxidative stress (Castillo et al., 2002). There are also the interactive effects between these two substances (Makino et al., 1994); it seems that partial H_2O_2 induced reactions could be diminished by treatment with diethyl maleate (Sasaki et al., 1998).

2.3.3 Characteristic redox responses were also observed at single-NPC-level assays

To further confirm that these crowding state changes for individual Nup are actually occurred at NPC, FRET measurement was performed at a single-NPC-level for Nup50 (DTT-sensitive), Nup62 (H_2O_2-sensitive), and Nup58 (insensitive).

There were 114, 73, and 68 single-NPCs analyzed for Nup50, Nup58, and Nup62, respectively. More than 20 images issued from at least two independent experiments for each condition were used for the analysis. As shown in Figure 2-11, the single-NPC-level crowding assays showed consistent results compare to NE level bulk crowding results (Figure 2-9).

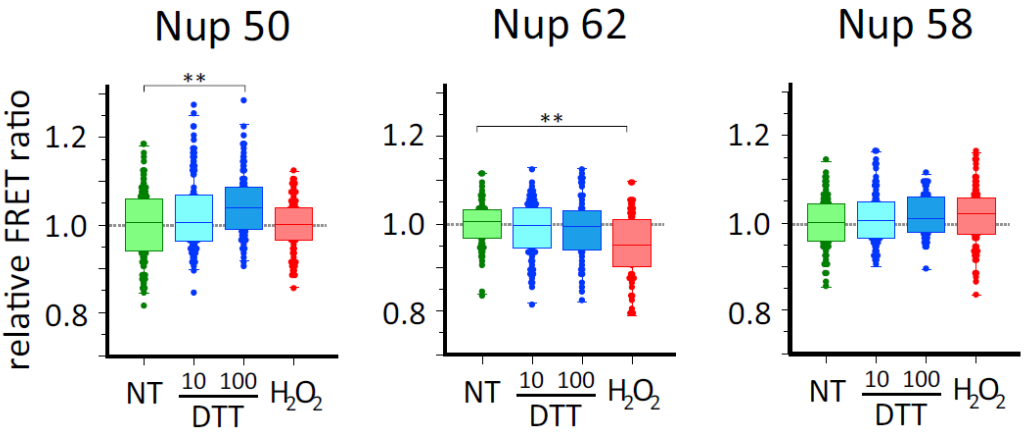

Figure 2-11 Single-NPC-level analysis of relative FRET ratios for HeLa cells expressing GimRET-Nups

Crowding states of HeLa cells under standard condition (green), reduced conditions (blue), and oxidative condition (red) (**indicates $p<0.01$, by Welch's t-test) were analyzed at the single-NPC-level.

A smaller degree of response between correlated conditions was observed for this single-NPC-level assay. This is due to the limitation in the single-NPC selection method. As shown below in Figure 2-12, there is a correlative tendency for the fluorescent intensity of CFP and FRET ratio. Even though I have chosen the same detection range for all parallel redox conditions in all experiments, compare to bulk assay under the same conditions, the single-NPC selection was limited to a narrower range of CFP intensity for several reasons. First, while selecting individual NPCs, highly zoomed images were acquired, with a signal-to-noise ratio optimized. This step has limited already the CFP signal to a certain range. Second, the detection using noise tolerance tool in ImageJ also preferentially choose NPCs with higher CFP signal, thus more crowded NPCs were chosen for further ratio analysis.

The results of the crowding assay suggested differential roles of Nups for environmental sensing: some are devoted to responding to oxidative conditions, while others are specialized to sense the reduced environments.

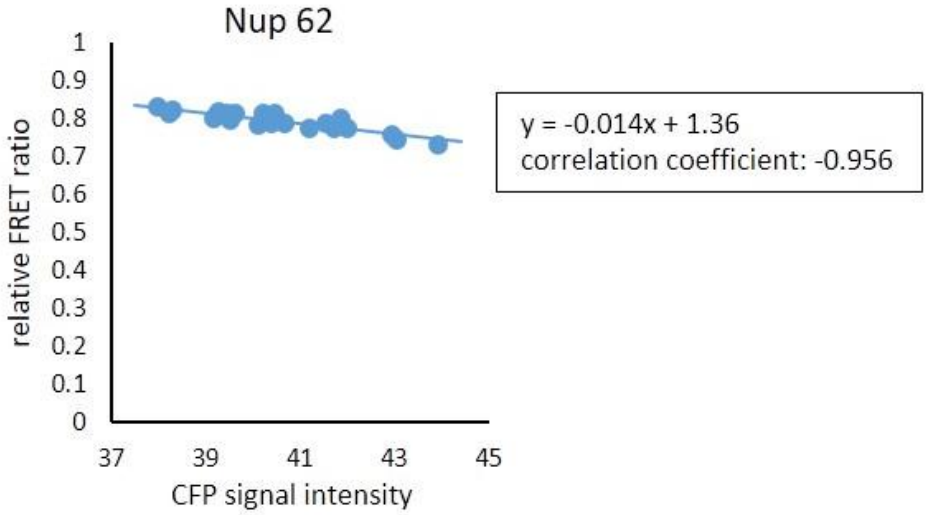

Figure 2-12 Correlations between GimRET-Nup62 expression level and the FRET ratio Plot graph of FRET ratio against CFP signal intensity, there is a negative correlation between FRET ratio and CFP intensity with a coefficient of -0.956.

2.3.4 Multiple mutations on cysteine residues abolished nuclear envelope localization of several Nups

A suppressed nuclear transport under oxidative stress was observed in a previous study of my laboratory (Yoshimura et al., 2013), in parallel with the formation of intermolecular disulfide bonds among Nups. Thus, multiple mutations were introduced to cysteine residues to investigate relationships between this formation of disulfide bonds and crowding states in the NPCs. As shown in Figure 2-13, four plasmid constructs of GimRET-fused Nups with CS mutants were prepared.

For the rat Nup62 that I have performed the experiments with, all those two cysteine residues on C-terminal have been replaced by serine residues (Figure 2-13, human Nup62 with an extra cysteine in IDR region was shown, in black color). Similarly, for Nup98, all three cysteines were substituted for serines. For Nup153 and Nup214, since they are large Nups with many cysteines distributed throughout the proteins, only the cysteines enriched regions were chosen for serine replacements. 21 out of total 28 cysteines were substituted to serines for Nup153; 8 out of 13 cysteines were substituted to serine for Nup214.

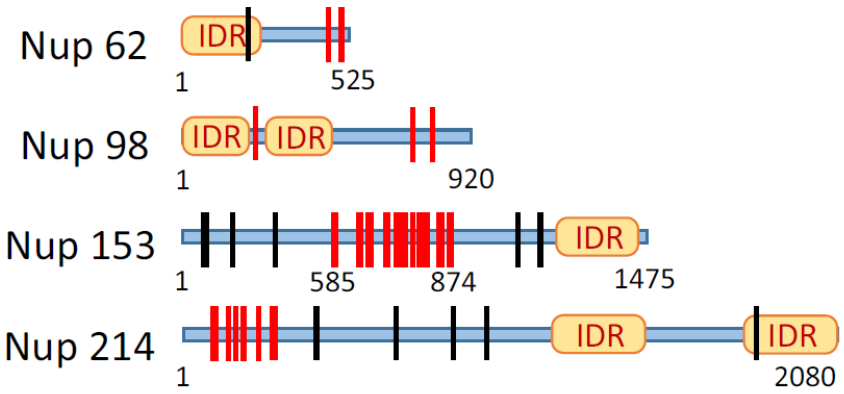

Figure 2-13 Summary of CS mutants for GimRET-fused Nups

Cysteine residues are indicated with vertical lines, substituted cysteine residues (to serine residues) are indicated with red color. IDRs are marked with yellow box (es) for each Nup. Molecular details for each Nup were collected from Uniprot database with accession numbers: Nup62 (P37198-1), Nup98 (P52948-1), Nup153 (P49790-1) and Nup214 (P35658-1).

As shown in Figure 2-14, several CS mutants showed distinct localization patterns compared to the WT (Figure 2-8). For Nup62 and Nup153, the CS mutants showed similar localization to WT constructs, which means an intensive localization of fluorescence signal at NE. In contrast, GimRET-Nup98CS and GimRET-214CS abolished their enriched localization at NE. The signals were detected in the entire nucleoplasm and cytoplasm, showing an essential role of cysteine residues in targeting these Nups to the NE.

To describe quantitatively this loss of localization effect, further analysis with plotline across the entire nucleus region for CFP image was performed. As shown in Figure 2-15, the enriched fluorescent signal at NE level, which corresponds to a peak or peak region across the nucleus could be observed in WT expressed cells, for both GimRET-Nup98 (Figure 2-15A) and GimRET-Nup214 (Figure 2-15B) cases. However, for cells expressing CS mutants, even partially mutated construct such as GimRET-Nup214CS, the enrichment of fluorescent signals on NE has disappeared.

From this result, the importance of cysteine residues for correct targeting of nucleoporins on NE was detected unexpectedly.

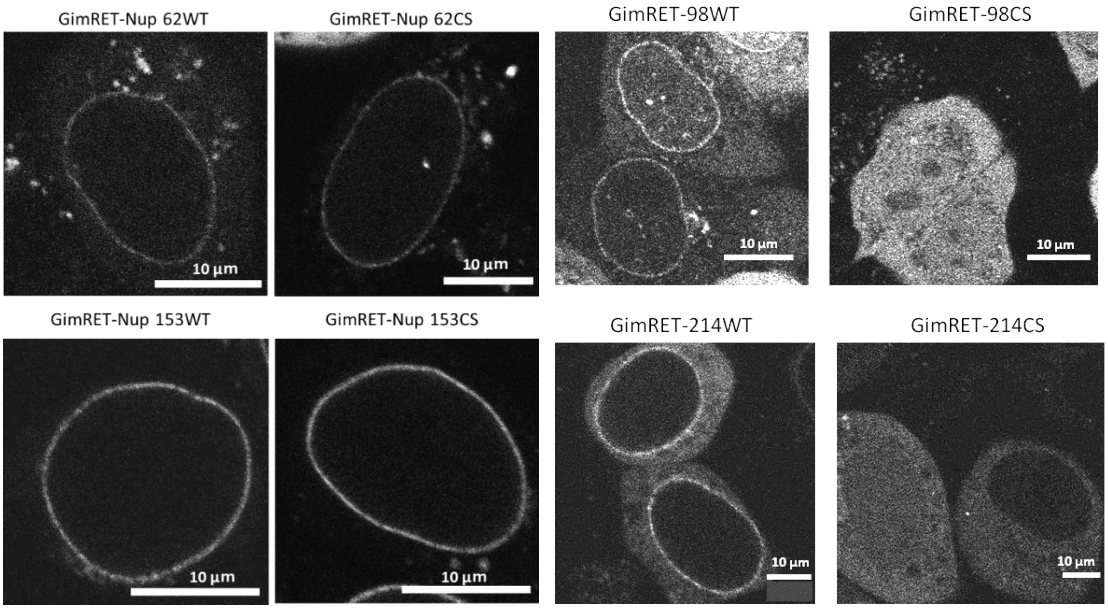

Figure 2-14 Localization of fluorescence signal in HeLa cells expressing GimRET-Nups WT vs. CS mutants

A similar fluorescent signal was observed, in HeLa cells expressing either WT or CS construct of GimRET-Nup62 and GimRET-Nup153. Localization of GimRET-Nups on the NE area was lost in CS mutant expressed HeLa cells, for both GimRET-Nup98 and Nup214 cases.

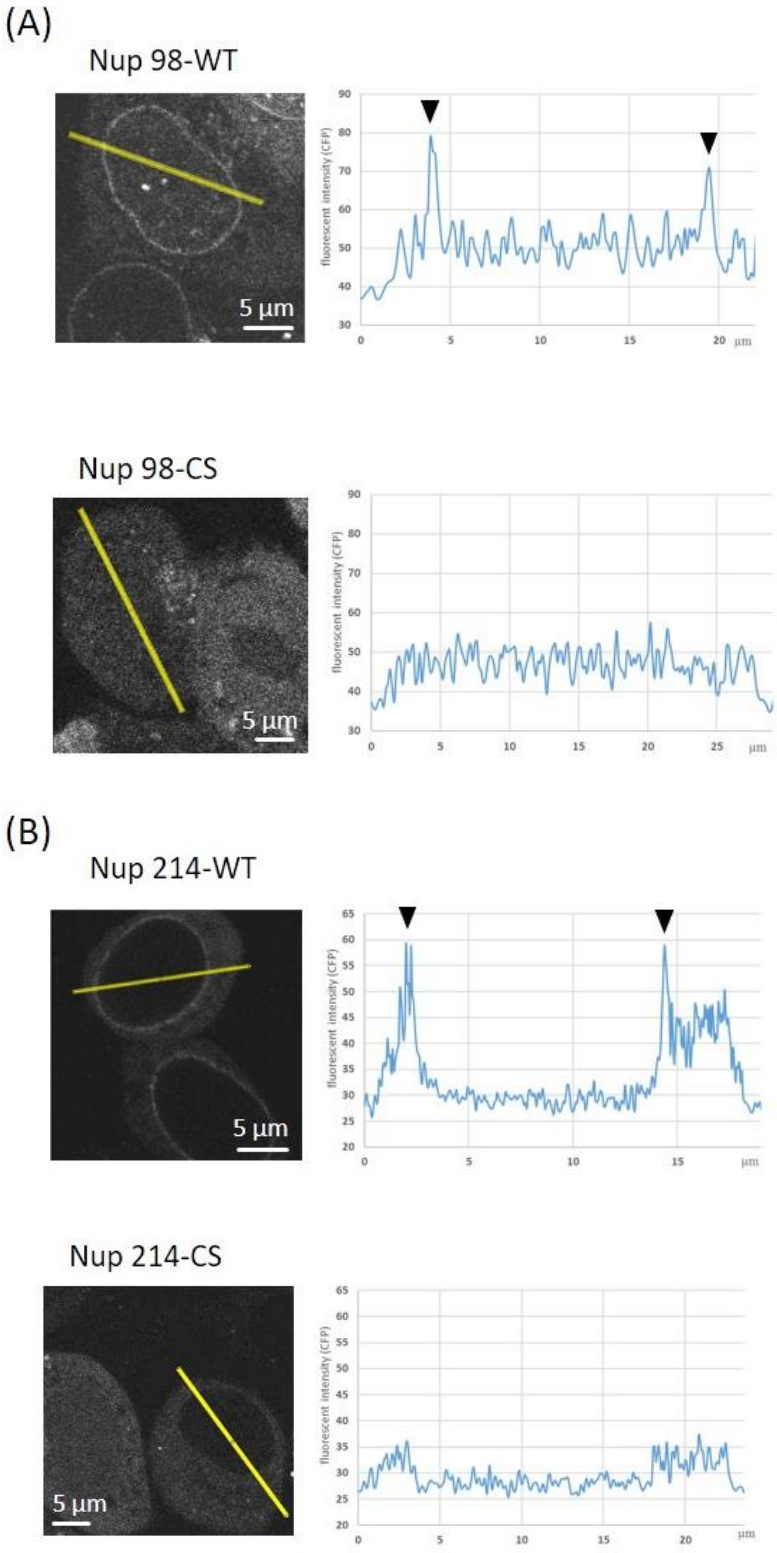

Figure 2-15 Targeting loss at NE for GimRET-Nup98CS and GimRET-Nup214CS

HeLa cells transfected with (A) GimRET-Nup98WT/CS and (B) GimRET-Nup214WT/CS are observed 30 h after transfection. The plotlines across the nucleus are drawn and analyzed with CFP images using ImageJ software; fluorescent intensities (y-axis) along the plotline (x-axis) are shown with the graph for each image.

2.3.5 Overexpression of CS mutant Nups abolished crowding control in response to oxidative stress

Single-NPC-level crowding analyses were performed for HeLa cells expressing GimRET-Nup62CS and GimRET-Nup153CS. As shown in Figure 2-16, the significant decrease of FRET ratio observed in WT was completely abolished in CS mutants.

For these single-NPC-level crowding assays, an average of 45 NPCs and 155 NPCs were analyzed under each condition for Nup62 and Nup153, respectively. This result suggested a direct involvement of cysteine residues in regulating molecular crowding states of Nups.

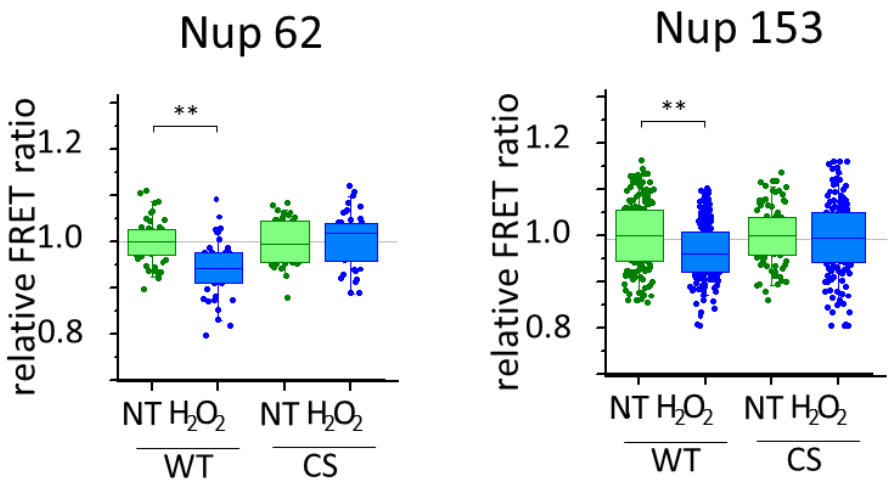

Figure 2-16 Crowding assays for WT and CS mutants of Nup62 and Nup153

Relative FRET ratio between WT and CS mutant of Nup62 and Nup153, under Non-treated condition (NT) and oxidative condition (H_2O_2) with 2 mM H_2O_2 (**indicate $p<0.01$, by Welch's test).

2.3.6 Formation of disulfide bonds was suppressed for Nup62CS and Nup153CS under oxidative stress

Western blot analyses were performed to detect the formation of disulfide bonds for WT and CS mutants. As described previously (Yoshimura et al., 2013), DTT-free SDS-PAGE was performed to separate disulfide bond-forming Nups as slow-migrating shift-bands.

Since GimRET (~58 kDa) tags were fused to Nup62 (~62 kDa) and Nup153 (~153 kDa), the theoretical molecular size for GimRET-Nup62 and GimRET-Nup153 are around 120 kDa and 210 kDa, respectively.

As shown in Figure 2-17, several shift-bands were observed for GimRET-Nup62WT and GimRET-Nup153 WT (red arrowheads). For Nup153 WT, the shift-bands were distinguishable for both standard (H_2O_2-, DTT-) condition and oxidative stressed condition (H_2O_2+, DTT-); whereas for Nup62WT, the shift-band was much enhanced for oxidative stressed sample (H_2O_2+, DTT-). These shift-bands were not observed after DTT treatment (H_2O_2+, DTT+).

For GimRET-Nup62CS and GimRET-Nup153CS, no visible shift-bands were observed, even under oxidative stress condition (H_2O_2+, DTT-).

This western blot result revealed that multiple cysteines are involved in the formation of intermolecular disulfide bonds under oxidative stress.

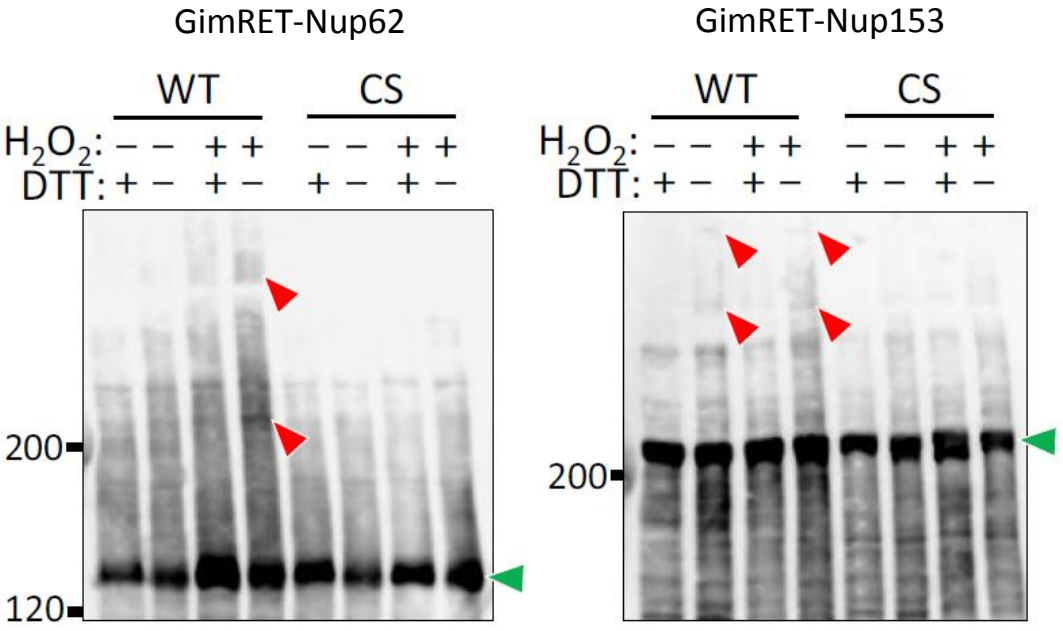

Figure 2-17 Shift-bands detection by western blot

Disulfide bonds related to shift-bands detection for GimRET-Nup62WT/CS (left panel) and GimRET-Nup153WT/CS (right panel) expressed HeLa cell nuclei lysates. Conditions with (+) or without (-) H_2O_2 and DTT treatments are summarized on the top of the membrane. Target protein positions are marked with green arrowheads; shift-bands are indicated with red arrowheads.

Chapter 3 Kinetic analysis of the cargos passing through the nuclear pore

3.1 Introduction

To investigate the molecular dynamics of nuclear transport under redox conditions, single-molecule fluorescence microscopy was applied. The experiments were performed by a former member of my research group, Ryuji Watanabe. I found that the dynamics of nuclear transport were drastically affected by redox conditions.

As shown in Figure 3-1, for standard condition (10 mM DTT), 421 events in 89 NPCs were observed. Among them, 68.2 % were detected within a single frame (≤ 15 msec); the incidence of the events persisted more than 150 msec was 23.5%. The number of detectable events at each NPC in the 60-second observation was ranged from 1 to 11.

The same single-molecule fluorescence measurement assays were performed under redox conditions using cells pre-incubated with 2 mM H_2O_2 for 1 hour or treated with 100 mM DTT. In total, 250 events in 64 NPCs and 585 events in 67 NPCs were detected for oxidative and reduced conditions, respectively. There was a significantly reduced incidence of the fast event under oxidative condition (56.0%), compared to reduced conditions (65.7%), which share a similar pattern with the standard condition (68.2%). The ratio was significantly higher in oxidative condition (35.6%) for events that persisted more than 150 msec, whereas that in reduced condition (19.5%) was similar to the standard condition (23.5%).

Under the reduced condition, the number of events for all NPCs ranged from 3 to 19, which was significantly higher than that under standard condition (1 to 11); whereas that under oxidative condition (2 to 9) was similar to the standard condition. Generally, under the reduced condition, the average number of nuclear transport is 8.7±3.7, which is significantly higher than standard condition (4.7±2.1) and oxidative condition (3.9±1.8).

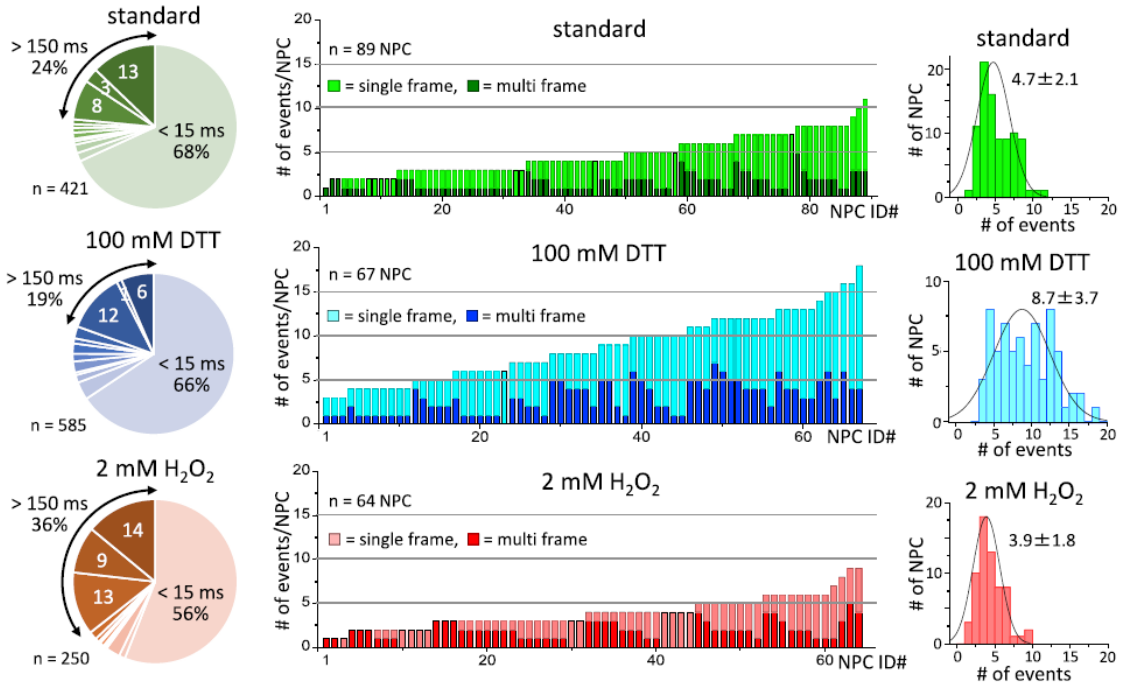

Figure 3-1 Transport patterns for NPCs under redox conditions

(Performed by Ryuji Watanabe)

Statistical results for single molecular transport assay. Transport patterns of fluorescent TMR-Impβ passing through NE were summarized, when permeabilized HeLa cells were exposed to standard condition (10 mM DTT, n = 89 NPCs, green), reduced condition (100 mM DTT, n = 67 NPCs, blue), and oxidative condition (2 mM H_2O_2, n = 64 NPCs, red). Percentages of fast single frame transport (≤ 15 ms) and long-last multiple frame transport (> 150 ms) were shown in the left panel. Detailed transport patterns per NPC in 60 s were shown in the middle panel, with ID of NPC on the x-axis and type of event on the y-axis (single frame even in the light color, and multi-frame event in the dark color). Histograms of the event frequency for NPCs under redox conditions were shown in the right panel, with the Gaussian distribution fitting.

In conclusion, it seems that the oxidative stress alters the NPC's property to hold transport molecules longer in the pore and suppress the transport efficiency, while the reduced environment acts on the NPCs to be more accessible for the transport molecules.

Based on these findings, I tried to elucidate how local molecular crowding states of Nups affect the nuclear permeability by FRAP experiments.

3.2 Materials and methods

3.2.1 DNA constructs

The WT and CS mutant fragments of Nup62 and Nup153 were cut from the GimRET expressing plasmid by double digestion using restriction enzyme pairs of BamHI+KpnI and BglII+SalI for Nup62 and Nup153, respectively. Then these fragments were inserted into the pEGFP-C1 vector, to get pEGF-Nup62 and pEGFP-Nup153 for WT and CS mutant constructs. The Impβ fragment was prepared by PCR with the previously constructed plasmid of pEGFP-Impβ (Kumeta et al., 2018), with the restriction site of SalI (indicated in italic letters) added to both ends of the fragment. The forward primer 5' acc*gtcgac*atggagctcataaccatcc 3' and the reverse primer 5' ggt*gtcgac*ctaagcctggttcttcagt 3' were used. After PCR amplification, the Impβ fragment was inserted into the pmCherry-C1 vector digested by the same restriction enzyme SalI.

3.2.2 Evaluation of endogenous and exogenous Nups in HeLa cells

To evaluate the relative amount of endogenous and exogenous Nups, HeLa cell lysate samples for non-transfected (NT) cells and EGFP-Nups (both WT and CS mutant) expressing cells were prepared with 5% SDS and 1 h incubation at room temperature.

The monoclonal mAb414 antibody was used for detection and quantification of bands that correspond to endogenous and exogenous Nups in western blot.

3.2.3 FRAP experiment

Plasmid DNA of pEGFP-Nup and pmCherry-Impβ were co-transfected into HeLa cells on the next day of seeding (cellular confluency 60%~70%), using Effectene (QIAGEN). Three concentrations of H_2O_2 for oxidative conditions (0, 2, and 10 mM) were tested in FRAP assays. To keep consistent treatment for every condition, a workflow for dish preparation was carried out, as shown in Figure 3-2.

In the case of Nup62, 24 h after transfection (30 h for Nup153), a standard medium without phenol red (DMEM + 10% FBS), with or without H_2O_2 was supplied to the dish and incubated for 50 min at 37℃ with 5% CO_2. Then the dish was mounted to the microscope stage with a heater at 37℃ to settle down for 10 min before the start of the FRAP experiment.

A preliminary experiment (data not shown) proved that cells started to exhibit an abnormal morphology around 120 min incubation with the highest concentration of H_2O_2 (2 mM), which was caused by the accumulated oxidative damage in cells. Therefore, the FRAP observation for each dish was limited to 30 min after 1 h H_2O_2 treatment at 37℃ (within 90 min of H_2O_2 incubation). A final concentration of 10 mM HEPES was added to the observation medium, which stabilizes the pH in the culture medium during the 30 min observation period.

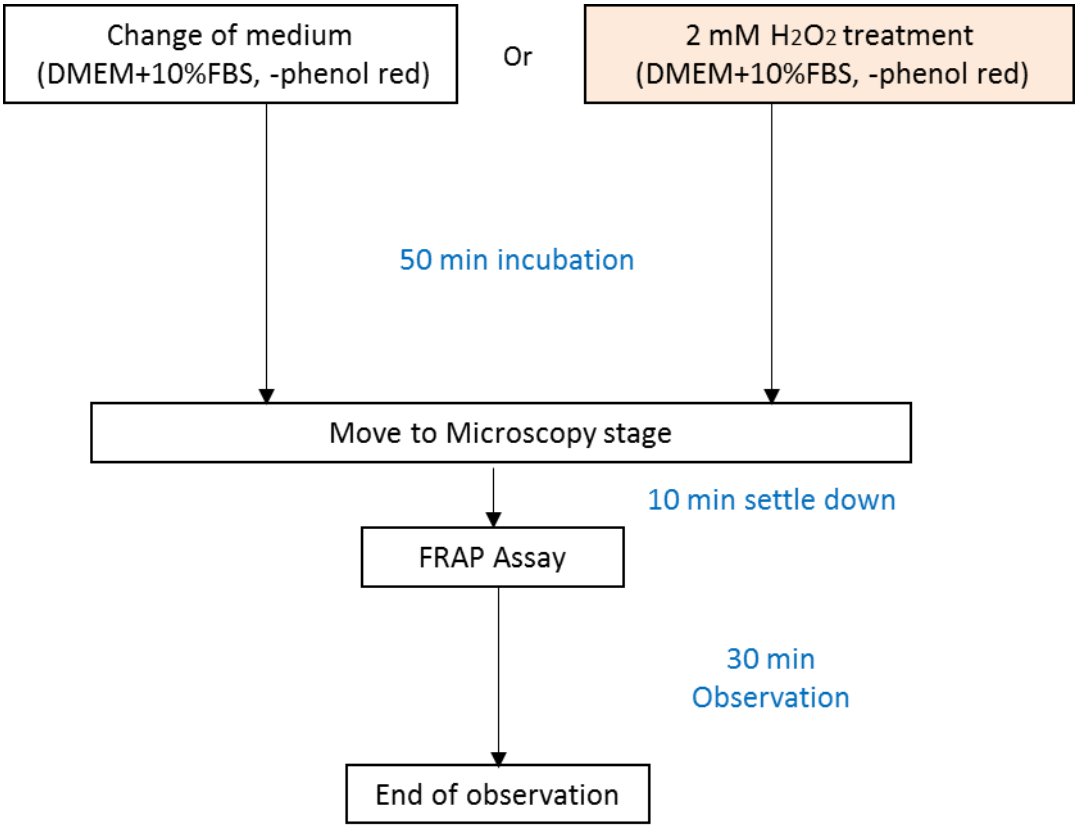

Figure 3-2 Workflow for HeLa cells preparation

Either for non-treated condition and oxidative condition (2 mM H_2O_2), cell culture medium has been changed 1 h before observation, for HeLa cells co-expressing EGFP-Nups WT/CS and mCherry-Impβ in the glass bottom dish. 10 min before observation, the dish was placed to the stage of microscopy for settling down. A total of 30 min of FRAP observation was performed for each dish.

For the time-lapse imaging of FRAP, photobleaching, observation, and image acquisition were performed by confocal laser scanning microscopy (Olympus FV 1200). Three images were acquired before bleaching; the post-bleaching images were acquired with 1% laser intensity to reduce the bleaching during imaging. The entire nucleus was photo-bleached at maximum output for 10 s for the mCherry-Impβ (excitation wavelength at 559 nm). Images were captured every 5 s for 150 s. Fluorescence recovery of the nucleus was obtained and expressed as the fluorescence intensity relative to maximum recovered intensity. Curve fitting and other kinetic analyses of obtained data were performed by Origin software (Light Stone), with the following fitting functions:

$$y = \exp(-x \times k_{out}) \times Y_0 + (k_{in}/k_{out}) \times (1-\exp(-x \times k_{out}))$$

3.2.4 Knockdown of endogenous Nup153 by siRNA

Endogenous Nup153 in HeLa cells was knocked down by siRNAs that targeting to the 3'-UTR region of human Nup153: ggguuaucugaagucagaucugccu for sense, aggcagaucugacuucagauaaccc for antisense sequences. For the rescue condition, siRNA transfection was performed with Lipofectamine 3000 (Thermo) 48 h before the assay, followed by the transfection of pEGFP-Nup153WT/CS and pmCherry-Impβ by Effectene (QIAGEN) 30 h before the assay. Cell lysates of Nup153 knock-down sample and Nup153 knock-down with overexpressing EGFP-Nup153 (WT or CS) samples were collected, as previously described, for western blot quantification.

3.2.5 Co-immunoprecipitation assay for Ran-Nup153

HeLa cells transfected with pEGFP-Nup153 WT and CS by Effectene (QIAGEN), with or without H_2O_2 treatment, were collected 30 h after transfection. The cell lysate was

prepared by suspending cells in Lysis buffer (20 mM HEPES (pH 7.4), 120 mM NaCl, 5 mM $MgCl_2$, 2 mM EGTA, 1 mM DTT, and protease inhibitor cocktail (Nacalai)). A mild sonication (10% duty cycle, output 1 for 20-30 s) was carried out after suspension, and then 1% Triton was added and incubated for 20 min on ice. After a centrifuge at 2000 × g for 20 min at 4℃, the cell lysate (supernatant) was collected and incubated with equilibrated GFP beads (Rat IgG2a, monoclonal (GF090R), CC, Agarose Conjugate beads, Nacalai) for overnight incubation at 4℃. After three times of wash with Lysis buffer, the GFP beads were subjected to SDS-PAGE and proceeded for immunoblotting against GFP (MBL) and Ran (BD).

3.3 Results

3.3.1 Overexpression of Nups containing multiple CS mutations did not alter the nuclear envelope localization of Nups and Impβ

As shown in Figure 3-3, the co-expression of EGFP-Nup and mCherry-Impβ in HeLa cells did not interrupt their native localization. The EGFP-Nups signal was enriched on the NE, similar to the case of GimRET-Nups expressed HeLa cells (Figure 2-8). The mCherry-Impβ signal was found in both the nucleus and cytoplasm, with an enriched signal on the NE, similar to the case of EGFP-Impβ expressed in HeLa cells (Kumeta et al., 2018). In addition, there was no big difference for distributions of Nups and Impβ in co-transfected HeLa cells, between WT and CS mutant cases.

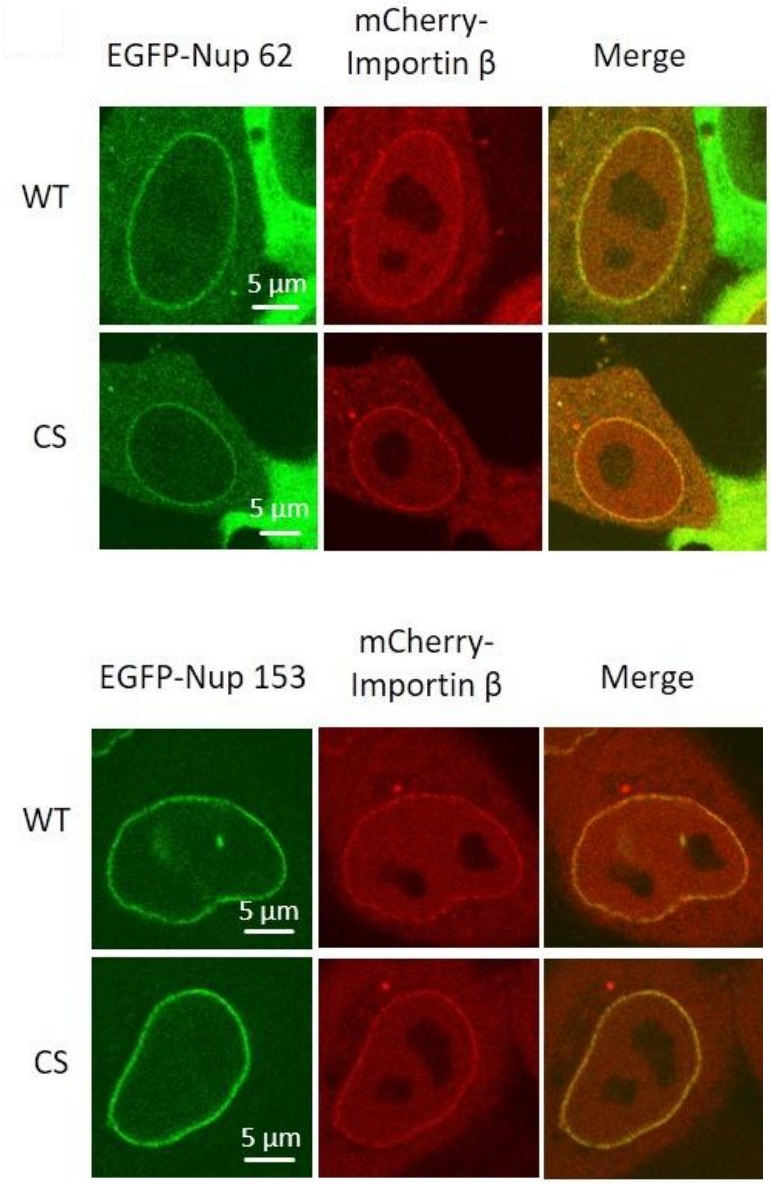

Figure 3-3 Co-expression of EGFP-Nup and mCherry-Impβ in HeLa cells

Images of HeLa cells co-expressed EGFP-Nup62WT or CS with mCherry-Impβ are shown on the upper panel; images for the Nup153 set are shown on the lower panel. No significant difference between WT and CS expressed cells for the distribution of fluorescent signals.

3.3.2 Relative amount of endogenous and exogenous Nup62 and Nup153 for HeLa cells coexpressing EGFP-Nups and mCherry-Impβ

The ratio between endogenous and exogenous Nups was quantified by western blot analysis using mAb414 (recognize Nup62, Nup153, Nup214 and Nup358). As shown in Figure 3-4, by comparing with the non-transfected (NT) sample lane, the bands corresponding to exogenous Nups were identified.

The band intensity was quantified with ImageJ software. The ratio of exogenous Nups to endogenous Nups were 1.39 and 1.48 for WT and CS Nup62, and 1.35 and 1.05 for WT and CS Nup153, respectively.

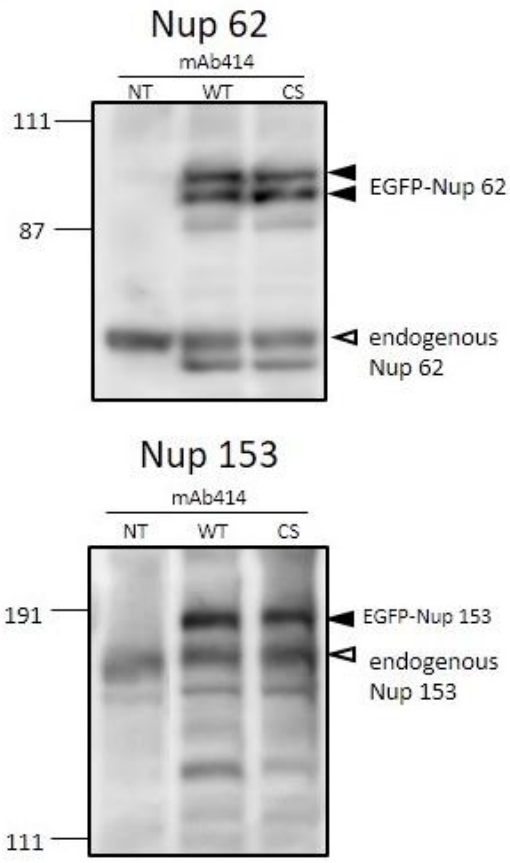

Figure 3-4 Western blot quantification of exogenous and endogenous Nups

Quantification of the exogenous Nup amounts to the endogenous molecules by the western blot. Nuclear lysates were prepared from HeLa cells non-transfected (NT), transfected with WT Nups (WT), and CS Nups (CS) as described previously (Yoshimura et al., 2013). Western blot was performed using monoclonal antibody mAb414 which recognizes 4 FG-Nups (Nup62, 153, 214, 358).

3.3.3 HeLa cells expressing Nup62CS or Nup153CS failed to restrain the transport kinetics of Impβ under oxidative condition

The effect of overexpressing CS mutant Nups on nuclear transport of cargo molecule was investigated by the FRAP analysis; kinetics in cells expressing WT Nups were considered as reference. mCherry-Impβ was co-expressed with WT or CS mutant Nups, and its transport kinetics was measured by bleaching the entire nucleoplasmic region. Captured images of the time-lapse imagining were shown in Figure 3-5.

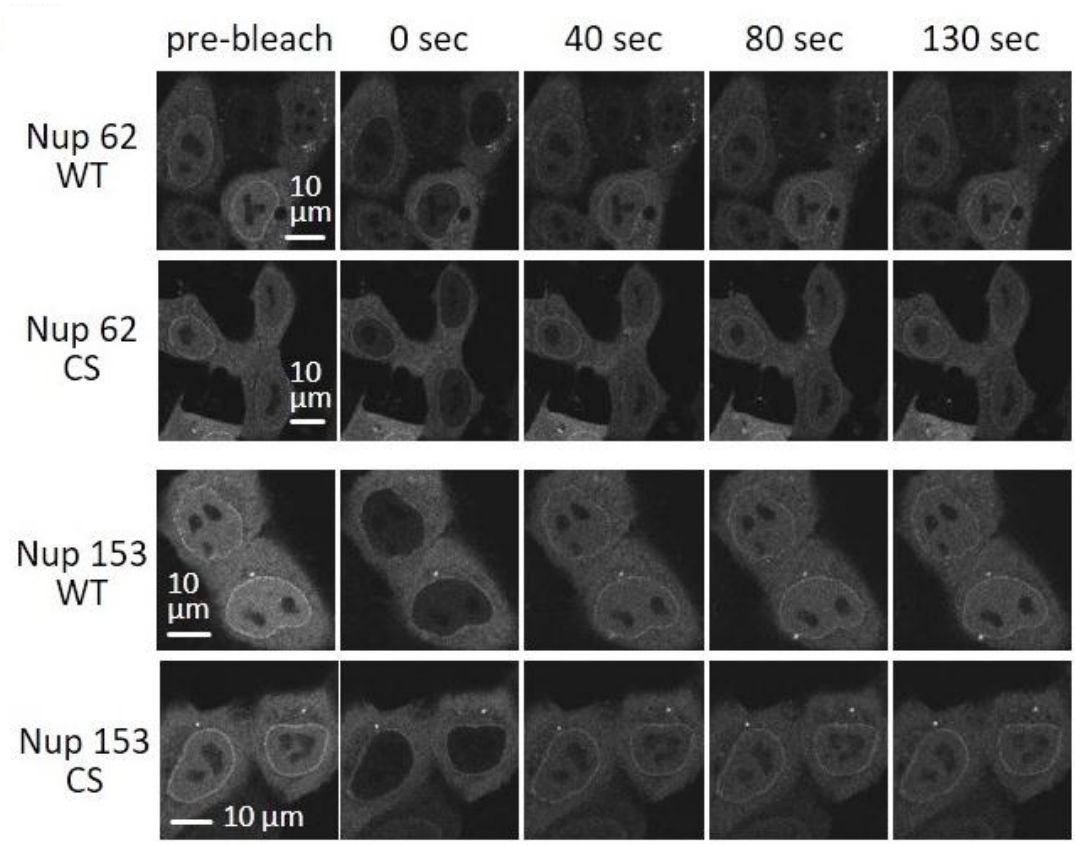

Figure 3-5 Time-lapse images for FRAP experiment

HeLa cells expressing EGFP-fused Nup and mCherry-fused Impβ were subjected to FRAP analysis. Captured images for the mCherry channel at the indicated time after bleaching are shown.

For both Nup62 and Nup153, three independent FRAP experiments were performed. After statistical analysis and curve fitting process, import rates of Impβ (k_{in}) in each condition were obtained and summarized in Figure 3-6.

Under 2 mM H_2O_2-treated condition, HeLa cells overexpressed with CS mutant Nups showed higher k_{in} compare to those overexpressed with WT Nups. HeLa cells started to sense the oxidative stress with a quite low concentration of H_2O_2 (0.2 mM) in both WT and CS mutant expressed conditions. At this point, fluctuant transport kinetics among cells for both types was detected. Compare to Nup62, Nup153 expressing cells showed a bigger fluctuation at 0.2 mM H_2O_2, maybe due to the remote spatial localization of Nup153 (nuclear basket). With an increase of H_2O_2 concentration (1 mM), severe suppression of nuclear transport was observed, both in WT and CS mutant expressing cells. Until this point, the molecular kinetics of Impβ were similar in HeLa cells expressing WT or CS mutant of Nups. It was only with an effective concentration of H_2O_2 (2 mM), the CS mutant expressing cells showed higher transport kinetics compare to cells expressing WT.

Therefore, in Nups-CS mutant expressing cells (both Nup62 and Nup153), not only the adaptive response of local crowding was deprived but also higher transport kinetics was observed under significant oxidative stress, compared to Nups WT expressing cells. This result suggested that there were concurrent events of adaptive crowding response of Nups and a nuclear transport related effect that depends partially on Nups while facing oxidative stress.

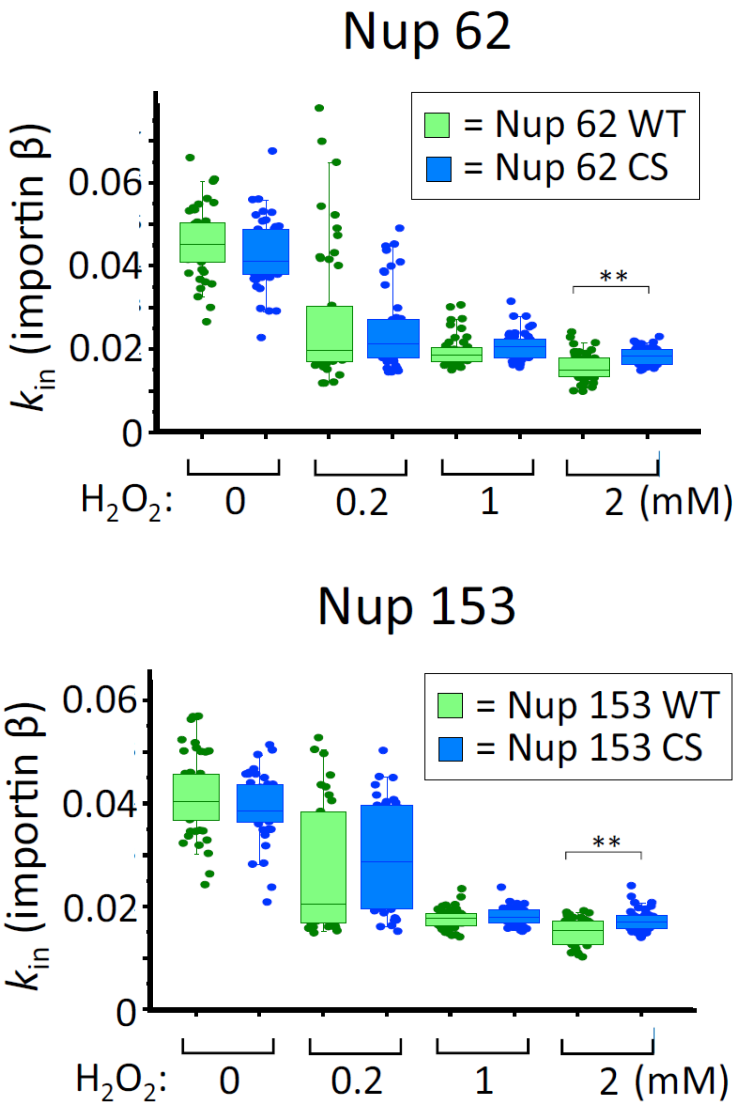

Figure 3-6 Statistical results for FRAP experiment

Statistical analysis for FRAP recovery rate of nucleoplasmic mCherry-fused Impβ observed in HeLa cells expressing WT (green) and CS mutants (bleu) of Nup62 and Nup153, respectively. The averaged k_{in} for measurements under non-treated conditions (0 mM) and different concentrations of H_2O_2 (0.2 mM, 1 mM, and 2 mM) are presented (**indicates $p<0.01$, by Welch's t-test).

The FRAP experiment uncovered the functional importance of cysteine residues in Nups. Combined with previous findings, these cysteine residues participate in the adaptive structural response under oxidative stress. Replacement of cysteine residues to serine residues, either total substitutions (Nup62CS) or partial mutations (Nup153CS), leads to more accessible NPCs under oxidative stress, which reflects a partial loss of control at NPCs. This indicates the crowding state of individual Nups has a direct effect on nuclear transport; the ability to alternating crowding states also contribute to the general regulatory mechanism under oxidative stress, and cysteine residues play important roles in both cases.

3.3.4 Transport kinetics of mCherry-Impβ in HeLa cells with endogenous Nup153 knocked down under oxidative condition

To highlight the effect of exogenous EGFP-Nups (WT or CS mutants) in FRAP assay, I performed a FRAP assay with endogenous Nup153 knocked down HeLa cells, which co-expressing exogenous EGFP-Nup153 (WT or CS) and mCherry-Impβ transiently.

Using siRNA against its 3'UTR, HeLa cells transfected with siRNAs showed a 69% and 84% decrease of endogenous Nup153 for 24 h and 48 h effects, respectively (Figure 3-7A). For HeLa cells with endogenous Nup153 knocked down and simultaneously expressing exogenous EGFP-Nup153WT/CS with mCherry-Impβ, about 75% endogenous Nup153 was depleted after 48 h; the ratios of exogenous EGFP-Nup153 were 0.82 and 0.90 for WT to CS, respectively, for HeLa cells 30 h after DNA transfection (Figure 3-7B).

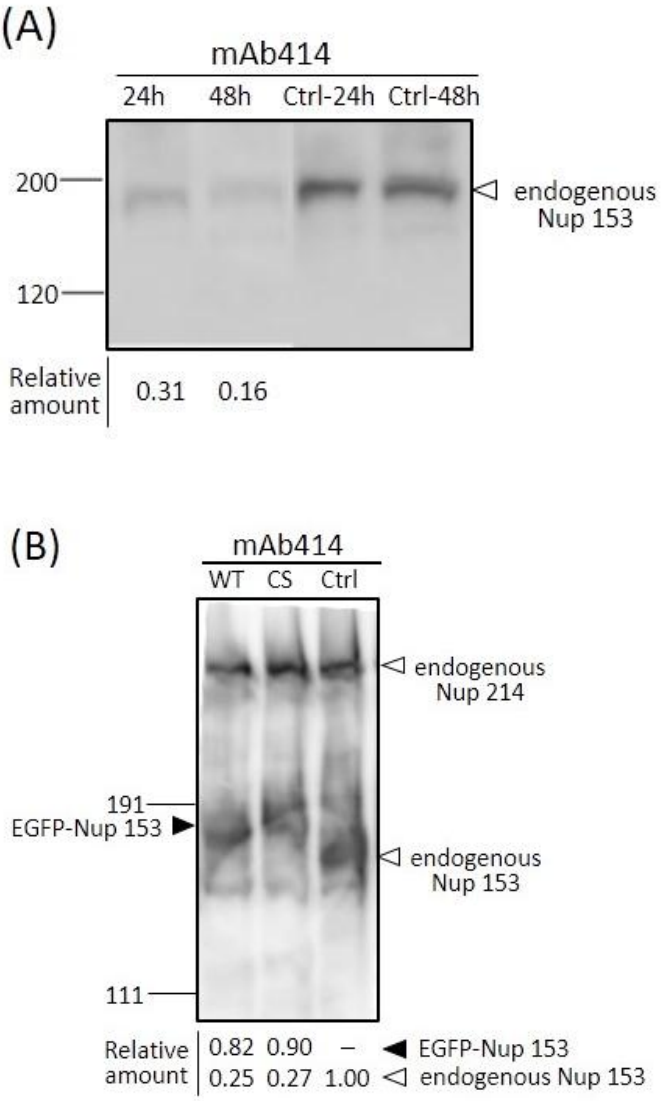

Figure 3-7 Evaluation of siRNA Nup153 knock-down and exogenous expressing of pEGFP-Nup153 WT/CS

(A) Quantification of the knockdown efficiency of siRNA against Nup153. HeLa cells were transfected with the siRNA and subjected to the western blot analysis by mAb414 24 and 48 hours after transfection. Cells transfected with nonsense siRNA (siRNA targeting Luciferase gene) were used as the negative control. (B) Quantification of the knockdown and expression of exogenous Nup153. For a total incubation of 48 hours after siRNA transfection against endogenous Nup153, the transfection of exogenous pEGFP-Nup153 was performed 30 hours after siRNA transfection.

The FRAP assay with a similar procedure was applied to HeLa cells with endogenous Nup153 knocked down and expression of EGFP-Nup153 (WT/CS). The statistical result of FRAP assays was shown in Figure 3-8.

The FRAP analysis in these cells revealed that knockdown of Nup153 drastically decreased the molecular kinetics of Impβ, thus the import rate was largely affected. This effect was partly rescued by introducing exogenous Nup153 both WT and CS mutant. When treated with 2 mM H_2O_2, CS mutant expressing cells fail to restrain the kinetics of Impβ; similar to the previous results (Figure 3-6, 2 mM H_2O_2) in cells with the expression of exogenous Nup153 CS only, compare to Nup153WT. These results clearly demonstrated the role of disulfide bonds in regulating NPCs' permeability.

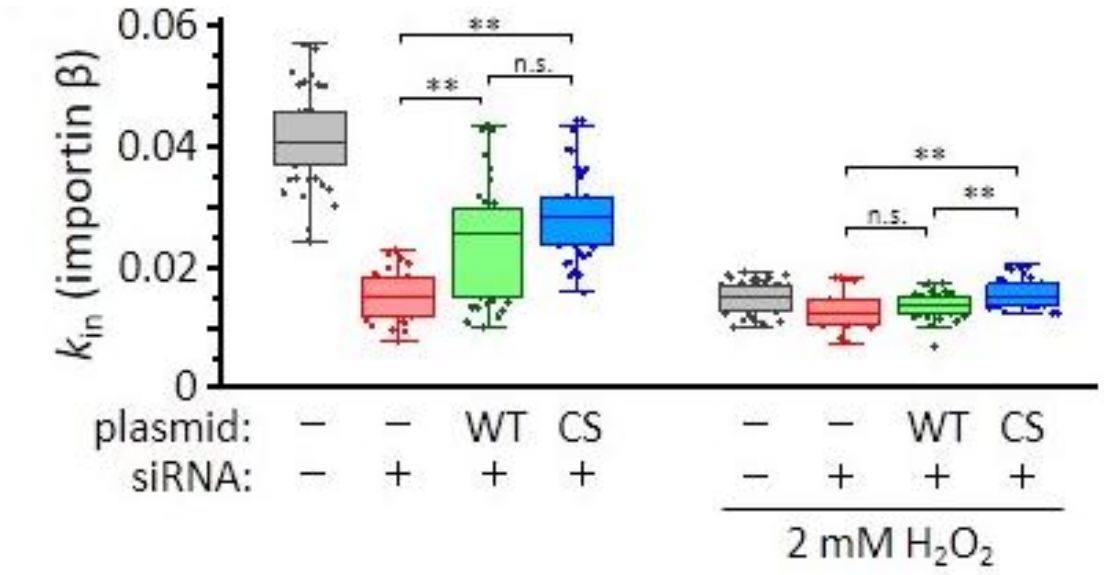

Figure 3-8 FRAP assay result for HeLa cells knocking down endogenous Nup153 and expressing exogenous EGFP-Nup153

Import rates of mCherry-fused Impβ measured by FRAP analyses in HeLa cells transfected with siRNA against Nup153 and plasmid to express siRNA-resistant Nup153 WT and CS mutant (**indicates $p<0.01$, n.s. indicates no significant differences, by Welch's t-test).

3.3.5 Nuclear import rates for other nuclear shuttling molecules

To get a general aspect of permeability at the NE level, other nuclear shuttling molecules were further analyzed (Lolodi et al., 2016). EGFP-Snail (cargo of Impβ1), EGFP-importin α, NLS-EGFP, EGFP-eIF1A (NLS-dependent cargo of Imp13), and EGFP were expressed in HeLa cells, and the nuclear import rates were analyzed by the FRAP analyses under standard (-) and 2 mM H_2O_2-treated (+) conditions, as shown in Figure 3-9.

EGFP-Snail and EGFP-Impα showed significant decreases in their import rates under oxidative stress. The molecular kinetics of small NLS-cargo (NLS-EGFP), passively diffusing molecule (EGFP), and cargo of other Kap (EGFP-eIF1A) were not affected by oxidative stress. These results suggested that redox-dependent crowding control potentially affects a broad range of nuclear shuttling molecules, especially for molecules that translocate through NPC with the help of Impβ and Impα.

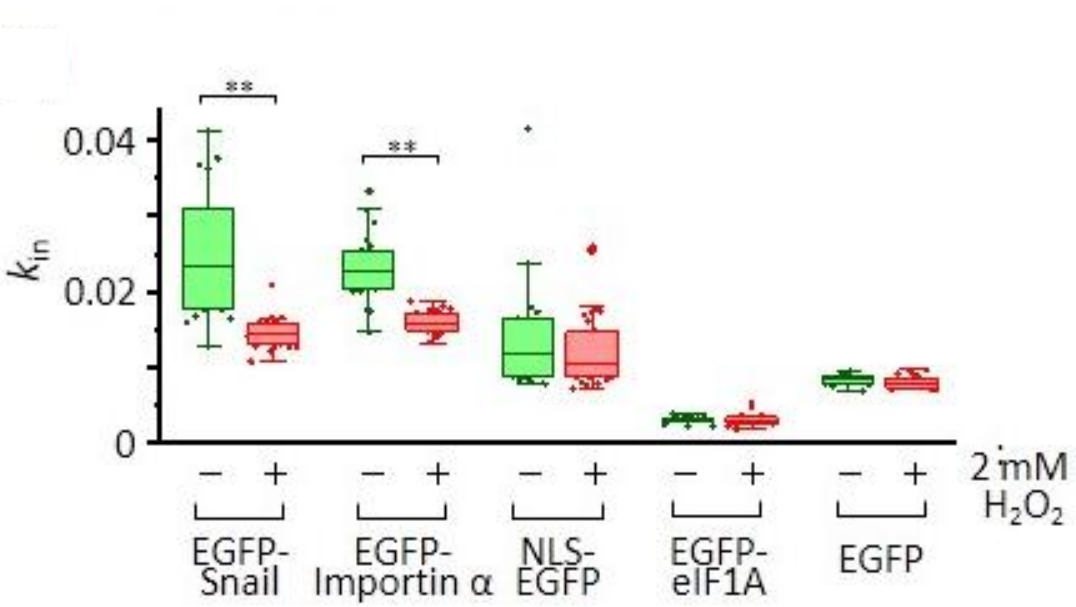

Figure 3-9 FRAP assay for other cargos in karyopherin-related transport

Nuclear import rates obtained by the FRAP analyses of EGFP-Snail, EGFP-Importin α, NLS-EGFP, EGFP-eIF1A, and EGFP expressed in HeLa cells in the presence (+) or absence (-) of 2 mM H_2O_2 (**indicates $p<0.01$, by Welch's t-test)

3.3.6 Binding potential of NupCS mutants with nuclear transport related molecules

From the molecular architecture view, as shown in Figure 3-10, all cysteine residues were mutated to serine residues for Nup62 (C478 and C509); and a total of 21 cysteines from residue 585 to residue 874 were mutated in Nup153. Compare to their molecular structure shown in Figure 2-13, I found that all these cysteine residues locate inside a structural region for both Nups.

For rat Nup62, the α-helical region (amino acid residues 362-425) corresponds to a dynamic fragment that contributes to homodimeric or homotrimeric structure with Nup54 or Nup54 and Nup58, respectively (Dewangan et al., 2017). Therefore, cysteine residues are potentially involved directly in conformational changes of Nup62, thus their role in altering crowding states is reasonable.

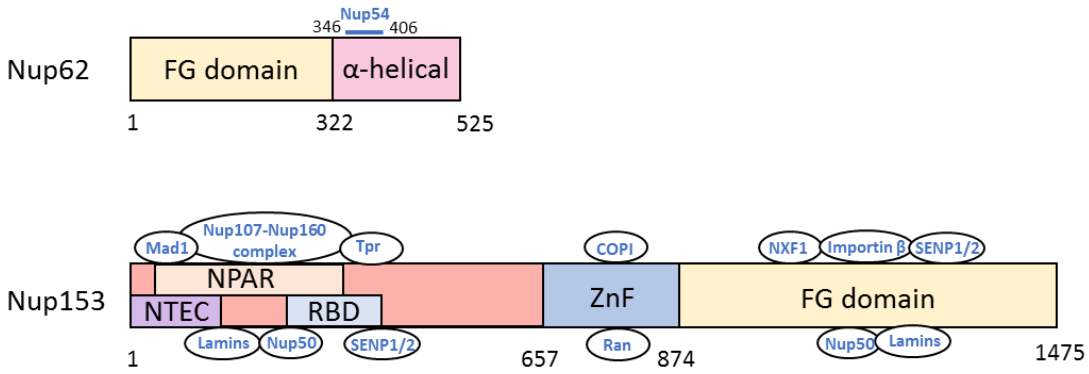

Figure 3-10 Molecular details about Nup62 and Nup153

Nup62 molecule adapted from (Solmaz et al., 2013); interaction region with Nup54 is marked with blue bar, Unsaturated "valences" region is marked with a yellow bar. Nup153 molecule adapted from Atlas of Genetics and Cytogenetics in Oncology and Haematology (Open Access Journal at CNRS-INIST, Version Nov.2019) (http://atlasgeneticsoncology.org/Categories/Nuclear_membrane.html)

For Nup153, the cysteines that I mutated to serines were located within the zinc finger (ZnF) domains of Nup153, which is the region that responsible for interaction with Ran according to several studies (Schrader et al., 2008) (Partridge and Schwartz, 2009) (Lowe et al., 2015). Co-immunoprecipitation assay of Ran by WT and CS Nup153 was performed to assess the effect of CS mutation in Ran-binding activity. The results shown in Figure 3-11A revealed that the averaged relative amount of co-precipitated Ran was 1: 0.94 for WT and CS from three independent experiments, demonstrating a limited effect of CS mutation in Ran-binding activity of Nup153.

Crystallographic structural information in ZnF domains of Nup153 and Ran in complex with GDP showed that cysteines are located near the major interactive residues and suggested to play a supportive role in their interaction (Partridge and Schwartz, 2009), as shown in Figure 3-11B.

Among four cysteine residues in ZnF2, at least two of them (Cys727 and Cys730) are proven to be irrelevant to Ran binding (Partridge and Schwartz, 2009). In addition, the Cys744 to serine mutation did not affect Ran binding process, since the interaction is based on the backbone of Cys744 (Partridge and Schwartz, 2009), which was not altered by the mutation.

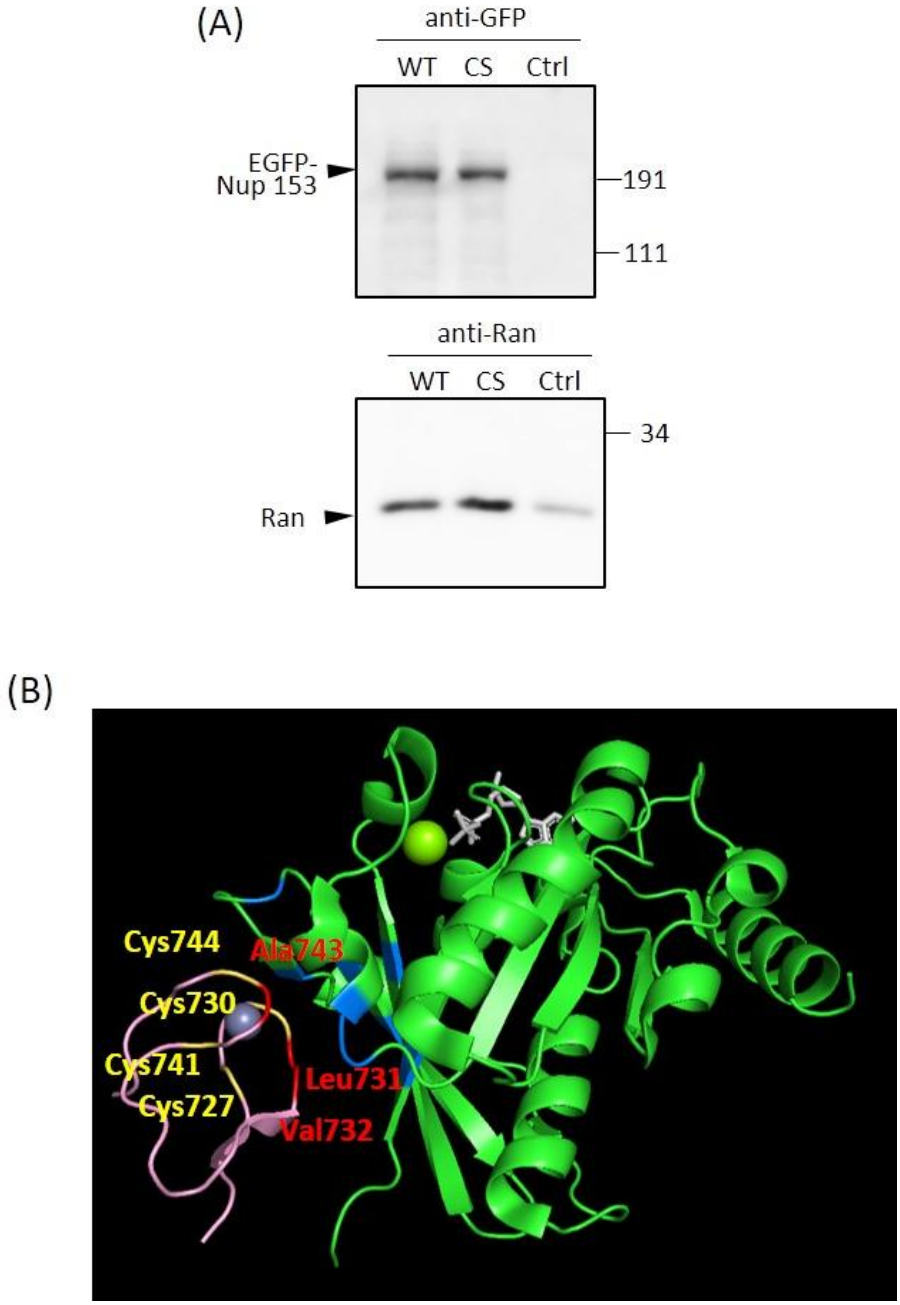

Figure 3-11 CS mutants and Ran-binding ability in Nup153

(A) Co-precipitation analysis of Nup153 with Ran. HeLa cells expressing EGFP-Nup153 WT/CS were lysed and subjected to the immunoprecipitation using an anti-GFP antibody. (B) 3D molecular image of the interaction domains between Nup153 (purple) and Ran (green) (PDB: 3GJ3). Nup153 ZnF2 is shown in purple, with its key interactive amino acid residues in red (Leu731, Val732, Ala743, LVA motif) and cysteine residues in yellow (Cys727, 730, 741, 744). RanGDP is shown in the green ribbon model, with its key interactive residues colored in blue (Lys12, Lys38, Leu43, Val47, Pro49, Trp64, Ile81, Gln82).

Taken together with the results for molecular crowding assays (Figure 2-16) and FRAP (Figure 3-6) assays under standard condition (similar between WT and CS), alteration in the nuclear permeability by redox-sensitive cysteines of Nup153 are independent of Ran binding process. It is reasonable to conclude that the impaired molecular crowding adjustments for CS mutants of Nup62 and Nup153 under oxidative stress were indeed due to the failed formation of disulfide bonds, either intermolecularly and/or intramolecularly among individual Nups within NPCs.

Chapter 4 Discussion and Conclusion

Proper control of nuclear permeability/transport is essential for eukaryotic cells; it is not only important for cellular activities under physiological conditions but also plays pivotal roles in adaptive regulation under stressed conditions. In this chapter, I discuss the molecular mechanisms and physiological significance underlying the redox-sensitive control of nuclear transport revealed in this study, referring to redox signaling and cellular redox homeostasis.

4.1 Oxidative stress and cellular responses

4.1.1 Reactive oxygen species (ROS)

In general, oxidative stress is issued from the reactive oxygen species (ROS). Typical cellular oxidative molecules, both radical and non-radical ROS (Phaniendra et al., 2014), are shown in Table 4-1.

Radicals	Non-radicals
$O_2^{\bullet -}$ (Superoxide)	H_2O_2 (Hydrogen peroxide)
OH• (Hydroxyl)	$^1O_2$ (Singlet oxygen)
RO• (Alkoxyl)	O_3 (Ozone)
ROO• (Peroxyl)	ROOH (Organic peroxide)
	HOCl (Hypochlorous acid)
	HOBr (Hypobromous acid)

Table 4-1 List of radical and non-radical ROS molecules

4.1.2 Redox signaling pathways

For oxidative stress-related signaling, ASK1 (apoptosis signal-regulating kinase 1) and ATM (Ataxia telangiectasia mutated kinase) pathways are well known (Guo et al., 2010). When ASK1 is activated under oxidative stress, the downstream JNK (c-Jun N-terminal kinase) and p38 MAPK (Mitogen-activated protein kinase) pathways are activated, which leads to adaptive responses for survival in cells; or apoptosis when cells are severely damaged. On the other hand, H_2O_2 also activates ATM in the absence of double-strand breaks, through disulfide-cross-linking dimerization of ATM, which process makes ATM a crucial redox-sensor for oxidative stress defense system in cells (Guo et al., 2010).

Other pathways such as PI3K/AKT (Phosphatidylinositol 3-kinase (PI3K) /protein kinase B (AKT)) also help to accommodate redox homeostasis (Samakova et al., 2019). The transcription factors such as Nrf2 (Zhang et al., 2015) (Sajadimajd and Khazaei, 2018), NF-κB (nuclear factor kappa B) (Enesa et al., 2008), p53 (tumor protein p53) (Beyfuss and Hood, 2018), and HIF-1 (Hypoxia-inducible factors 1) (Dewhirst, 2009) (Miyata et al., 2011) also act as regulators under oxidative environment.

4.1.3 Redox reactive cysteine residues

Either for oxidative stress sensing or regulation pathways, cysteine residues play crucial roles (Ray et al., 2012), known as redox-reactive cysteine residues. For example, ASK1 is activated by oxidation of its two cysteine residues: cys-32 and cys-35, hence an intramolecular disulfide bond was formed. Other important regulatory targets such as cGMP-dependent protein kinase (PKG), protein kinase A (PKA), and PKC are all affected directly by ROS; with the formation of either intermolecular (PKG1α) or intramolecular (PKA) disulfide bonds, these proteins regulate MAPK pathways.

Inspired by these regulation factors that rely on cysteine residues as redox-sensor and a previous study of my lab (Yoshimura et al., 2013), I propose a control model with cysteine residues as an essential factor for molecular crowding control for each Nup, which will further be employed to explain the nuclear transport pattern under redox conditions.

4.2 Crowding control and the hydrodynamic dimension of Nups

As previously mentioned, based on the responses of individual Nups under redox conditions (Figure 2-9), there are three types of Nups: the DTT-sensitive (Nup50, 54 and 88), the H_2O_2-sensitive (Nup62, 98, 153, 214, and Pom121) and the insensitive Nup58. When I compare the potential crowding range of these Nups with the hydrodynamic dimension that proposed by Yamada. J group (Yamada et al., 2010), there is a consistency between them, shown as Figure 4-2. Nups with smaller dimensions such as Nup50 and Nup54 are found to be involved in DTT-sensitive decrease of molecular crowding, while Nups with a larger dimension such as Nup62, 98, 153, and 214 are sensitive for H_2O_2. In addition, the insensitive Nup58 is one of the Nups with the smallest hydrodynamic dimension.

This hydrodynamic dimension model could explain the results of the crowding assays for individual Nups regarding their shrinking or extending potentials for hydrodynamic dimension. For example, Nups with large dimension (Nup62, 98, 153, 214) has more potential to shrink their hydrodynamic dimension compare to small dimension Nups such as Nup50 and 54. Oxidative stress may act as a trigger for this shrinking process.

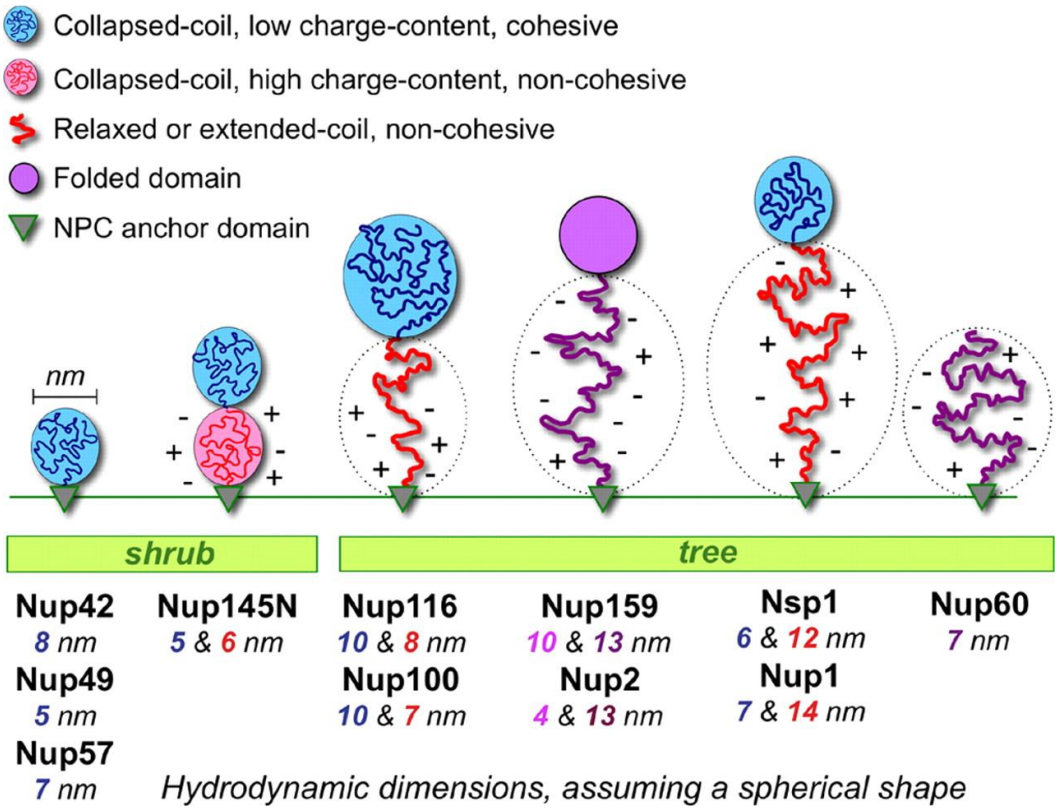

Figure 4-2 Classification of FG-Nups based on hydrodynamic dimensions in *S. cerevisiae* (Yamada et al., 2010))

Homolog Nups in *homo sapiens* are listed as below, with original *S. cerevisiae* Nups in parentheses: Nup42 (Nup42), Nup58 (Nup49), Nup54 (Nup57), Nup98 (Nup145N), Nup98 (Nup116 and Nup100), Nup214 (Nup159), Nup50 (Nup2), Nup62 (Nsp1), Nup153 (Nup1). These FG-Nups are classified as ‘shrub-’ or ‘tree-’ type Nups, based on their hydrodynamic dimensions.

4.3 Transport kinetics and forest model

In agreement with the hydrodynamic dimension model, the forest model for the NPC barrier (Figure 1-6B) serves as a model to interpret the nuclear transport pattern under oxidative stress, which was extracted from the single molecular transport assay. As shown in Figure 3-1, both the single-frame (≤ 15 msec) fast transport event and multi-frame long-lasting transport events (> 150 msec) were affected under oxidative stress (56% and 36%, respectively), compared to the standard condition (68% and 24%, respectively).

According to the forest model, the central cavity of NPC is divided into two zones. The fast nuclear transports within a single frame may share the path with passive diffusion in zone 2 (Figure 4-3, yellow zone). The slow nuclear transports that are mediated by TRs mainly pass through zone 1 (green zone), which may correspond to multi-frame transports in this study (Figure 3-1) under standard/physiological condition. When cells are facing oxidative stress, with an increase of crowding state (or shrinking of dimension) of 'tree' type Nups, the zone 2 area is decreased compared to standard condition, therefore NPCs restrain the passage of fast nuclear transport (68% to 56%). Since the dimension of NPC's central cavity is limited, zone 1 shall be slightly expanded reciprocally while zone 2 is shrunken under oxidative stress, which leads to an increase of multiple-frame long-lasting transport events (24% to 36%).

On the other hand, even though the nuclear transport feature under oxidative condition could be explained by the forest model, the transport pattern under reduced condition does not fit in this model, because both single-frame (especially single-frame fast transport) and multiple-frame nuclear transports are enhanced under reduced environment.

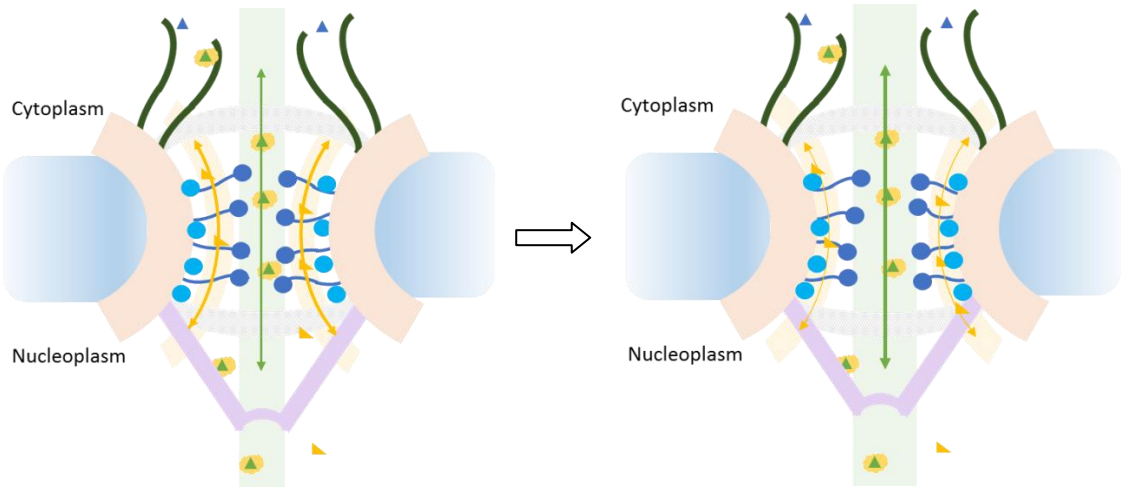

Figure 4-3 Theoretical alternation of transport zones according to the forest model under standard condition (left) and oxidative condition (right)

The nuclear membrane is illustrated with blue color, a schematic NPC is simplified with membrane and scaffold Nups in pink color, cytoplasmic filament Nups in dark green, nucleoplasmic basket in violet. FG-Nups in ‘shrub’ conformation are shown in cyan disks; FG-Nups with ‘tree’ conformation are shown in dark blue disks with an extended coiled in the same color. Under standard condition (left panel), the central cavity of NPC is divided into two transport zones: active transports pass through zone1 (green area, with green arrows that indicate transport orientations); passive diffusion or small molecular transports pass through NPC via zone 2 (yellow area, with orange arrows that indicate transport orientations). Under oxidative condition (right panel), FG-Nups with ‘tree’ conformation shrunken their hydrodynamic dimension, which leads to an expanded zone 1 and a decreased zone 2, compared to the standard condition (left panel).

4.4 Adaptive changes for the crowding states of Nups within sub-complexes

The location of DTT-sensitive and H_2O_2-sensitive Nups are 'well-balanced' within sub-complex structures of NPC (Figure 4-4).

For example, within the Nup214 sub-complex, there are DTT-sensitive Nup88 and H_2O_2-sensitive Nup214 (Xylourgidis et al., 2006), and for the Nup62 sub-complex, there are DTT-sensitive Nup54, H_2O_2-sensitive Nup62, and insensitive Nup58 (Chug et al., 2015). Another example is in the spatial interaction partnerships substructure, between DTT-sensitive Nup50 and H_2O_2-sensitive Nup153 (Kosako et al., 2009). For all sub-complexes mentioned above, there is a co-existence of different types of Nups. This co-existence is well balanced, either with an equivalent presence of two opposite types of Nups or all three types of Nups in each sub-complex. Furthermore, these redox-sensitive Nups localize to almost every sub-structures of the NPC, including the transmembrane region (Pom121) and peripheral regions of both cytoplasmic and nucleoplasmic sides (Nup98), which suggests an overall structural adaptation within NPCs while facing redox conditions.

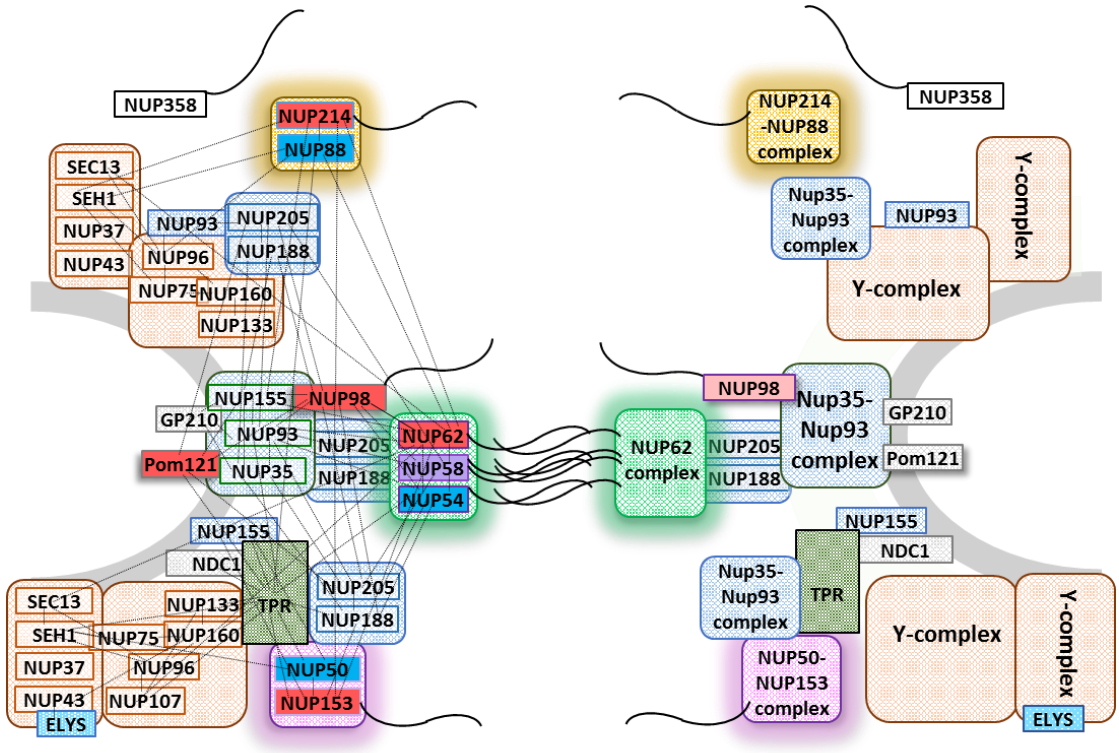

Figure 4-4 Schematic Structure of NPC

Distribution of redox-sensitive Nups in the NPC. Sub-complex structures are shown on the right panel, and detailed constituent Nups in each sub-complex are shown on the left panel, with known interactions identified by cross-linking mass spectrometry (Kosinski et al., 2016) (Kim et al., 2018). Nups that are sensitive to reduced condition (indicate in blue) and oxidative condition (red) co-exist within several sub-complex units. The insensitive Nup58 is shown in purple.

This feature of co-existence of different types of Nups in sub-complex structure (or spatial interaction partners) may imply a functional balanced structure for overall NPC since these sub-complexes are also be considered as functional modules (Gaik et al., 2015) (Mackay et al., 2017). This balanced distribution of Nups may allow NPC to adapt to a broad range of redox situations.

4.5 Cysteine residues and redox regulation in NPC

4.5.1 Conservation of cysteine residues in Nup62 and Nup153

The redox-sensitive cysteines are evolutionally conserved among species, according to the multiple protein sequence alignments of Nup62 and Nup153 for higher vertebrates (Figure 4-5).

As shown in Figure 4-5, the C-terminal cysteine residues in Nup62 are conserved among species. As for the cysteine-enriched ZnF regions of Nup153 (C585 to C874 of human Nup153), 18 cysteine residues out of total 21 residues are conserved among species.

(A) Nup 62

```
HUMAN   458   LNTSGAPADTSDPLQQICKILNAHMDSLQWIDQNSALLQRKVEEVTKVCEGRRKEQERSF   517
RAT     461   LNMAGGPADTSDPLQQICKILNAHMDSLQWVDQSSALLQRRVEEASRVCESRRKEQERSL   520
MOUSE   462   LNMAGGPADTSDPLQQICKILNAHMDSLQWVDQSSALLQRRVEEASRVCEGRRKEQERSL   521
BOVIN   456   LNTSGGPADTSDPLQQICKILNAHMDSLQWIDQNSALLQRKVEEVTKVCEGRRKEQERSF   515
CHICK   510   LNTSGRPADTSDPLQQICKILNAHMDSLQWIDQNSALLQRKVEEVTKVCESRRKEQERSF   569
```

(B) Nup 153

```
HUMAN   536   EANVLPPS-SIGFTFSVPVAKTAELSGSSSTLEPIISSSA--HHVTTVNSTNCKKTPPED   592
RAT     536   QADVLPPA-SIGFTFSVPLAKT-ELSGPNSSSETVLSSSVTAQDNTVVN-SSSSKKRSAP   592
MOUSE   534   QAAVLPPA-SIGFTFSVPLAKT-EFSGSNSSSETVLSSS--AQDITAVN-SSSYKKRSAP   588
BOVIN   537   ESDVLPPS-SIGFTFSVPVAKTAELSGPSSVSEPITSSSA--QDTTAVNSTSCKKKQDED   593
CHICK   532   EAEVLPPLSQIGFTFSVPVVKSAERSGSSDTPVT----SLLTRDTTTVNSISNKKEEKEE   587

HUMAN         CEGPFRPAEILKEGSVLDILKSPGFASPKIDSVAAQPTATSPVVYTRPAISSFSSSGIGF   652
RAT           CEDPFTPAKILREGSVLDILKTPGFMSPKVDSPALQPTTTSSIVYTRPAISTFSSSGVEF   652
MOUSE         CEDPFTPAKILREGSVLDILKTPGFASPKVDSPALQPTTTSSIVYTRPAISTFSSSGIEY   648
BOVIN         CESPFRVAKTLKEGSVLDILKSPGFASSKADSLAAQPGTTSPVVHTRPAISSFSSSGTGF   653
CHICK         YDGPFKPAKVLKEGSVLDILRSPGFTSVKTHSSASAQPITSTAVYTRPAISSFSAGK---   644

HUMAN         GESLKAGSSWQCDTCL--LQNKVTDNKCIACQAAKLSPRDTAKQTGIETPNKSGKTTLSA   710
RAT           GESLKAGSSWQCDTCL--LQNKVTDNKCIACQAAKLPLKETAKQTGIGTPSKSDKPAS--   708
MOUSE         GESLKAGSSWQCDTCL--LQNKVTDNKCIACQAAKLPLKETAKQTGTGTPSKSDKPAS--   704
BOVIN         GEGLKAGSSWQCDTCL--LQNKVTDNKCVACQATKLLPKDSAKQTAAGTPSKSGKVTLST   711
CHICK         ETPKQASSYWQSDPCDPCSQNKAADSKCVTCQAAKVSTAESTKQTTSSSPSGSTKAAAPP   704

HUMAN         SG-TGFGDKFKPVIGTWDCDTCLVQNKPEAIKCVACETPKPGTCVKRALTLTVVSESAET   769
RAT           TSGTGFGDKFKPAIGTWDCDTCLVQNKPEAVKCVACETPKPGTGVKRALPLTVASESPVT   768
MOUSE         TSGTGFGDKFKPAIGTWDCDTCLVQNKPEAVKCVACETPKPGTGVKRALTLTVASESPVT   764
BOVIN         PGTAGFGDKFKPAVGTWDCDTCLVQNKPEAIKCVACETPKPGTGVKRVLTLPVASESAVT   771
CHICK         VGMLGFGDKFKAAPGTWDCDTCLVQNKPEATKCVACETPKPGMGVMPTLALPVTTESSVT   764

HUMAN         MTASSSSCTVTTGTLGFGDKFKRPIGSWECSVCCVSNNAEDNKCVSCMSEKPGSSVPASS   829
RAT           A---SSSTTVTTGTLGFGDKFKRPVGSWECPVCCVSNKAEDSRCVSCTSEKPGLVSASSS   825
MOUSE         A---SSSTTVTTGTLGFGDKFKRPVGSWECPVCCVCNKAEDNRCVSCTSEKPGLVSASSS   821
BOVIN         VAASSSSCTVTTGALGFADKFKRPVGSWECPVCCVSNNAEDNKCVSCMSEKPGSSVPVSS   831
CHICK         VTSSSS-STDTTVTLGFGDKFKKPKGSWDCATCFVSNKAEDSKCVACQSEKPGSSVPVTS   823

HUMAN         SSTVP-VSLPSGGSLGLEKFKKPEGSWDCELCLVQNKADSTKCLACESAKPGTKSGFKGF   888
RAT           --NSVPVSLPSGGCLGLDKFKKPEGSWDCEVCLVQNKADSTKCIACESAKPGTKSEFKGF   883
MOUSE         --SPAPVSLSSGGCLGLDKFKKPEGSWDCEVCLVQNKADSAKCIACESAKPGTKSEFKGF   879
BOVIN         SSMAPSISLSSGGCLGLDKFKKPEGSWNCEVCLVQNKADSTKCIACETVKSHTKPEFTGF   891
CHICK         SSA-SAFAAPSGDLLDLDKFKKPEGSWDCEVCLVQNKAEATKCVACESAKPGTKAEFKGF   882
```

Figure 4-5 Conservation of cysteine residues in Nup62 and Nup153

Amino-acid sequences of cysteine-containing regions of Nup62 (C475 and C506 of human Nup62) and Nup153 (cysteine cluster between C585 and C874 of human Nup153) are shown. Multi-alignments were performed using the Clustal Omega server (https://www.ebi.ac.uk/Tools/msa/clustalo/). Cysteine residues are highlighted with yellow color. Source of the amino acid sequences from different species are listed as follows (A) Nup62: human (Uniprot: P37198-1), rat (Uniprot: P17955-1), mouse (Uniprot: Q63850-1), bovine (Uniprot: A0A3Q1M9H9-1), chicken (Uniprot: F1NFA8-1). (B) Nup153: human (Uniprot: P49790-1), rat (Uniprot: P49791-1), mouse (Uniprot: E9Q3G8-1), bovine (Uniprot: A0A3Q1MAS6-1), chicken (Uniprot: A0A1D5PXQ1-1).

Besides Nup153, similar conservative cysteines within ZnF motifs have been revealed in several other redox sensors/regulator proteins, for example, a bacterial redox-sensitive molecular chaperone Hsp33 (Jakob et al., 2000). Hsp33 releases zinc ion and is activated under oxidative stress (Graumann et al., 2001). After releasing zinc, two disulfide bonds are formed between specific pairs of cysteines and stabilize the structure (Ilbert et al., 2007). Another very recent study of a DNA repair protein XPA (Xeroderma pigmentosum complementation group A) revealed that its ZnF domain could sense quite a low concentration of H_2O_2 and thus may function as a highly sensitive redox sensor in cells (Witkiewicz-Kucharczyk et al., 2020). More examples can also be found in a prokaryotic RNA polymerase regulator DksA (Henard et al., 2014), bacterial recombination protein RecR (Tang et al., 2014), and T4 phase intron endonuclease I-TevI (Robbins et al., 2011), etc. All these examples suggested a conservative ZnF based redox-sensitive mechanism; sometimes these ZnF are even irrelevant to molecular stability but specific to the redox sensing process.

Therefore, from the case of Nup62 and Nup153, we found that the formation of disulfide bonds is important for molecular crowding adjustment in NPCs. By forming disulfide bonds, functional domains that contain cysteine residues may also play a role as a redox-sensitive module within NPCs.

4.5.2 Position of cysteine residues in Nups

The position of cysteine residues within all the human Nups is summarized in Figure 4-6.

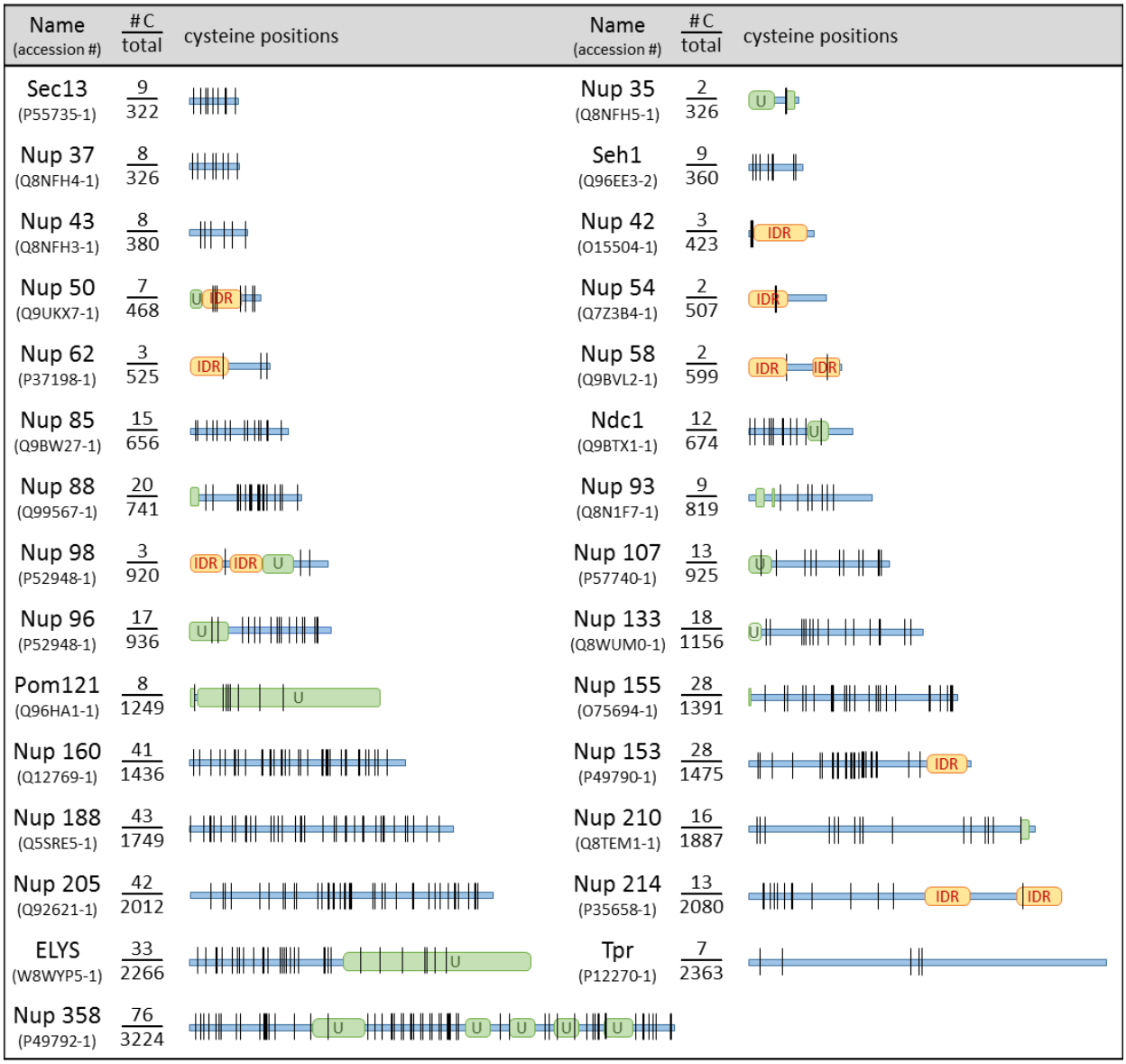

Figure 4-6 Localization of cysteine residues in nucleoporins

Sources of the amino acid sequences are listed with Uniprot accession numbers. The number of cysteines and total amino acid number are also listed. Intrinsically disordered regions (IDR) and unstructured regions (U) are shown in yellow and green boxes, respectively. Cysteine residues are indicated with vertical black lines.

It seems that cysteines are located preferably in structural regions of Nups. If these cysteine residues are similar to those in Nup62 and Nup153, they may play essential roles in dynamic control of crowding states of each Nups, and the permeability of NPCs under redox conditions may also be affected by these cysteine residues. Further studies of cysteine residues within structural domains may also find uncovered redox-sensitive modules, such as the ZnF motif in Nup153.

4.6 A model of redox-sensitive alteration of NPC barrier

Based on the results of the crowding assays and FRAP experiments, a model of redox-sensitive alteration of nuclear transport was proposed, as shown in Figure 4-7.

Nups contain cysteines in their structured regions, which spontaneously form disulfide bonds and serve as ‘sensors’ for redox environments. Under the reduced conditions, DTT-sensitive Nups (Nup50, 54, and 88) sense the environment and disrupt disulfide bonds. This disruption of disulfide bonds leads to a decrease of the molecular crowding states and makes the NPC more accessible to transport molecules. In oxidative conditions, inter- or intramolecular disulfide bonds are formed between H_2O_2-sensitive Nups (Nup62, 98, 153, 214, and Pom121). Under this situation, NPC becomes more crowded and keeps transport molecules longer in the pore. Therefore, transport activity is enhanced in reduced condition and suppressed in oxidative condition.

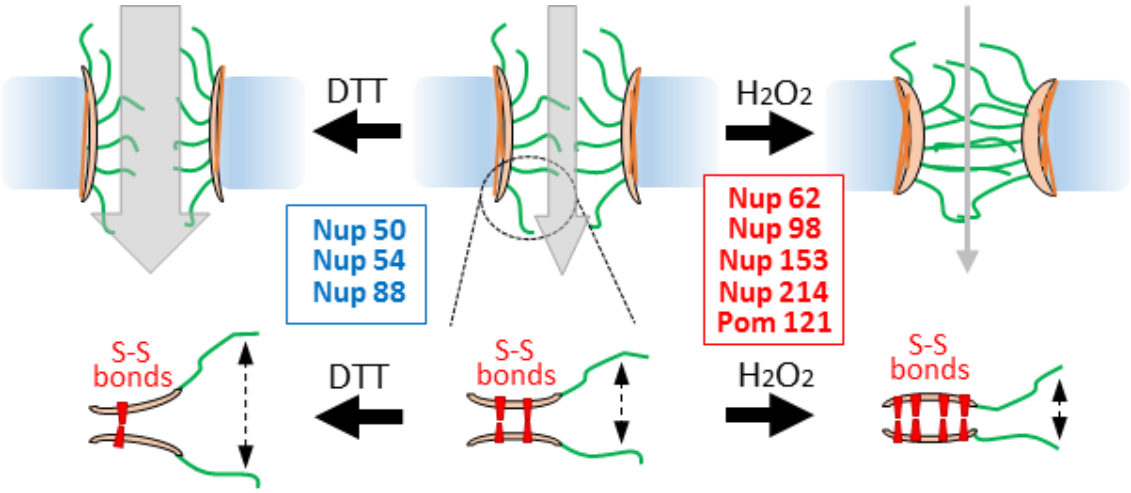

Figure 4-7 Regulation model for nuclear transport under redox conditions

Under physiological conditions, certain numbers of disulfide bonds are pre-established, probably by the DTT-sensitive Nups. These disulfide bonds could be disrupted when cells are facing reduced conditions, resulting in a less crowded NPC which facilitates nuclear transport. The formation of disulfide bonds could also be enhanced when cells are facing oxidative conditions; strengthened NPC by these disulfide bonds may inhibit the nuclear transport in the meantime.

Based on these ideas, I propose a conceptual model of dynamic regulation of molecular crowding states *in vivo*, named the proximal control model (Figure 4-8). The key feature of this model is the separate role of environmental sensing and phase separation regions within a molecule.

As shown in Figure 4-8, the phase separation is maintained by weak and multivalent interactions of IDRs among Nups. Bonding between IDRs (internal control) directly restricts the free movements of the peptides, and probably affects the physiological features of IDRs too, which may have an influence on the phase separation phenomenon. Therefore, the internal control is unsuitable for the adaptive regulation of phase separation. The proximal control model suggested the bonding of structured regions next to the IDRs provides seamless control of the crowding status of IDRs.

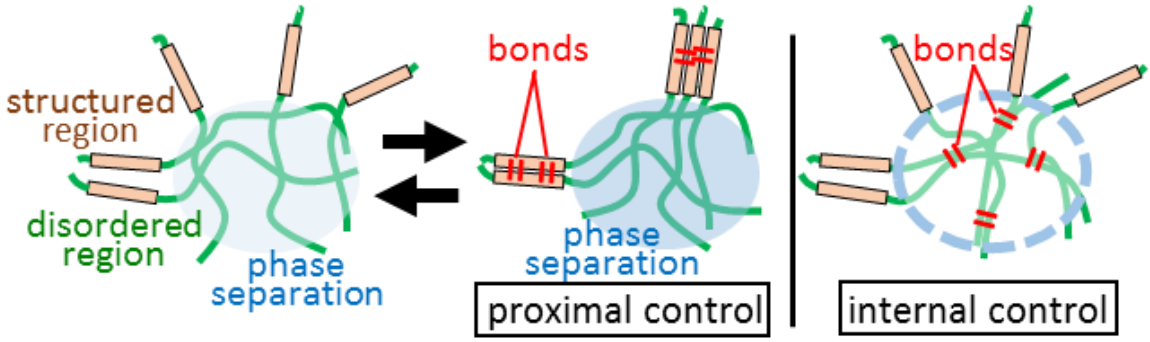

Figure 4-8 General models for *in vivo* phase separation mechanism

Phase separation inside NPC could be controlled by forming or disrupting disulfide bonds at structural proximal regions of IDRs (proximal control). Disulfide bonds within IDRs (internal control) may influence the phase separation phenomenon which may be not suitable for adaptive regulation.

A recently published simulation study of the NPC barrier supports my model (Gu et al., 2019). The simulation proceeded with a coarse-grained model; it suggested that the increase in cohesiveness among IDRs of Nups leads to a decrease in their permeability. They predicted a decrease of NPC's permeability with a high grafting density of Nup-IDRs, which is consistent with our observation of nuclear transport under oxidative stress (Figure 3-1). Under the low grafting density situation, which corresponds to the reduced environment in my study, the permeability was predicted to be enhanced due to a moderate increase of cohesiveness of FG-Nups.

Our findings and proximal control model provide molecular insights of how molecular crowding state is actually controlled *in vivo*: dynamic control at 'sensor' regions leads to the spatial limitation for 'effector' regions to alter their graft density and eventually control the NPC permeability. In addition, since the proximal control of the crowding barrier is mediated by conservative redox-sensitive cysteines, this control model could be an evolutionarily conserved mechanism. Further studies may provide more information on this subject.

4.7 Conclusion and future perspectives

Taken together, data from this study revealed that under redox conditions, nuclear transport through the NPC is either facilitated (reduced condition) or suppressed (oxidative condition). The disulfide bond formation among Nups contributes to this adaptive process. In addition, the mechanism of the nuclear transport regulation by the crowding regulation serves as a model case for phase separation dynamics *in vivo*, which provides insights into the cellular strategy to orchestrate molecular activities at a low energy cost.

Furthermore, I believe that the proximal control of NPCs could be integrated into

the bigger picture of redox cellular homeostasis, as shown in Figure 4-9.

From the “mild” level of ROS, cells initiate the redox regulation by previously mentioned pathways such as ATM (Yan et al., 2014) (Tolbert et al., 2019), p38 MAPK (Zhang et al., 2018), PI3K/AKT (Samakova et al., 2019). Multiple redox-sensitive transcriptional factors were triggered; translocations of Nrf2, NF-κB from the cytoplasm to nucleoplasm are particularly interested (Bellezza et al., 2018). When the concentration of ROS exceeded a certain range, cells can no longer handle the oxidative stress which ultimately leads the apoptosis. From “mild” oxidative stress to “severe” oxidative stress that triggers apoptosis, various cellular processes would occur, such as the disruption of RanGTP gradient (Datta et al., 2014) (Chatterjee and Paschal, 2015), the interruption of nuclear transport, the degradation of Nup153 (Kodiha et al., 2004), the mislocalization of nuclear transport factors (Impα and Crm1) (Miyamoto et al., 2004) (Crampton et al., 2009) and nucleoporins (FG-Nups, Nup88 and Nup153) (Kodiha et al., 2008), and even the lipid peroxidation (Ramana et al., 2017) regarding phospholipids of the nuclear membrane.

Therefore, NPCs play important roles in cellular homeostasis through different mechanisms. The cell could adapt to a certain range of oxidative stress by adjusting nuclear transport in general, and/or by triggering the translocations of crucial transcriptional factors for rescue. At last, the apoptosis would occur with cleavage of Nups (Lindenboim et al., 2020), in response to unbearable oxidative stress.

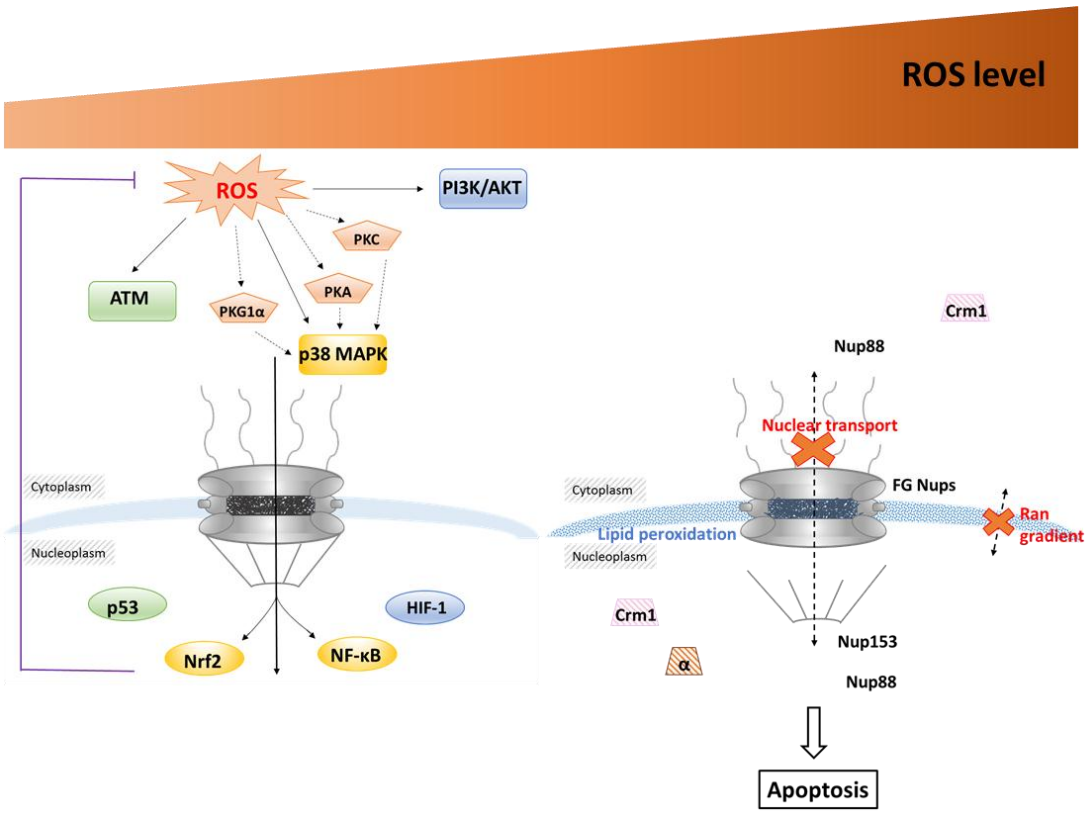

Figure 4-9 NPCs centered redox regulation

The “Mild” oxidative stress would trigger multiple regulation pathways, including the translocation of transcription factors of Nrf2, NF-κB from the p38 MAPK pathway. Retroactive regulation from downstream pathways inhibits the damage of ROS. The “Severe” oxidative stress would induce serious damage in cells, including the disruption of nuclear transport, the lipid peroxidation of the nuclear membrane, the mislocalization of Nups, etc., which may lead to cell apoptosis.

This study provides a new point of view to evaluate the functional role of NPC. The idea of NPC being a regulation hub in cellular redox regulation raises some questions: Are there some Nups that play dominant roles under redox conditions? Are there any other conformational adaptations of Nups in NPCs that specific to stress environments? The answers to these questions will provide more information on nuclear transport and cellular homeostasis.

References

Abu-Arish, A., Kalab, P., Ng-Kamstra, J., Weis, K., and Fradin, C. (2009). Spatial distribution and mobility of the Ran GTPase in live interphase cells. Biophys J *97*, 2164-2178.

Alam, S.G., Lovett, D., Kim, D.I., Roux, K.J., Dickinson, R.B., and Lele, T.P. (2015). The nucleus is an intracellular propagator of tensile forces in NIH 3T3 fibroblasts.

Andrade Ma Fau - Bork, P., and Bork, P. (1995). HEAT repeats in the Huntington's disease protein.

Aramburu, I.V., and Lemke, E.A. (2017). Floppy but not sloppy: Interaction mechanism of FG-nucleoporins and nuclear transport receptors.

Askjaer, P., Bachi, A., Wilm, M., Bischoff, F.R., Weeks, D.L., Ogniewski, V., Ohno, M., Niehrs, C., Kjems, J., Mattaj, I.W*., et al.* (1999). RanGTP-regulated interactions of CRM1 with nucleoporins and a shuttling DEAD-box helicase. Mol Cell Biol *19*, 6276-6285.

Azimi, M., and Mofrad, M.R. (2013). Higher nucleoporin-Importinbeta affinity at the nuclear basket increases nucleocytoplasmic import.

Bayliss, R., Littlewood, T., and Stewart, M. (2000). Structural basis for the interaction between FxFG nucleoporin repeats and importin-beta in nuclear trafficking. Cell *102*, 99-108.

Bayliss, R., Littlewood, T., Strawn, L.A., Wente, S.R., and Stewart, M. (2002). GLFG and FxFG nucleoporins bind to overlapping sites on importin-beta. J Biol Chem *277*, 50597-50606.

Bellezza, I., Giambanco, I., Minelli, A., and Donato, R. (2018). Nrf2-Keap1 signaling in oxidative and reductive stress.

Bernad, R., van der Velde, H., Fornerod, M., and Pickersgill, H. (2004). Nup358/RanBP2 attaches to the nuclear pore complex via association with Nup88 and Nup214/CAN and plays a supporting role in CRM1-mediated nuclear protein export. Mol Cell Biol *24*, 2373-2384.

Beyfuss, K.A.-O., and Hood, D.A. (2018). A systematic review of p53 regulation of oxidative stress in skeletal muscle.

Bischoff, F.R., and Gorlich, D. (1997). RanBP1 is crucial for the release of RanGTP from importin beta-related nuclear transport factors. Febs Lett *419*, 249-254.

Bischoff, F.R., Krebber, H., Smirnova, E., Dong, W., and Ponstingl, H. (1995). Co-activation of RanGTPase and inhibition of GTP dissociation by Ran-GTP binding protein RanBP1. EMBO J *14*, 705-715.

Bogerd, H.P., Fridell, R.A., Benson, R.E., Hua, J., and Cullen, B.R. (1996). Protein sequence requirements for function of the human T-cell leukemia virus type 1 Rex nuclear export signal delineated by a novel in vivo randomization-selection assay. Mol Cell Biol *16*, 4207-4214.

Cagatay, T., and Chook, Y.M. (2018). Karyopherins in cancer. Curr Opin Cell Biol *52*, 30-42.

Capelson, M., Doucet, C., and Hetzer, M.W. (2010). Nuclear pore complexes: guardians of the nuclear genome. Cold Spring Harb Symp Quant Biol *75*, 585-597.

Castillo, E.A., Ayté J Fau - Chiva, C., Chiva C Fau - Moldón, A., Moldón A Fau - Carrascal, M., Carrascal M Fau - Abián, J., Abián J Fau - Jones, N., Jones N Fau - Hidalgo, E., and Hidalgo, E. (2002). Diethylmaleate activates the transcription factor Pap1 by covalent modification of critical cysteine residues.

Chatterjee, M., and Paschal, B.M. (2015). Disruption of the ran system by cysteine oxidation of the nucleotide exchange factor RCC1.

Cheshire, W.P., Jr. (2016). Thermoregulatory disorders and illness related to heat and cold stress.

Chook, Y.M., and Blobel, G. (1999). Structure of the nuclear transport complex karyopherin-beta2-Ran x GppNHp. Nature *399*, 230-237.

Chook, Y.M., and Blobel, G. (2001). Karyopherins and nuclear import. Curr Opin Struct Biol *11*, 703-715.

Chook, Y.M., and Suel, K.E. (2011). Nuclear import by karyopherin-betas: recognition and inhibition. Biochim Biophys Acta *1813*, 1593-1606.

Chug, H., Trakhanov, S., Hulsmann, B.B., Pleiner, T., and Gorlich, D. (2015). Crystal structure of the metazoan Nup62*Nup58*Nup54 nucleoporin complex. Science *350*, 106-110.

Cingolani, G., Lashuel, H.A., Gerace, L., and Muller, C.W. (2000). Nuclear import factors importin alpha and importin beta undergo mutually induced conformational changes upon association. Febs Lett *484*, 291-298.

Cingolani, G., Petosa, C., Weis, K., and Muller, C.W. (1999). Structure of importin-beta bound to the IBB domain of importin-alpha. Nature *399*, 221-229.

Conti, E., and Izaurralde, E. (2001). Nucleocytoplasmic transport enters the atomic age. Curr Opin Cell Biol *13*, 310-319.

Conti, E., Muller, C.W., and Stewart, M. (2006). Karyopherin flexibility in nucleocytoplasmic transport. Curr Opin Struct Biol *16*, 237-244.

Conti, E., Uy, M., Leighton, L., Blobel, G., and Kuriyan, J. (1998). Crystallographic analysis of the recognition of a nuclear localization signal by the nuclear import factor karyopherin alpha. Cell *94*, 193-204.

Crampton, N., Kodiha, M., Shrivastava, S., Umar, R., and Stochaj, U. (2009). Oxidative Stress Inhibits Nuclear Protein Export by Multiple Mechanisms That Target FG Nucleoporins and Crm1. Molecular Biology of the Cell *20*, 5106-5116.

Crisp, M., and Burke, B. (2008). The nuclear envelope as an integrator of nuclear and cytoplasmic architecture.

Cushman, I., Palzkill, T., and Moore, M.S. (2006). Using peptide arrays to define nuclear carrier binding sites on nucleoporins. Methods *39*, 329-341.

Datta, S., Snow Cj Fau - Paschal, B.M., and Paschal, B.M. (2014). A pathway linking oxidative stress and the Ran GTPase system in progeria.

Denning, D.P., and Rexach, M.F. (2007). Rapid evolution exposes the boundaries of domain structure and function in natively unfolded FG nucleoporins. Mol Cell Proteomics *6*, 272-282.

Dewangan, P.S., Sonawane, P.J., Chouksey, A.R., and Chauhan, R. (2017). The Nup62 Coiled-Coil Motif Provides Plasticity for Triple-Helix Bundle Formation. Biochemistry *56*, 2803-2811.

Dewhirst, M.W. (2009). Relationships between cycling hypoxia, HIF-1, angiogenesis and oxidative stress.

Donnaloja, F., Jacchetti, E., Soncini, M., and Raimondi, M.T. (2019). Mechanosensing at the Nuclear Envelope by Nuclear Pore Complex Stretch Activation and Its Effect in Physiology and Pathology. Front

Physiol *10*.

Eisele, N.B., Frey, S., Piehler, J., Gorlich, D., and Richter, R.P. (2010). Ultrathin nucleoporin phenylalanine-glycine repeat films and their interaction with nuclear transport receptors. Embo Reports *11*, 366-372.

Elosegui-Artola, A., Andreu, I., Beedle, A.E.M., Lezamiz, A., Uroz, M., Kosmalska, A.J., Oria, R., Kechagia, J.Z., Rico-Lastres, P., Le Roux, A.L*., et al.* (2017). Force Triggers YAP Nuclear Entry by Regulating Transport across Nuclear Pores.

Enesa, K., Ito, K., Luong le, A., Thorbjornsen, I., Phua, C., To, Y., Dean, J., Haskard, D.O., Boyle, J., Adcock, I*., et al.* (2008). Hydrogen peroxide prolongs nuclear localization of NF-kappaB in activated cells by suppressing negative regulatory mechanisms. J Biol Chem *283*, 18582-18590.

Engelsma, D., Bernad, R., Calafat, J., and Fornerod, M. (2004). Supraphysiological nuclear export signals bind CRM1 independently of RanGTP and arrest at Nup358. Embo Journal *23*, 3643-3652.

Fahrenkrog, B., and Harel, A. (2018). Perturbations in Traffic: Aberrant Nucleocytoplasmic Transport at the Heart of Neurodegeneration. Cells *7*, 232.

Finan, J.D., and Guilak, F. (2010). The effects of osmotic stress on the structure and function of the cell nucleus.

Finan, J.D., Leddy Ha Fau - Guilak, F., and Guilak, F. (2011). Osmotic stress alters chromatin condensation and nucleocytoplasmic transport.

Fiserova, J., Spink, M., Richards, S.A., Saunter, C., and Goldberg, M.W. (2014). Entry into the nuclear pore complex is controlled by a cytoplasmic exclusion zone containing dynamic GLFG-repeat nucleoporin domains. J Cell Sci *127*, 124-136.

Floer, M., and Blobel, G. (1999). Putative reaction intermediates in Crm1-mediated nuclear protein export. J Biol Chem *274*, 16279-16286.

Fogelson, B., and Keener, J.P. (2018). Enhanced Nucleocytoplasmic Transport due to Competition for Elastic Binding Sites. Biophysical Journal *115*, 108-116.

Folker, E.S., Ostlund C Fau - Luxton, G.W.G., Luxton Gw Fau - Worman, H.J., Worman Hj Fau - Gundersen, G.G., and Gundersen, G.G. (2011). Lamin A variants that cause striated muscle disease are defective in anchoring transmembrane actin-associated nuclear lines for nuclear movement.

Fornerod, M., vanDeursen, J., vanBaal, S., Reynolds, A., Davis, D., Murti, K.G., Fransen, J., and Grosveld, G. (1997). The human homologue of yeast CRM1 is in a dynamic subcomplex with CAN/Nup214 and a novel nuclear pore component Nup88. Embo Journal *16*, 807-816.

Forwood, J.K., Lange, A., Zachariae, U., Marfori, M., Preast, C., Grubmuller, H., Stewart, M., Corbett, A.H., and Kobe, B. (2010). Quantitative structural analysis of importin-beta flexibility: paradigm for solenoid protein structures. Structure *18*, 1171-1183.

Frey, S., Rees, R., Schunemann, J., Ng, S.C., Funfgeld, K., Huyton, T., and Gorlich, D. (2018). Surface Properties Determining Passage Rates of Proteins through Nuclear Pores. Cell *174*, 202-+.

Frey, S., Richter, R.P., and Gorlich, D. (2006). FG-rich repeats of nuclear pore proteins form a three-dimensional meshwork with hydrogel-like properties. Science *314*, 815-817.

Fung, H.A.-O., Fu, S.C., and Chook, Y.A.-O. (2017). Nuclear export receptor CRM1 recognizes diverse conformations in nuclear export signals. LID - 10.7554/eLife.23961 [doi] LID - e23961 [pii].

Gaik, M., Flemming, D., von Appen, A., Kastritis, P., Mücke, N., Fischer, J., Stelter, P., Ori, A., Bui, K.H., Baßler, J.*, et al.* (2015). Structural basis for assembly and function of the Nup82 complex in the nuclear pore scaffold.

Gamini, R., Han, W., Stone, J.E., and Schulten, K. (2014). Assembly of Nsp1 Nucleoporins Provides Insight into Nuclear Pore Complex Gating. Plos Computational Biology *10*.

Gilbert, P.M., and Weaver, V.M. (2017). Cellular adaptation to biomechanical stress across length scales in tissue homeostasis and disease.

Gorlich, D., and Kutay, U. (1999). Transport between the cell nucleus and the cytoplasm. Annu Rev Cell Dev Bi *15*, 607-660.

Gorlich, D., Pante, N., Kutay, U., Aebi, U., and Bischoff, F.R. (1996). Identification of different roles for RanGDP and RanGTP in nuclear protein import. EMBO J *15*, 5584-5594.

Gorlich, D., Seewald, M.J., and Ribbeck, K. (2003). Characterization of Ran-driven cargo transport and the RanGTPase system by kinetic measurements and computer simulation. EMBO J *22*, 1088-1100.

Goulev, Y.A.-O., Morlot, S., Matifas, A., Huang, B.A.-O., Molin, M., Toledano, M.B., and Charvin, G.A.-O. (2017). Nonlinear feedback drives homeostatic plasticity in H(2)O(2) stress response. LID - e23971 [pii] LID - 10.7554/eLife.23971 [doi].

Graumann, J., Lilie H Fau - Tang, X., Tang X Fau - Tucker, K.A., Tucker Ka Fau - Hoffmann, J.H., Hoffmann Jh Fau - Vijayalakshmi, J., Vijayalakshmi J Fau - Saper, M., Saper M Fau - Bardwell, J.C., Bardwell Jc Fau - Jakob, U., and Jakob, U. (2001). Activation of the redox-regulated molecular chaperone Hsp33--a two-step mechanism.

Grima, J.C., Daigle, J.G., Arbez, N., Cunningham, K.C., Zhang, K., Ochaba, J., Geater, C., Morozko, E., Stocksdale, J., Glatzer, J.C.*, et al.* (2017). Mutant Huntingtin Disrupts the Nuclear Pore Complex. Neuron *94*, 93-107.e106.

Gu, C., Vovk, A., Zheng, T., Coalson, R.D., and Zilman, A. (2019). The Role of Cohesiveness in the Permeability of the Spatial Assemblies of FG Nucleoporins. Biophys J *116*, 1204-1215.

Guilluy, C., Osborne, L.D., Van Landeghem, L., Sharek, L., Superfine, R., Garcia-Mata, R., and Burridge, K. (2014). Isolated nuclei adapt to force and reveal a mechanotransduction pathway in the nucleus.

Guo, L., Kim, H.J., Wang, H., Monaghan, J., Freyermuth, F., Sung, J.C., O'Donovan, K., Fare, C.M., Diaz, Z., Singh, N.*, et al.* (2018). Nuclear-Import Receptors Reverse Aberrant Phase Transitions of RNA-Binding Proteins with Prion-like Domains. Cell *173*, 677-692.e620.

Guo, Z., Kozlov S Fau - Lavin, M.F., Lavin Mf Fau - Person, M.D., Person Md Fau - Paull, T.T., and Paull, T.T. (2010). ATM activation by oxidative stress.

Hampoelz, B., Andres-Pons, A., Kastritis, P., and Beck, M. (2019). Structure and Assembly of the Nuclear Pore Complex. Annu Rev Biophys *48*, 515-536.

Henard, C.A., Tapscott T Fau - Crawford, M.A., Crawford Ma Fau - Husain, M., Husain M Fau - Doulias, P.-T., Doulias Pt Fau - Porwollik, S., Porwollik S Fau - Liu, L., Liu L Fau - McClelland, M., McClelland M Fau -

Ischiropoulos, H., Ischiropoulos H Fau - Vázquez-Torres, A., and Vázquez-Torres, A. (2014). The 4-cysteine zinc-finger motif of the RNA polymerase regulator DksA serves as a thiol switch for sensing oxidative and nitrosative stress.

Hodel, A.E., Harreman, M.T., Pulliam, K.F., Harben, M.E., Holmes, J.S., Hodel, M.R., Berland, K.M., and Corbett, A.H. (2006). Nuclear localization signal receptor affinity correlates with in vivo localization in Saccharomyces cerevisiae. J Biol Chem *281*, 23545-23556.

Hodel, M.R., Corbett, A.H., and Hodel, A.E. (2001). Dissection of a nuclear localization signal. J Biol Chem *276*, 1317-1325.

Hoffman, L.M., Smith, M.A., Jensen, C.C., Yoshigi, M., Blankman, E., Ullman, K.S., and Beckerle, M.C. (2020). Mechanical stress triggers nuclear remodeling and the formation of transmembrane actin nuclear lines with associated nuclear pore complexes.

Hutten, S., and Kehlenbach, R.H. (2006). Nup214 is required for CRM1-dependent nuclear protein export in vivo. Mol Cell Biol *26*, 6772-6785.

Hutten, S., and Kehlenbach, R.H. (2007). CRM1-mediated nuclear export: to the pore and beyond. Trends Cell Biol *17*, 193-201.

Ilbert, M., Horst J Fau - Ahrens, S., Ahrens S Fau - Winter, J., Winter J Fau - Graf, P.C.F., Graf Pc Fau - Lilie, H., Lilie H Fau - Jakob, U., and Jakob, U. (2007). The redox-switch domain of Hsp33 functions as dual stress sensor.

Imasaki, T., Shimizu, T., Hashimoto, H., Hidaka, Y., Kose, S., Imamoto, N., Yamada, M., and Sato, M. (2007). Structural basis for substrate recognition and dissociation by human transportin 1. Mol Cell *28*, 57-67.

Jahed, Z., Soheilypour, M., Peyro, M., and Mofrad, M.A.-O. (2016). The LINC and NPC relationship - it's complicated!

Jakob, U., Eser M Fau - Bardwell, J.C., and Bardwell, J.C. (2000). Redox switch of hsp33 has a novel zinc-binding motif.

Kaspar, J.W., Niture Sk Fau - Jaiswal, A.K., and Jaiswal, A.K. (2009). Nrf2:INrf2 (Keap1) signaling in oxidative stress.

Kaur, P., Kalia S Fau - Bansal, M.P., and Bansal, M.P. (2006). Effect of diethyl maleate induced oxidative stress on male reproductive activity in mice: redox active enzymes and transcription factors expression.

Kehlenbach, R.H., Dickmanns, A., Kehlenbach, A., Guan, T., and Gerace, L. (1999). A role for RanBP1 in the release of CRM1 from the nuclear pore complex in a terminal step of nuclear export. J Cell Biol *145*, 645-657.

Kerr, A.R., and Schirmer, E.C. (2011). FG repeats facilitate integral protein trafficking to the inner nuclear membrane. Commun Integr Biol *4*, 557-559.

Kim, S.J., Fernandez-Martinez, J., Nudelman, I., Shi, Y., Zhang, W., Raveh, B., Herricks, T., Slaughter, B.D., Hogan, J.A., Upla, P*., et al.* (2018). Integrative structure and functional anatomy of a nuclear pore complex. Nature *555*, 475-482.

Kobayashi, J., and Matsuura, Y. (2013). Structural basis for cell-cycle-dependent nuclear import mediated by the karyopherin Kap121p. J Mol Biol *425*, 1852-1868.

Kodiha, M., Chu, A., Matusiewicz, N., and Stochaj, U. (2004). Multiple mechanisms promote the inhibition of classical nuclear import upon exposure to severe oxidative stress. Cell Death Differ *11*, 862-874.

Kodiha, M., Tran D Fau - Qian, C., Qian C Fau - Morogan, A., Morogan A Fau - Presley, J.F., Presley Jf Fau - Brown, C.M., Brown Cm Fau - Stochaj, U., and Stochaj, U. (2008). Oxidative stress mislocalizes and retains transport factor importin-alpha and nucleoporins Nup153 and Nup88 in nuclei where they generate high molecular mass complexes.

Konishi, H.A., Asai, S., Watanabe, T.M., and Yoshimura, S.H. (2017). In vivo analysis of protein crowding within the nuclear pore complex in interphase and mitosis. Sci Rep *7*, 5709.

Kosako, H., Yamaguchi, N., Aranami, C., Ushiyama, M., Kose, S., Imamoto, N., Taniguchi, H., Nishida, E., and Hattori, S. (2009). Phosphoproteomics reveals new ERK MAP kinase targets and links ERK to nucleoporin-mediated nuclear transport. Nat Struct Mol Biol *16*, 1026-1035.

Kosinski, J., Mosalaganti, S., von Appen, A., Teimer, R., DiGuilio, A.L., Wan, W., Bui, K.H., Hagen, W.J., Briggs, J.A., Glavy, J.S*., et al.* (2016). Molecular architecture of the inner ring scaffold of the human nuclear pore complex. Science *352*, 363-365.

Koyama, M., and Matsuura, Y. (2010). An allosteric mechanism to displace nuclear export cargo from CRM1 and RanGTP by RanBP1. EMBO J *29*, 2002-2013.

Kubitscheck, U., and Siebrasse, J.P. (2017). Kinetics of transport through the nuclear pore complex. Seminars in Cell & Developmental Biology *68*, 18-26.

Kumeta, M., Konishi, H., Zhang, W., Sakagami, S., and Yoshimura, S. (2018). Prolines in the α-helix confer the structural flexibility and functional integrity of importin-β. LID - jcs206326 [pii] LID - 10.1242/jcs.206326 [doi].

Kutay, U., and Guttinger, S. (2005). Leucine-rich nuclear-export signals: born to be weak. Trends Cell Biol *15*, 121-124.

la Cour, T., Gupta, R., Rapacki, K., Skriver, K., Poulsen, F.M., and Brunak, S. (2003). NESbase version 1.0: a database of nuclear export signals. Nucleic Acids Res *31*, 393-396.

la Cour, T., Kiemer, L., Molgaard, A., Gupta, R., Skriver, K., and Brunak, S. (2004). Analysis and prediction of leucine-rich nuclear export signals. Protein Eng Des Sel *17*, 527-536.

Labokha, A.A., Gradmann, S., Frey, S., Hulsmann, B.B., Urlaub, H., Baldus, M., and Gorlich, D. (2013). Systematic analysis of barrier-forming FG hydrogels from Xenopus nuclear pore complexes. EMBO J *32*, 204-218.

Lai, M.C., Lin, R.I., Huang, S.Y., Tsai, C.W., and Tarn, W.Y. (2000). A human importin-beta family protein, transportin-SR2, interacts with the phosphorylated RS domain of SR proteins. J Biol Chem *275*, 7950-7957.

Lee, B.J., Cansizoglu, A.E., Suel, K.E., Louis, T.H., Zhang, Z., and Chook, Y.M. (2006). Rules for nuclear localization sequence recognition by karyopherin beta 2. Cell *126*, 543-558.

Lee, S.J., Imamotos, N., Sakai, H., Nakagawa, A., Kose, S., Koike, M., Yamamoto, M., Kumasaka, T., Yoneda, Y., and Tsukihara, T. (2000). The adoption of a twisted structure of importin-beta is essential for the

protein-protein interaction required for nuclear transport. J Mol Biol *302*, 251-264.

Lim, R.Y., Fahrenkrog, B., Koser, J., Schwarz-Herion, K., Deng, J., and Aebi, U. (2007). Nanomechanical basis of selective gating by the nuclear pore complex. Science *318*, 640-643.

Lin, D.H., and Hoelz, A. (2019). The Structure of the Nuclear Pore Complex (An Update). Annu Rev Biochem *88*, 725-783.

Lin, D.H., Stuwe, T., Schilbach, S., Rundlet, E.J., Perriches, T., Mobbs, G., Fan, Y., Thierbach, K., Huber, F.M., Collins, L.N.*, et al.* (2016). Architecture of the symmetric core of the nuclear pore. Science *352*, aaf1015-aaf1015.

Lindenboim, L., Zohar, H., Worman, H.J., and Stein, R. (2020). The nuclear envelope: target and mediator of the apoptotic process.

Liu, Q., Pante N Fau - Misteli, T., Misteli T Fau - Elsagga, M., Elsagga M Fau - Crisp, M., Crisp M Fau - Hodzic, D., Hodzic D Fau - Burke, B., Burke B Fau - Roux, K.J., and Roux, K.J. (2007). Functional association of Sun1 with nuclear pore complexes.

Liu, S.M., and Stewart, M. (2005). Structural basis for the high-affinity binding of nucleoporin Nup1p to the Saccharomyces cerevisiae importin-beta homologue, Kap95p. J Mol Biol *349*, 515-525.

Lolodi, O., Yamazaki, H., Otsuka, S., Kumeta, M., and Yoshimura, S.H. (2016). Dissecting in vivo steady-state dynamics of karyopherin-dependent nuclear transport.

Lowe, A.R., Tang, J.H., Yassif, J., Graf, M., Huang, W.Y., Groves, J.T., Weis, K.A.-O.h.o.o.X., and Liphardt, J.T. (2015). Importin-beta modulates the permeability of the nuclear pore complex in a Ran-dependent manner. LID - 10.7554/eLife.04052 [doi].

Ma, J., Goryaynov, A., and Yang, W. (2016). Super-resolution 3D tomography of interactions and competition in the nuclear pore complex. Nat Struct Mol Biol *23*, 239-247.

Mackay, D.A.-O., Howa, A.C., Werner, T.L., and Ullman, K.S. (2017). Nup153 and Nup50 promote recruitment of 53BP1 to DNA repair foci by antagonizing BRCA1-dependent events.

Maertens, G.N., Cook, N.J., Wang, W., Hare, S., Gupta, S.S., Oztop, I., Lee, K., Pye, V.E., Cosnefroy, O., Snijders, A.P.*, et al.* (2014). Structural basis for nuclear import of splicing factors by human Transportin 3. Proc Natl Acad Sci U S A *111*, 2728-2733.

Makino, N., Mochizuki Y Fau - Bannai, S., Bannai S Fau - Sugita, Y., and Sugita, Y. (1994). Kinetic studies on the removal of extracellular hydrogen peroxide by cultured fibroblasts.

Miao, L., and Schulten, K. (2010). Probing a Structural Model of the Nuclear Pore Complex Channel through Molecular Dynamics. Biophysical Journal *98*, 1658-1667.

Miao, L.L., and Schulten, K. (2009). Transport-Related Structures and Processes of the Nuclear Pore Complex Studied through Molecular Dynamics. Structure *17*, 449-459.

Milles, S., Huy Bui, K., Koehler, C., Eltsov, M., Beck, M., and Lemke, E.A. (2013). Facilitated aggregation of FG nucleoporins under molecular crowding conditions. EMBO Rep *14*, 178-183.

Milles, S., and Lemke, E.A. (2011). Single molecule study of the intrinsically disordered FG-repeat nucleoporin 153. Biophys J *101*, 1710-1719.

Milles, S., Mercadante, D., Aramburu, I.V., Jensen, M.R., Banterle, N., Koehler, C., Tyagi, S., Clarke, J.,

Shammas, S.L., Blackledge, M.*, et al.* (2015). Plasticity of an ultrafast interaction between nucleoporins and nuclear transport receptors. Cell *163*, 734-745.

Miyamoto, Y., Saiwaki T Fau - Yamashita, J., Yamashita J Fau - Yasuda, Y., Yasuda Y Fau - Kotera, I., Kotera I Fau - Shibata, S., Shibata S Fau - Shigeta, M., Shigeta M Fau - Hiraoka, Y., Hiraoka Y Fau - Haraguchi, T., Haraguchi T Fau - Yoneda, Y., and Yoneda, Y. (2004). Cellular stresses induce the nuclear accumulation of importin alpha and cause a conventional nuclear import block.

Miyata, T., Takizawa S Fau - van Ypersele de Strihou, C., and van Ypersele de Strihou, C. (2011). Hypoxia. 1. Intracellular sensors for oxygen and oxidative stress: novel therapeutic targets.

Morikawa, T.J., Fujita, H., Kitamura, A., Horio, T., Yamamoto, J., Kinjo, M., Sasaki, A., Machiyama, H., Yoshizawa, K., Ichimura, T.*, et al.* (2016). Dependence of fluorescent protein brightness on protein concentration in solution and enhancement of it. Sci Rep *6*, 22342.

Moussavi-Baygi, R., Jamali, Y., Karimi, R., and Mofrad, M.R. (2011). Brownian dynamics simulation of nucleocytoplasmic transport: a coarse-grained model for the functional state of the nuclear pore complex. PLoS Comput Biol *7*, e1002049.

Nemergut, M.E., and Macara, I.G. (2000). Nuclear import of the Ran exchange factor, RCC1, is mediated by at least two distinct mechanisms. J Cell Biol *149*, 835-849.

O'Reilly, A.J., Dacks, J.B., and Field, M.C. (2011). Evolution of the karyopherin-beta family of nucleocytoplasmic transport factors; ancient origins and continued specialization. PLoS One *6*, e19308.

Ogawa, Y., and Imamoto, N.A.-O. (2018). Nuclear transport adapts to varying heat stress in a multistep mechanism.

Oka, M., Asally, M., Yasuda, Y., Ogawa, Y., Tachibana, T., and Yoneda, Y. (2010). The Mobile FG Nucleoporin Nup98 Is a Cofactor for Crm1-dependent Protein Export. Molecular Biology of the Cell *21*, 1885-1896.

Otsuka, S., Iwasaka, S., Yoneda, Y., Takeyasu, K., and Yoshimura, S.H. (2008). Individual binding pockets of importin-beta for FG-nucleoporins have different binding properties and different sensitivities to RanGTP. P Natl Acad Sci USA *105*, 16101-16106.

Palmeri, D., and Malim, M.H. (1999). Importin beta can mediate the nuclear import of an arginine-rich nuclear localization signal in the absence of importin alpha. Mol Cell Biol *19*, 1218-1225.

Partridge, J.R., and Schwartz, T.U. (2009). Crystallographic and biochemical analysis of the Ran-binding zinc finger domain. J Mol Biol *391*, 375-389.

Patel, V.P., and Chu, C.T. (2011). Nuclear transport, oxidative stress, and neurodegeneration. Int J Clin Exp Pathol *4*, 215-229.

Phaniendra, A., Jestadi, D.B., and Periyasamy, L. (2014). Free radicals: properties, sources, targets, and their implication in various diseases.

Pomatto, L.C.D., and Davies, K.A.-O. (2017). The role of declining adaptive homeostasis in ageing.

Rahal, A., Kumar, A., Singh, V., Yadav, B., Tiwari, R.A.-O., Chakraborty, S.A.-O., and Dhama, K.A.-O. (2014). Oxidative stress, prooxidants, and antioxidants: the interplay.

Ramana, K.A.-O., Srivastava, S., and Singhal, S.S. (2017). Lipid Peroxidation Products in Human Health

and Disease 2016.

Raveh, B., Karp, J.M., Sparks, S., Dutta, K., Rout, M.P., Sali, A., and Cowburn, D. (2016). Slide-and-exchange mechanism for rapid and selective transport through the nuclear pore complex. P Natl Acad Sci USA *113*, E2489-E2497.

Ray, P.D., Huang Bw Fau - Tsuji, Y., and Tsuji, Y. (2012). Reactive oxygen species (ROS) homeostasis and redox regulation in cellular signaling.

Ribbeck, K., and Gorlich, D. (2001). Kinetic analysis of translocation through nuclear pore complexes. Embo Journal *20*, 1320-1330.

Ribbeck, K., and Gorlich, D. (2002). The permeability barrier of nuclear pore complexes appears to operate via hydrophobic exclusion. EMBO J *21*, 2664-2671.

Robbins, J.B., Smith D Fau - Belfort, M., and Belfort, M. (2011). Redox-responsive zinc finger fidelity switch in homing endonuclease and intron promiscuity in oxidative stress.

Sajadimajd, S., and Khazaei, M. (2018). Oxidative Stress and Cancer: The Role of Nrf2.

Samakova, A., Gazova A Fau - Sabova, N., Sabova N Fau - Valaskova, S., Valaskova S Fau - Jurikova, M., Jurikova M Fau - Kyselovic, J., and Kyselovic, J. (2019). The PI3k/Akt pathway is associated with angiogenesis, oxidative stress and survival of mesenchymal stem cells in pathophysiologic condition in ischemia.

Sasaki, K., Bannai S Fau - Makino, N., and Makino, N. (1998). Kinetics of hydrogen peroxide elimination by human umbilical vein endothelial cells in culture.

Schmidt, H.B., and Gorlich, D. (2015). Nup98 FG domains from diverse species spontaneously phase-separate into particles with nuclear pore-like permselectivity. LID - 10.7554/eLife.04251 [doi].

Schoch, R.L., Kapinos, L.E., and Lim, R.Y. (2012). Nuclear transport receptor binding avidity triggers a self-healing collapse transition in FG-nucleoporin molecular brushes. Proc Natl Acad Sci U S A *109*, 16911-16916.

Schrader, N., Koerner, C., Koessmeier, K., Bangert, J.A., Wittinghofer, A., Stoll, R., and Vetter, I.R. (2008). The crystal structure of the Ran-Nup153ZnF2 complex: a general Ran docking site at the nuclear pore complex. Structure *16*, 1116-1125.

Seewald, M.J., Korner, C., Wittinghofer, A., and Vetter, I.R. (2002). RanGAP mediates GTP hydrolysis without an arginine finger. Nature *415*, 662-666.

Shimi, T., and Goldman, R.D. (2014). Nuclear lamins and oxidative stress in cell proliferation and longevity.

Sieprath, T., Darwiche R Fau - De Vos, W.H., and De Vos, W.H. (2012). Lamins as mediators of oxidative stress.

Solmaz, S.R., Blobel, G., and Melcak, I. (2013). Ring cycle for dilating and constricting the nuclear pore. Proc Natl Acad Sci U S A *110*, 5858-5863.

Soniat, M., and Chook, Y.M. (2015). Nuclear localization signals for four distinct karyopherin-beta nuclear import systems. Biochem J *468*, 353-362.

Stanley, G.J., Fassati, A., and Hoogenboom, B.W. (2017). Biomechanics of the transport barrier in the

nuclear pore complex. Semin Cell Dev Biol *68*, 42-51.

Stewart, M. (2007). Molecular mechanism of the nuclear protein import cycle. Nat Rev Mol Cell Biol *8*, 195-208.

Stoffler, D., Feja, B., Fahrenkrog, B., Walz, J., Typke, D., and Aebi, U. (2003). Cryo-electron tomography provides novel insights into nuclear pore architecture: Implications for nucleocytoplasmic transport. J Mol Biol *328*, 119-130.

Stuwe, T., Bley, C.J., Thierbach, K., Petrovic, S., Schilbach, S., Mayo, D.J., Perriches, T., Rundlet, E.J., Jeon, Y.E., Collins, L.N.*, et al.* (2015). Architecture of the fungal nuclear pore inner ring complex.

Suel, K.E., Gu, H., and Chook, Y.M. (2008). Modular organization and combinatorial energetics of proline-tyrosine nuclear localization signals. PLoS Biol *6*, e137.

Tajik, A.A.-O., Zhang, Y., Wei, F., Sun, J., Jia, Q., Zhou, W., Singh, R., Khanna, N., Belmont, A.S., and Wang, N. (2016). Transcription upregulation via force-induced direct stretching of chromatin.

Tang, Q., Liu, Y.P., Yan, X.X., and Liang, D.C. (2014). Structural and functional characterization of Cys4 zinc finger motif in the recombination mediator protein RecR.

Timney, B.L., Raveh, B., Mironska, R., Trivedi, J.M., Kim, S.J., Russel, D., Wente, S.R., Sali, A., and Rout, M.P. (2016). Simple rules for passive diffusion through the nuclear pore complex. J Cell Biol *215*, 57-76.

Tolbert, C.E., Beck, M.V., Kilmer, C.E., and Srougi, M.C. (2019). Loss of ATM positively regulates Rac1 activity and cellular migration through oxidative stress.

Tomlin, C.a. (1950). Experimental studies on amphibian oocyte nuclei. I. Investigation of the structure of the nuclear membrane by means of the electron microscope.

Veening, J.W., Smits, W.K., Hamoen, L.W., Jongbloed, J.D., and Kuipers, O.P. (2004). Visualization of differential gene expression by improved cyan fluorescent protein and yellow fluorescent protein production in Bacillus subtilis. Appl Environ Microbiol *70*, 6809-6815.

Walde, S., and Kehlenbach, R.H. (2010). The Part and the Whole: functions of nucleoporins in nucleocytoplasmic transport. Trends Cell Biol *20*, 461-469.

Watson, M.L. (1959). Further Observations on the Nuclear Envelope of the Animal Cell. J Biophys Biochem Cy *6*, 147-&.

Weberruss, M., and Antonin, W. (2016). Perforating the nuclear boundary - how nuclear pore complexes assemble. J Cell Sci *129*, 4439-4447.

Weis, K. (2003). Regulating access to the genome: nucleocytoplasmic transport throughout the cell cycle. Cell *112*, 441-451.

Witkiewicz-Kucharczyk, A., Goch, W.A.-O., Olędzki, J., Hartwig, A.A.-O., and Bal, W. (2020). The Reactions of H(2)O(2) and GSNO with the Zinc Finger Motif of XPA. Not A Regulatory Mechanism, But No Synergy with Cadmium Toxicity. LID - 10.3390/molecules25184177 [doi] LID - 4177.

Xu, D., Farmer, A., and Chook, Y.M. (2010). Recognition of nuclear targeting signals by Karyopherin-beta proteins. Curr Opin Struct Biol *20*, 782-790.

Xu, D., Farmer, A., Collett, G., Grishin, N.V., and Chook, Y.M. (2012). Sequence and structural analyses of nuclear export signals in the NESdb database. Mol Biol Cell *23*, 3677-3693.

Xylourgidis, N., Roth P Fau - Sabri, N., Sabri N Fau - Tsarouhas, V., Tsarouhas V Fau - Samakovlis, C., and Samakovlis, C. (2006). The nucleoporin Nup214 sequesters CRM1 at the nuclear rim and modulates NFkappaB activation in Drosophila.

Yamada, J., Phillips, J.L., Patel, S., Goldfien, G., Calestagne-Morelli, A., Huang, H., Reza, R., Acheson, J., Krishnan, V.V., Newsam, S.*, et al.* (2010). A bimodal distribution of two distinct categories of intrinsically disordered structures with separate functions in FG nucleoporins. Mol Cell Proteomics *9*, 2205-2224.

Yan, S., Sorrell M Fau - Berman, Z., and Berman, Z. (2014). Functional interplay between ATM/ATR-mediated DNA damage response and DNA repair pathways in oxidative stress.

Yang, W., Gelles J Fau - Musser, S.M., and Musser, S.M. (2004). Imaging of single-molecule translocation through nuclear pore complexes.

Yang, W., and Musser, S.M. (2006). Nuclear import time and transport efficiency depend on importin beta concentration. J Cell Biol *174*, 951-961.

Yoshimura, S.H., Kumeta, M., and Takeyasu, K. (2014). Structural mechanism of nuclear transport mediated by importin beta and flexible amphiphilic proteins. Structure *22*, 1699-1710.

Yoshimura, S.H., Otsuka, S., Kumeta, M., Taga, M., and Takeyasu, K. (2013). Intermolecular disulfide bonds between nucleoporins regulate karyopherin-dependent nuclear transport. J Cell Sci *126*, 3141-3150.

Zachariae, U., and Grubmuller, H. (2008). Importin-beta: structural and dynamic determinants of a molecular spring. Structure *16*, 906-915.

Zeitler, B., and Weis, K. (2004). The FG-repeat asymmetry of the nuclear pore complex is dispensable for bulk nucleocytoplasmic transport in vivo. J Cell Biol *167*, 583-590.

Zhang, H., Davies, K.J.A., and Forman, H.J. (2015). Oxidative stress response and Nrf2 signaling in aging.

Zhang, H., Yuan, B., Huang, H., Qu, S., Yang, S., and Zeng, Z. (2018). Gastrodin induced HO-1 and Nrf2 up-regulation to alleviate H2O2-induced oxidative stress in mouse liver sinusoidal endothelial cells through p38 MAPK phosphorylation.

Zwerger, M., Jaalouk De Fau - Lombardi, M.L., Lombardi Ml Fau - Isermann, P., Isermann P Fau - Mauermann, M., Mauermann M Fau - Dialynas, G., Dialynas G Fau - Herrmann, H., Herrmann H Fau - Wallrath, L.L., Wallrath Ll Fau - Lammerding, J., and Lammerding, J. (2013). Myopathic lamin mutations impair nuclear stability in cells and tissue and disrupt nucleo-cytoskeletal coupling.